Advances in renal (patho)physiology using multiphoton microscopy

PhD dissertation

Arnold Sipos, M.D.

Semmelweis University
PhD School of Basic Medical Sciences

Supervisors: László Rosivall, M.D., Ph.D., Med. habil., D.Sc.Med.
János Peti-Peterdi, M.D., Ph.D.

Official opponents: Szabolcs Osváth, Ph.D.
József Balla, M.D., Med. habil., D.Sc.Med.

Chair of Exam Comitee: Emil Monos, M.D., Ph.D., Med. habil., D.Sc.Med.

Members of the Exam Comitee: Jenő Bartha, M.D., Ph.D.
István Kiss, M.D., Ph.D.

Budapest
2009

TABLE OF CONTENT

ABBREVIATIONS

A1 receptor	adenosine A1 receptor
AA	afferent arteriole
ANOVA	analysis of variance
arg	arginine
ATP	adenozin-triphosphate
B	blood
$[Ca^{2+}]ic$	intracellular Ca^{2+} concentration
cAMP	cyclic adenosine monophosphate
CCD	cortical collecting duct
CNT	connecting tubule
Cntrl	control
cTAL	cortical thick ascending limb
Cx30	connexin 30
DIC	differential interference contrast
DME	Dulbecco`s modified eagle
DMEM	Dulbecco`s modified eagle medium
EA	efferent arteriole
EC_{50}	half maximal effective concentration
ENaC	epithelial Na^+ channel
G	glomerulus
GFR	glomerular filtration rate
IC	intercalated cell
ID	internal diameter
ip.	intraperitoneal
JGA	juxtaglomerular apparatus
KO	gene knockout
MAP	mean arterial pressure
MD	macula densa
MW	molecular weight

[NaCl]	NaCl concentration
NHE2	Na^+-H^+ exchanger type 2
NHE3	Na^+-H^+ exchanger type 3
NKCC2	Na^+-K^+-$2Cl^-$ cotransporter
NO	nitric oxide
nNOS	neuronal type of the nitric oxide synthase
P2X	ligand gated, cation-permeable purinergic receptor family
P2X1	type 1 receptor from the ligand gated, cation-permeable purinergic receptor family
P2Y2	type 2 receptor from the G-protein coupled purinergic receptor family
PBS	phosphate buffer solution
PC	principal cell
PC12	Rattus norvegicus (rat) derived pheochromocytoma cell line
PGE2	prostaglandin E2
PI 3-K	phosphotidylinositol-3-kinase
PIP2	phosphatidylinositol 4,5-bisphosphate
PIP3	phosphatidylinositol 3,4,5-trisphosphate
PPi	pyrophosphate
ROMK	renal outer medullary K^+ channel
SE	standard error
TGF	tubuloglomerular feedback
U	urine
wk.	week
wt	weight
WT	wild type animal

1. INTRODUCTION

Multiphoton fluorescence microscopy offers a state-of-the-art imaging technique for deep optical sectioning of living tissues and organs with minimal deleterious effects. Dynamic regulatory processes and multiple functions in the intact kidney or isolated tissue can be quantitatively visualized in real time, noninvasively. Recent advances in our knowledge of renal (patho)physiological processes made possible by the use of this imaging technology. Also, this novel, innovative technique enables us to revisit the classical fields of the renal physiology, like the tubuloglomerular feedback (TGF), and to study it in real-time with submicron resolution. Using this approach, in my experiments I focused on the effect of the tubular flow on the TGF and on the sodium reabsorption of the cortical collecting duct aiming to reveal so far hidden details of these complex regulatory processes.

1.1 THE TUBULOGLOMERULAR FEEDBACK

The tubuloglomerular feedback is a major regulatory process which function is to stabilize NaCl delivery into the late part of the nephron and thereby to stabilize NaCl excretion. Deviations of luminal NaCl concentration ([NaCl]) at the macula densa (MD) serves as an input signal initiating fine control of glomerular arteriolar vasomotor tone that results in inverse changes of glomerular filtration rate. The structural basis of TGF is the juxtaglomerular apparatus, which is a most important structural component of the renin-angiotensin system and is an essential regulatory site of renal salt and water conservation and blood pressure maintenance. The juxtaglomerular apparatus forms a close anatomical link between the macula densa segment of the early distal tubule and the glomerular vessels. This creates the possibility of a feedback mechanism: to balance the tubular salt and water delivery by adjusting the pre- and postglomerular vascular tone. The most important vascular adjustment is the vasoconstriction of the afferent arteriole as NaCl concentration at the macula densa increases (1).

TGF is a hallmark of the kidney function which was always in the focus of the renal physiologists. Despite of the strong attention and thorough work of several research groups details of the exact mechanism of the TGF is still debated. One of this so far less understood component of the existing model is the role of the tubular flow in

the TGF. The flow-effect was proposed long ago. However, current paradigm describes that MD cells respond to elevation in luminal [NaCl] but it lacks to reflect the flow-effect. It is recognized that changes in the NaCl delivery also accompanied by alterations in the fluid flow. If these two components of the tubular fluid are dependent on one another it would assume that the sensor (MD cells) could respond to both.

As part of my studies I aimed to approach the existing model of the TGF seeking evidences to support the role of the tubular fluid flow in the TGF mechanism.

1.1.1 Our current understanding on the TGF signaling pathway

It is the cortical thick ascending limb (cTAL), where the morphologically distinct tubular cells, called macula densa cells, reside. These cells monitor tubular fluid flow and composition and send signals that regulate renal hemodynamics and the rate of filtration (2, 3, 4, 5). Over the past few years there has been intense interest in understanding the biology and functional characteristics of macula densa cells and their role in the cell-to-cell communication process that forms the TGF signaling pathway.

The TGF signaling pathway involves an initial change in luminal fluid composition that is detected by macula densa cells. Macula densa cells then signal the underlying mesangial cells, which leads to the propagation of signals to other juxtaglomerular apparatus (JGA) structures, to the smooth muscle cells of the afferent and efferent arteriole moreover to intraglomerular elements: to the podocytes.

Because initiation of TGF involves concomitant changes in luminal fluid [NaCl] and osmolality, work has focused on defining and characterizing the transport processes in macula densa cells and how these processes may be involved in the detection of changes in luminal fluid composition.

At the apical membrane of the MD cell (figure 1.), there is the Na:K:2Cl cotransporter (NKCC2) that is the primary means for NaCl entry into macula densa cell (6). There are three splice variants of NKCC2 (A, B, and F) that vary in distribution along the cTAL, as well as demonstrate differences in ionic affinities and regulation (7, 8, 9). The luminal [NaCl] at the MD could be as low as 25mM. At this concentration NKCC2 cotransporter is still reabsorbing NaCl; however, it is operating at or near equilibrium values (6). With increases in luminal [NaCl], the cotransporter exhibits functional saturation and maximal transport rates at approximately 60 mM [NaCl] (9,

10). Under physiological circumstances the NKCC2 cotransporter is responsible for the ~80% of the NaCl uptake into the MD cell. The other apical pathway for sodium entry into MD cells is through the type 2 isoform of the Na^+/H^+ exchanger (NHE2) (figure 1.). This transporter is responsible for the remaining ~20% of apical Na^+ uptake (11, 12). However, unlike with the NKCC2 cotransporter, Na^+/H^+ exchanger activity does not saturate as luminal [NaCl] is elevated above 60 mM. In addition to influx of sodium, NHEs extrude hydrogen ions and so there is a luminal [NaCl] dependent cell alkalization with a linear increase in cell pH at least over the range of 25–150 mM [NaCl] (12). Therefore, the fact the NKCC2 cotransporter and NHE2 operate over different ranges in luminal [NaCl] provides the basis for suggesting that these two transport proteins may regulate separate paracrine signaling pathways.

Cellular extrusion of Na^+ take places against its electrochemical gradient, and the classic model by which this occurs is via basolateral Na/K-ATPase. However, as reported a number of years ago, macula densa cells do not have an abundance of this enzyme (13). Thus there was some early indication that macula densa cells might regulate intracellular [Na^+] in a novel manner (14). An almost linear increase in intracellular [Na^+] over the range of 0 to 60 mM NaCl, with no further increase in cell [Na^+] between 60 and 150 mM was found (14). This finding is remarkable because other cells appear to precisely regulate [Na^+] levels in response to external ion perturbations. The concept that has now emerged is that intracellular [Na^+] (and most likely [Cl^-]) tracks or reflects luminal [NaCl]. This seems logical in terms of the sensor function of macula densa cells: to have intracellular [NaCl] reflect changes in luminal [NaCl] over the range where TGF responses occur.

As reported in expression studies, some member of the H/K-ATPase family not only transports H^+ and K^+ but can also transport Na^+, albeit less efficiently than the Na/K-ATPase (15, 16). In macula densa cells, Na^+ extrusion and K^+ entry occur at the apical membrane via a Na-H/K-ATPase (figure 1.). The fact that intracellular [Na^+] tracks luminal [NaCl] may be due to the reduced efficiency of this pump for Na^+ removal. The finding that low levels of Na/K-ATPase are expressed at the basolateral membrane (17) suggests that this ATPase does not greatly participate in Na^+ dynamics under normal conditions. However, it is possible that physiological perturbations could increase the contribution of basolateral Na/K-ATPase to macula densa [Na] regulation.

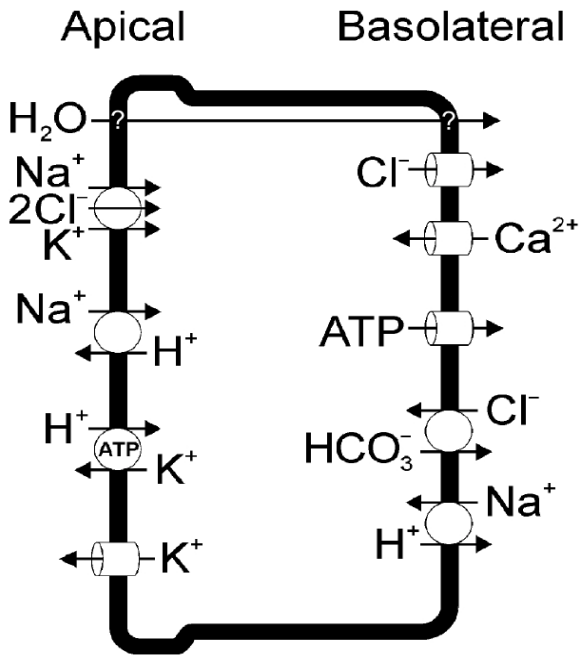

Figure 1. Review of the transport processes in the MD cell apical and basolateral membrane.

Using patch-clamp techniques, a high abundance of apical K^+ channels was detected in MD cells (18) (figure 1.). Because the cotransporter and the apical H^+/K^+-ATPase activities constitute a significant K^+ load into MD cells, a high-activity K^+ efflux pathway is required for sustainable coupling of apical Na^+ and K^+ transport. Moreover, the TAL luminal [K^+] is at or below plasma values (19, 20, 21, 22), continued NaCl transport requires that K^+ be continuously recycled from cell to lumen. ROMK (Renal Outer Medullary K^+ channel) has been identified immunologically in TAL and macula densa (23) and may be responsible for all or part of apical K^+ secretion. TGF responses and renal function are severely impaired in mice with Type II Bartters syndrome in which ROMK has been genetically deleted. This indicates that the apical K^+ recycling mechanism is also an essential component in the macula densa mediation of TGF signaling. In addition to K^+ recycling, this K^+ channel may be responsible for hyperpolarization and regulation of MD cell membrane potential.

There is functional evidence suggesting the existence of a substantial basolateral chloride conductance in MD cells (24) (figure 1.). This chloride permeability is proposed to be responsible for MD basolateral membrane depolarization in response to increased apical NaCl transport and increased intracellular chloride activity. Beside, maneuvers assumed to depolarize the macula densa cells were associated with TGF signaling (25 19). Because the cotransporter (NKCC2) is electro-neutral, membrane potential depolarization most likely reflects intracellular accumulation of Cl^-, with Cl^- efflux through a basolateral Cl channel. It is now clear that increasing luminal [NaCl] will, in fact, cause increases in cell pH, elevations in cellular [NaCl] and a modest elevation in macula densa [Ca^{2+}]ic as well (53). There is a ~20 pS non-selective cation channel in the basolateral membrane of macula densa cells (26) that is activated by depolarization and by elevations in [Ca^{2+}]. This channel has a moderate Ca^{2+} permeability. Is not clear whether this is the primary Ca^{2+} entry pathway.

Although macula densa cells and the rest of the juxtaglomerular apparatus are in close proximity, no cell-to-cell junctions between macula densa and mesangial cells have been proved. Therefore, these cells are thought to communicate with other components of juxtaglomerular apparatus though the release of paracrine factors (like ATP, PGE2, NO), also the release and degradation some of these factors is believed to be coupled to Ca^{2+} influx and subsequent intracellular signaling.

Increasing evidences show the importance of ATP in the regulation of renal microvascular tone. While desensitizing juxtaglomerular purinergic receptors, inhibits TGF responses (27) suggesting that ATP may be involved in TGF signaling. Recently a large-conductance maxi-anion channel was identified on the basolateral membrane of MD (figure 1.), which is permeable to ATP (28). ATP release via this channel occurred over the same range of luminal [NaCl] as reported for TGF responses. Also like TGF (29, 30), ATP release was inhibited by luminal furosemide and enhanced by dietary salt restriction (31). At the present time, there is no firm evidence regarding what specifically regulates the activity of this basolateral anion channel. Presumably, it is associated with the luminal [NaCl]-dependent depolarization of the MD cell basolateral membrane, increase in the intracellular [Ca^{2+}] which in turn could regulate, possibly facilitate the opening of the maxi-anion channel. However, additional work is required to clarify this speculation. Once ATP is released, it should activate P2X receptors on the

extraglomerular mesangial field, and thereby evoke Ca^{2+} waves that propagate towards the vascular elements (32) causing depolarization, vasoconstriction of the vascular smooth muscle cells in the afferent arteriole and subsequent reduction in the diameter of the AA (figure 2.).

Besides the ATP release, MD cells express enzymes that are capable synthesize prostaglandin E2 (PGE2): the microsomal form of prostaglandin E2 synthase and the cyclooxygenase-2 (33, 34, 35). A recent study has provided direct evidence that MD cells synthesize and release PGE2 at the basolateral membrane in response to reduced luminal [NaCl] (36). During conditions of low extracellular fluid volume, reduced tubular salt delivery causes macula densa cells to synthesize and release prostaglandin E2, which in turn stimulates the proliferation of juxtaglomerular cells, the synthesis and release of renin, and the activation of the renin–angiotensin system (37). Finally, the activation of the renin–angiotensin system will result in enhanced angiotensin II production that contracts the AA and reduce the GFR.

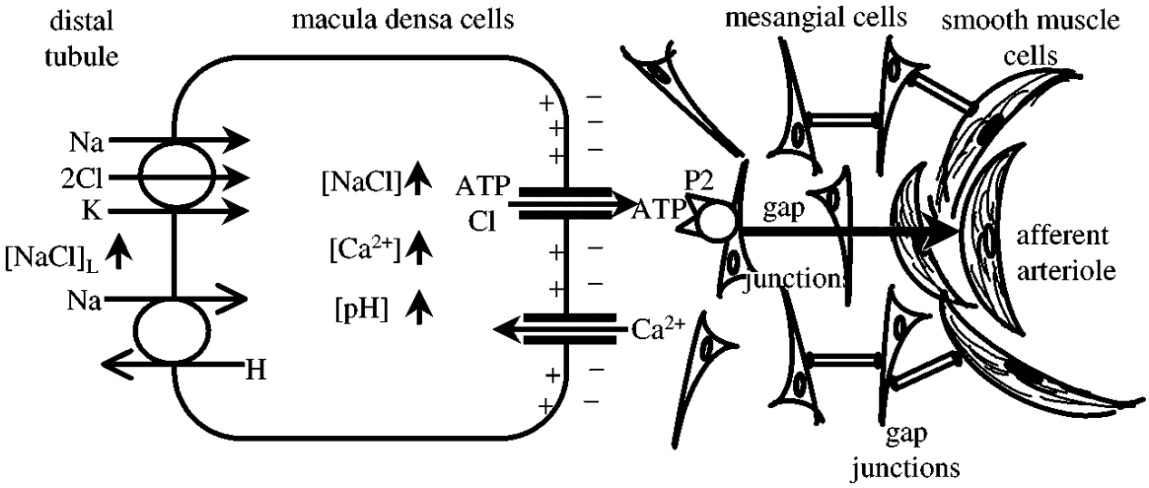

Figure 2. The TGF signaling pathway. *When the luminal [NaCl] is elevated Na^+, K^+, Cl^- enter into MD cell via NKCC2 cotransporter. Alternative Na^+ entry means is through Na/H exchanger resulting in elevated intracellular [Na^+], [Cl^-] and alkalic pH. The basolateral Cl^- efflux depolarizes the basolateral membrane of the MD cell and triggers the opening of nonselective cation channels. The alkalic pH and these ion currents with a so far unknown signaling pathway will lead to the opening of the basolateral maxi-anion channel causing ATP release and Ca^{2+} waves in the mesangial*

cells. The Ca^{2+} wave propagates via gap junctions to the VSMC of the AA causing depolarization, intracellular Ca^{2+} elevation, vasocontraction, reduction of diameter of the AA and reduced GFR.

A great deal of effort has been directed towards elucidating the role of the nitric oxide (NO) in the TGF. NO has been shown to attenuate TGF responses (38) and influence renin release from granular cells (39). This is based, to a large extent, on the high levels of neuronal-type nitric oxide synthase (nNOS) that have been immunologically detected in MD cells. TGF studies suggested that MD intracellular NO concentration increases with elevations in luminal [NaCl] (40, 41). Surprisingly, NO release was mostly stimulated by supraphysiological (above 60 mmol) luminal [NaCl]. In the range where the NKCC2 cotransporter is saturated and changes in luminal [NaCl] are not reflected in changes in intracellular [Na^+]. However, above 60mM luminal [NaCl] the pH of MD cells is further alkalized due to the activity of the Na^+/H^+ exchanger (11). Despite nNOS is traditionally thought to be a calcium sensitive enzyme, other work has reported that it is also pH sensitive (42). These might implicate that over 60mM luminal [NaCl] the MD cell alkalization could lead to enhanced nNOS activity and increased NO release and attenuated TGF respond.

1.2 THE PREGLOMERULAR SPHINCTER

1.2.1 Vasoconstrictor mediators in the TGF

In terms of the vasoconstrictor site along the length of the AA, it is known that the juxtaglomerular portion of the AA produces the highest vascular resistance (43). More proximal segments of the AA (i.e. far from the glomerulus) show only weak autoregulatory vasoconstriction (44). Also, the vasoconstrictor effects of both angiotensin II and adenosine are most pronounced in the glomerular entrance segment of the AA (45,46,47). Angiotensin II and adenosine are considered the key modulator (2) and mediator (48,49) of TGF, respectively. Angiotensin II is known to have a synergic effect on adenosine induced vasoconstriction of the AA (46,50,51).

ATP, another vasoconstrictor involved in renal autoregulation (52) and TGF (28) is likewise more effective in juxtaglomerular versus proximal AA segments (46).

Because this strong vasoconstrictor site overlaps with the renin-positive portion of the AA, it was speculated that renin granular cells could be the effector site of the TGF mechanism (43). However, renin-producing granular cells are considered non-contractile, due to the lack of myosin in these cells (53).

1.2.2 New approaches to study the TGF

Recently, a new experimental imaging approach has been established (102, 54) that uses multiphoton confocal fluorescence microscopy and allows visualization of the living and functioning JGA and glomerulus in striking detail and on single cell level. Using this method, preliminary findings from our laboratory (102, 54) indicated swelling/contraction of certain cells in the terminal, intraglomerular part of the AA during TGF. This contraction appeared to cause a very significant reduction of vessel diameter, nearly to the point of complete closure of the AA. Therefore, we have named it the "glomerular sphincter" based on similarities with the precapillary sphincter in other vascular beds. In my studies I aimed to characterize the morphology and function of the preglomerular sphincter.

1.3 CX30 – DISTAL NEPHRON ATP RELEASE

The changes in the tubular flow rate are known to alter the function of the proximal nephron but these also influence the function of the distal nephron (i.e. sodium reabsorption by the ENaC). The epithelial Na^+ channel (ENaC) forms a pathway for the transport of Na^+ across a variety of epithelia, including tubular epithelium in the kidney. The rate of Na^+ transport must vary dramatically to maintain Na^+ and volume homeostasis in the face of extremes of Na^+ intake. Thus, ENaC function is tightly regulated. It has been known for a long time that ATP is one of the major local regulators of the nephron function. In terms of the body sodium homeostasis it is important that ATP can reduce the sodium excretion by decreasing the activity of the epithelial sodium channel (55) present in the principal cells in the cortical collecting duct (CCD). However, recent studies indicate that this is not a direct effect on ENaC, since ENaC itself is insensitive to extracellular ATP (56), rather than purinergic receptor mediated inhibition. Although the localization and function of the purinergic

receptors are widely studied in the kidney (57), our knowledge of the possible ATP source is limited. One important factor that should also be taken account is the short half life of ATP (for example the half-life of nucleotides in perfused lung is ~0.2 s (57)) due to the metabolic activity of the extracellular membrane-bound ecto-nucleotidases. This fact let us suppose that the ATP source and the site of action are in close proximity.

1.3.1 Gap junctions as ATP channels

Recently, it was shown, that ATP can be released via connexon (58). This is a novel concept since the gap junction hemichannels were believed to be active only in the junctional membrane lipid rafts. It was the earlier work of our laboratory, which described at the first time that connexin 30 (Cx30) gap junction protein is expressed in a non-junctional plasma membrane: in the apical membrane of the intercalated cells in the CCD (59) (figure 3.). Based on this observation and similarities between connexon hemichannels, we suppose that ATP can also be released from intercalated cells through Cx30 and act on the neighboring principal cells. This way Cx30 could even closer couple this morphologically and functionally different two cell types (intercalated and principal cells) forming a local regulatory network in the CCD.

Sodium is the major ion of the extracellular fluid, and total body sodium is an important determinant of the extracellular fluid volume. The mechanisms regulating salt balance tend to be geared towards retaining salt and water in the body in an attempt to preserve the extracellular fluid volume and maintain adequate blood circulation. Increased generation of the adrenal hormone aldosterone is a major mechanism in the preservation of salt and water in response to sodium depletion. However, in the presence of a sustained large salt intake, body fluid volumes do not increase indefinitely; normally, urinary sodium excretion is increased to match the higher sodium intake, thereby preventing overt and dangerous expansion of the extracellular fluid volume. Besides the regulation of sodium intake, the modulation of renal sodium excretion is a key process in the maintenance of sodium balance (60).

The epithelial sodium channel in the renal distal nephron is an important component in the overall control of sodium balance. However it is responsible only for a relatively small proportion of the sodium re-absorbed (<5%), it nevertheless

constitutes the rate-limiting step for renal sodium reabsorption and therefore is of fundamental importance in the control of blood volume and thereby of blood pressure.

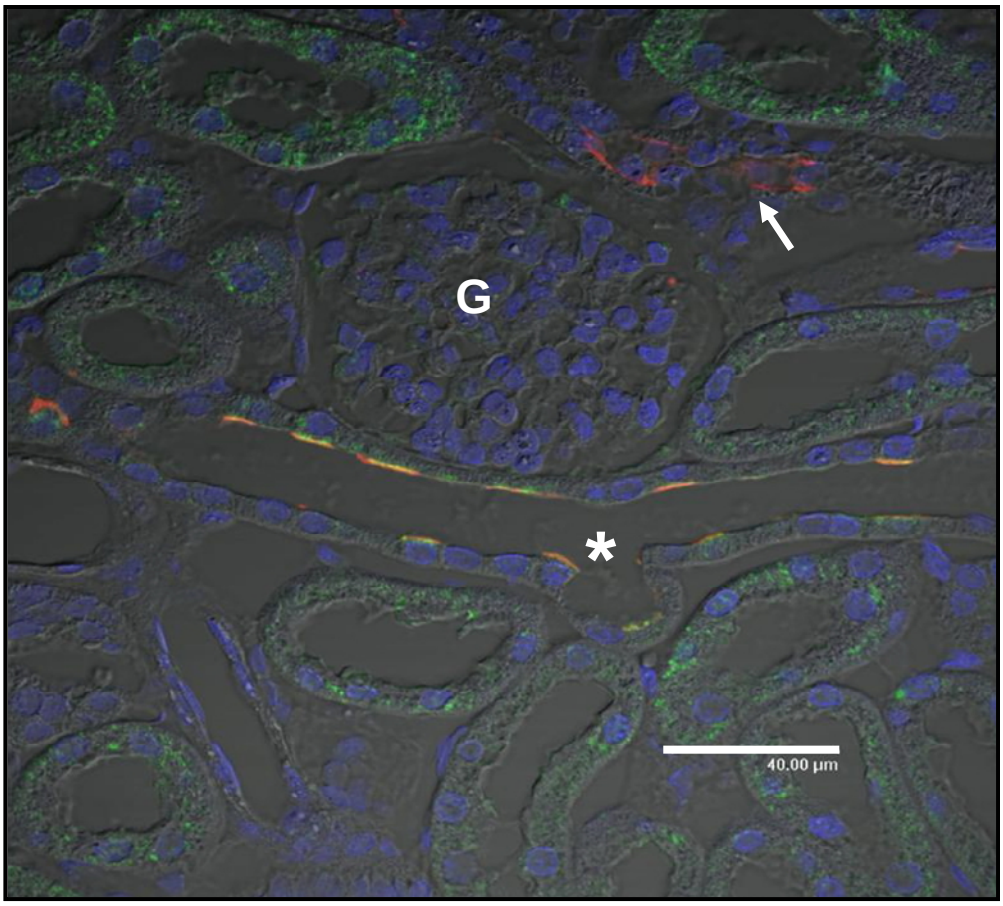

Figure 3. Immunofluorescence labeling of Cx30 in the rabbit kidney. *Pendrin (green) and Cx30 (red) staining in the apical membrane of select cells in the CNT and CCD. Present image demonstrates colocalization of Cx30 and pendrin (yellow) in type B and non-A, non-B intercalated cells of the CNT and CCD (*). Apical membrane of the cTAL (arrow) next to the glomerulus (G) is also positive for Cx30. The nuclei of the cells were stained by Hoechst 33342 (blue). Image source: (59).*

Indeed, the significance of ENaC in the control of sodium balance and blood pressure is clearly demonstrated by rare genetic disorders of sodium-channel activity such as Liddle's syndrome (61, 62).

The ENaC is also relevant in the regulation of sodium transport in other epithelia, such as the alveolar epithelium, distal colon, salivary duct and sweat glands (63).

ENaCs are composed of three homologous subunits, termed α-, β- and γENaC (64, 65, 66). These subunits assemble to form a hetero-oligomeric, Na^+-selective ion channel with a subunit stoichiometry of 2α:1β:1γ (67, 68), although an alternative subunit stoichiometry has been proposed (69, 70). All three Na^+ channel subunits have cytoplasmic amino and carboxyl termini, two transmembrane domains (termed M1 and M2), and a large ectodomain (71, 72).

1.3.2 Purinergic control of ENaC

The rate of Na^+ transport must vary dramatically to maintain Na^+ and volume homeostasis in the face of extremes of Na^+ intake. Thus, ENaC function is tightly regulated. In contrast to voltage- and ligand-gated ion channels, which are regulated through rapid changes in channel gating (opening and closing), ENaC is regulated in large part through mechanisms that control its expression at the cell surface, akin to the regulation of many receptors and transporters. Although such a mechanism mostly sacrifices speed, its advantage is a potentially larger dynamic range. Previous work suggests that ENaC trafficking is highly regulated (73, 74, 75), both at the level of ENaC movement to the cell surface, as well as ENaC endocytosis and degradation. Moreover, defects in ENaC trafficking are responsible for inherited forms of hypertension and hypotension (76). Thus, elucidating the mechanisms that regulate ENaC trafficking is critical to our understanding of Na^+ transport and Na^+ homeostasis.

Besides of the long term regulation of channel activity, the Na^+ permeability of ENaC can be modified by paracrine bioactive molecules such as ATP. This field has been in the focus of researches over the last decade. There has been rapid progress in understanding the regulation of ENaC activity since the constituent subunits were cloned (65). Interestingly, a number of factors that are known to regulate ENaC activity—such as changes in intracellular cations, changes in cAMP levels, and the activation of regulatory G proteins—can be modulated by nucleotide receptors (e.g. by P2 receptors).

The purinergic receptors are divided into three families:

- P1 receptors: G-protein-coupled receptors with adenosine as the endogenous ligand (77).
- P2Y receptors: G protein-coupled receptors stimulated by nucleotides such as ATP, ADP, UTP, UDP and UDP-glucose. To date, 12 P2Y receptors have been cloned in humans (78). P2Y receptors are present in almost all human tissues where they exert various biological functions based on their G-protein coupling.
- P2X receptors: the ligand gated, cation-permeable ion channels. To date, seven separate genes coding for P2X subunits have been identified, and referred to as P2X1 through P2X7 (79, 80). These receptors, with the exemption of P2X7, are capable of forming heteromeric P2X receptors with at least one other subunit type.

Several lines of evidence show that both P2X and P2Y receptors can inhibit ENaC activity. Concerning P2Y receptors, recent studies confirmed that ATP stimulation of purinergic P2Y receptors hydrolyzes PIP_2 (81, 82) and that aldosterone stimulation of steroid receptors induces PIP_3 formation (83). These studies together suggest that one primary mechanism for regulating ENaC is by alteration of plasma membrane bound anionic phospholipids and that the receptor-mediated and hormonal regulation of ENaC works through a variety of signaling pathways, but many of these pathways finally alter ENaC activity by regulating the formation or degradation of anionic phospholipids. Therefore, changes in the concentration of PIP_2 and PIP_3 are hypothesized to participate in the regulation of ENaC by purinergic and corticoid receptors. The underlying mechanism may be associated with a physical interaction of the positively charged cytoplasmic domains of the β- and γ-ENaC with the negatively charged membrane phospholipids (figure 4.). However, the exact nature of this interaction will require further investigation.

Beside of P2Y receptors mediated inhibition of ENaC there are evidences for decreased ENaC activity after P2X receptor stimulation (84, 85) Increased expression of ENaC may result in the concomitant upregulation of P2X2, P2X2/6, and P2X5 receptors by decreased retrieval of these ion channels from the plasma membrane. Activation of P2X2, P2X4, P2X2/6, and/or P2X4/6 receptor ion channels by

endogenous extracellular ATP may result in an influx of Na^+ and Ca^{2+} and the subsequent downregulation of ENaC (85).

These data suggest that both P2Y and P2X receptor stimulation results in decreased ENaC activity via several mechanisms (by blocking the active pore or downregulation of the ion channel itself).

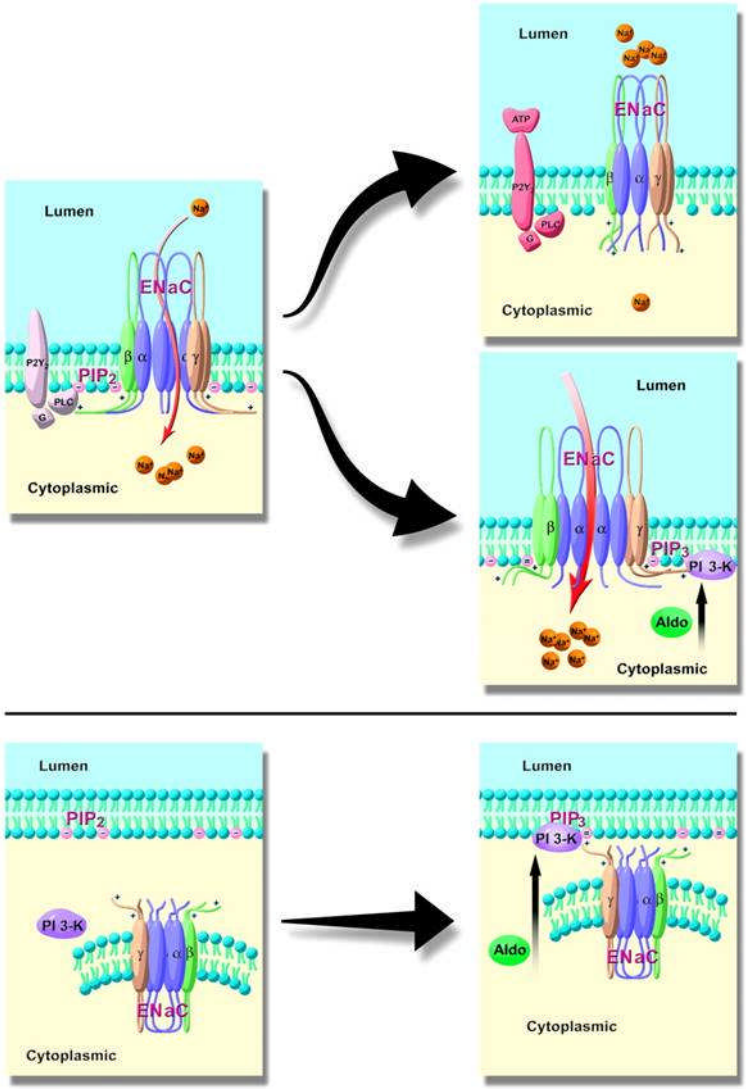

Figure 4. Hypothesis for ENaC regulation by either ATP via a decrease in membrane PIP_2 or aldosterone via an increase in membrane PIP_3. *Under resting conditions, the positively charged regions of the cytoplasmic termini of α- and β-ENaC are held in a certain position by the negatively charged PIP_2 located in the inner leaflet of plasma membrane (top left). After P2Y receptor activation, the concentration of PIP_2 is decreased as a result of the induction of PLC. Loss of PIP_2"unlocks" the cytoplasmic termini to release them from the inner surface of plasma membrane, subsequently*

leading to the decreased ENaC open probability (top right). Aldosterone elevates the concentration of PIP_3 by activating of phosphotidylinositol-3-kinase (PI 3-K). PIP_3 stimulates ENaC activity by further "locking" of the cytoplasmic termini to the inner surface of plasma membrane because of one more negative charges (middle right). In the absence of aldosterone, the inner leaflet of the plasma membrane contains PIP_2 rather than PIP_3 (bottom left). In the presence of aldosterone, PIP_3 is produced and somehow stimulates ENaC surface expression. Image source: (86).

1.3.3 Pressure natriuresis

Renal autoregulation keeps the renal blood flow (RBF) and glomerular filtration (GFR) rate constant when blood pressure varies between ~60 and ~150 mmHg. As a result, both RBF and GFR remain relatively constant with increases in blood pressure. This limits the effect of blood pressure in raising the glomerular blood flow and the glomerular filtration (figure 5.).

This regulation is not perfect and thus increases in blood pressure do produce increased excretion of salt and water. This phenomenon is called pressure natriuresis.

It is well established that pressure natriuresis plays a key role in long-term blood pressure regulation (87), but our understanding of the mechanisms underlying this process is incomplete. Pressure natriuresis is mainly mediated by inhibition of tubular sodium reabsorption, because both total renal blood flow and glomerular filtration rate are efficiently autoregulated. Because of the majority of the filtered sodium is reabsorbed in the proximal nephron the studies mainly focused on finding the role of the proximal nephron segments in the pressure natriuresis. Inhibition of active sodium transport both in the proximal (88, 89) and distal tubules are likely to contribute to pressure natriuresis.

Beside of these other mechanisms are also hypothesized to be taken part in this phenomenon: increased renal interstitial hydrostatic pressure is believed to inhibit sodium reabsorption by altering passive diffusion through paracellular pathways in 'leaky' tubular elements (90); the role of nitric oxide and products of cytochrome P450-dependent arachidonic acid metabolites (91, 92) are proven in pressure natriuresis, although their precise mechanisms remain to be determined.

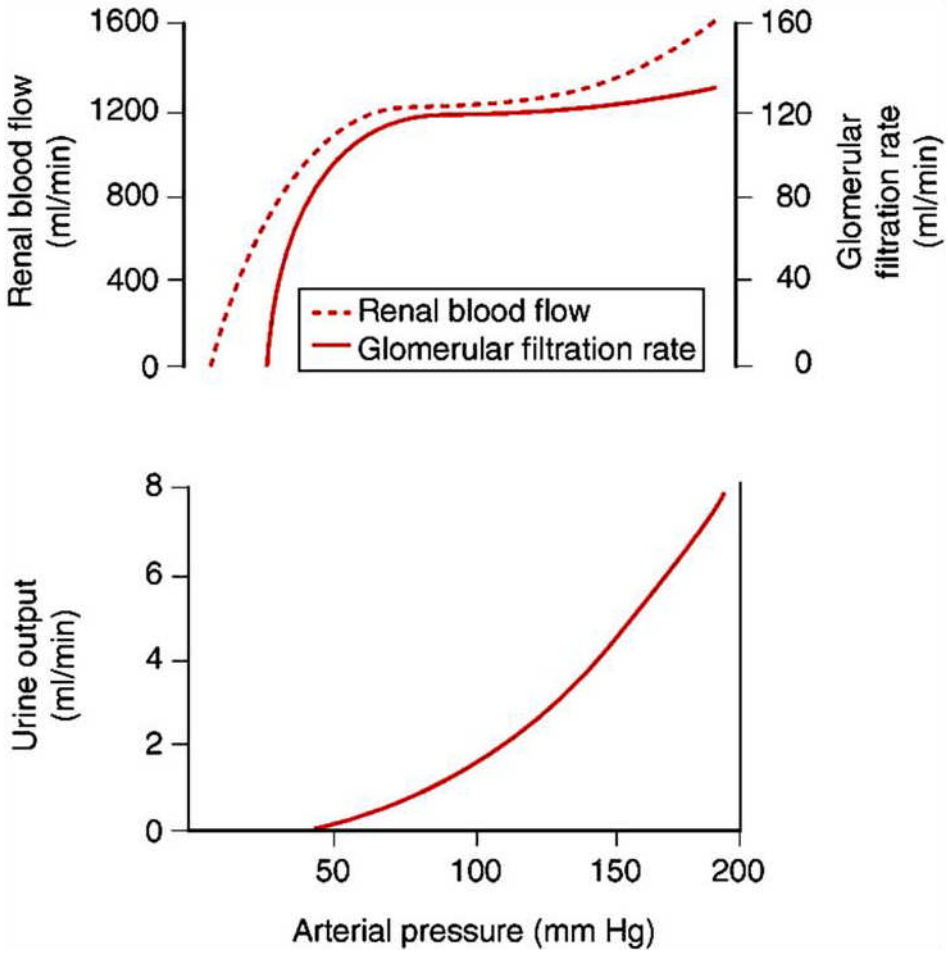

Figure 5. *Upper panel: renal autoregulation – relationship between arterial pressure and renal blood flow and glomerular filtration rate. Lower panel: pressure diuresis – relationship between arterial pressure and urine output.*

The key, unresolved question is: how does the kidney sense the increased renal arterial pressure? One proposal rests on the notion that blood flow in the renal medulla is poorly autoregulated, so that increased renal arterial pressure leads to increased renal medullary blood flow, which, in turn, builds up renal increased interstitial hydrostatic pressure. An alternative proposal favors the increased shear stress that is associated with the autoregulation of renal blood flow. The shear stress releases nitric oxide and perhaps products of cytochrome P450- dependent arachidonic acid metabolites, which, in turn, drive the cascade of events that inhibit sodium reabsorption.

To date the exact mechanism which is capable to describe the pressure natriuresis phenomenon in details, is not known. This creates the possibility of coexistence for several alternative theories. During my work I aimed to examine the role of the Cx30 hemichannels in the ATP release, study their function in the control of the distal nephron sodium reabsorption and in the pressure natriuresis.

2. HYPOTHESIS AND SPECIFIC AIMS

2.1 TUBULOGLOMERULAR FEEDBACK

In the current model of the TGF the input signal of the regulatory pathway is the tubular [NaCl] at the MD area. However, the alteration in the tubular [NaCl] is not an isolate change. NaCl is an osmotically active molecule. Whenever the tubular [NaCl] is elevated it also means that more water and in consequence higher tubular flow reaches the MD region. Because of this reason, changes in the tubular [NaCl] occur simultaneously with the alteration in the tubular flow rate. MD cells are capable to detect changes in the tubular [NaCl]. For the aforementioned reasons we suppose that the MD cells are also capable to sense the changes in the tubular flow rate.

Former studies using different type of tissue (canin, rat and human) has already reported that MD cells has a primer cilium (93, 94). Neither of these studies nor the latter ones were trying to find the function of this cilium. Recently, Pretorius et al. reported that cultured MDCK cells produce a Ca^{2+}-coupled intracellular signaling after flow stimuli (95). The author demonstrated that this response was due to the bending of the primary cilium of the MDCK cells. We suppose that if the MD cells possess a primary cilium than this might be the means how the MD cell might be able to detect changes in the tubular flow rate.

Our specific aims were:

1. To examine if the TGF can be initiated by changing the tubular flow rate per se without causing any alteration in the tubular [NaCl]
2. To find the tubular flow sensor in the distal tubule
3. To determine the effect of the changing tubular [NaCl] on the fluid flow induced TGF
4. To identify the signaling pathway that is involved in the flow induced TGF

2.2 PREGLOMERULAR SPHINCTER

Previous observations from our earlier experiments suggested the existence of a preglomerular capillary sphincter. The present studies were undertaken to characterize this sphincter in more detail and to directly visualize it in function during TGF activation by using state-of-the-art confocal imaging techniques.

Our specific aims were:

1. To visualize the preglomerular capillary sphincter both in vitro and in vivo using two photon microscopy
2. To identify the cellular components involved in the formation of the preglomerular capillary sphincter
3. To study the regulation of the preglomerular capillary sphincter
4. To examine if a similar postglomerular capillary sphincter exists at the juxtaglomerular part of the efferent artery

2.3 CX30 – DISTAL NEPHRON ATP RELEASE

Accumulating evidences suggest that ATP is released via gap junctions (32, 58, 96, 97). In our laboratory Cx30 hemichannel was localized at the apical membrane of the intercalated cells suggesting a release function and potential role in regulation of the cortical collecting duct function. If we suppose that Cx30 is an ATP-permeable luminal hemichannel -possible mechanosensor- and ATP-purinergic signaling inhibits renal Na^+ and water reabsorption then Cx30 may be involved in the pressure-natriuresis and diuresis phenomenon. To assess this theory, we applied our hypothesis in a pressure-natriuresis model with modulation on protocol earlier described (98). In this model both in vivo and in vitro we tried to demonstrate functional differences in the presence and in the lack of Cx30. Previous pressure-natriuresis studies (88, 89, 99) focused on the proximal tubule since the majority of the filtered sodium is reabsorbed in this segment of the nephron. Besides the importance of the proximal nephron elements in Na^+ reuptake, in our experiments we want to explore the “distal component” of the pressure-natriuresis, the contribution of the CCD to this phenomenon.

Our specific aims were:

1. To study if Cx30 hemichannel is capable releasing ATP using imaging approach (biosensor technique and confocal microscope)
2. To examine the role of Cx30 in pressure natriuresis and diuresis phenomenon in Cx30 animal model
3. To explore the contribution of the cortical collecting duct to the pressure natriuresis
4. To test if the Cx30 is involved in the regulation of the pH homeostasis

3. METHODS

3.1 MULTIPHOTON MICROSCOPY

3.1.1 Fundamentals of the two-photon microscopy

Multiphoton excitation fluorescence microscopy is a state-of-the-art confocal imaging technique ideal for deep optical sectioning of living tissues. Two-photon excitation employs a concept first described by Maria Göppert-Mayer in her 1931 doctoral dissertation (100).

The concept of two-photon excitation is based on the idea that two photons of low energy can excite a fluorophore in a quantum event, resulting in the emission of a fluorescence photon, typically at a higher energy than either of the two excitatory photons. The probability of the near-simultaneous absorption of two photons is extremely low. Therefore a high flux of excitation photons is typically required, usually a femtosecond laser.

The first pioneering researcher in the two-photon microscopy field was Winfried Denk who combined the idea of two-photon absorption with the use of a laser scanner (101). In two-photon excitation microscopy an infrared laser beam is focused through an objective lens. Normally, the titanium-sapphire laser is used, which has a pulse width of approximately 100 femtoseconds and a repetition rate of about 80 MHz, allowing the high photon density and flux required for two photons absorption and is tunable across a wide range of wavelengths.

The two-photon microscope is capable of performing ultrasensitive, quantitative imaging of organ functions in health and disease (102) with high spatial and temporal resolution which other imaging modalities cannot achieve (figure 6.).

The most commonly used fluorophores have excitation spectra in the 400–500 nm range, whereas the laser used to excite the fluorophores lies in the ~700–1000 nm (infrared) range. If the fluorophore absorbs two infrared photons simultaneously, it will absorb enough energy to be raised into the excited state. The fluorophore will then emit a single photon with a wavelength that depends on the type of fluorophore used (typically in the visible spectrum). Because two photons need to be absorbed to excite a

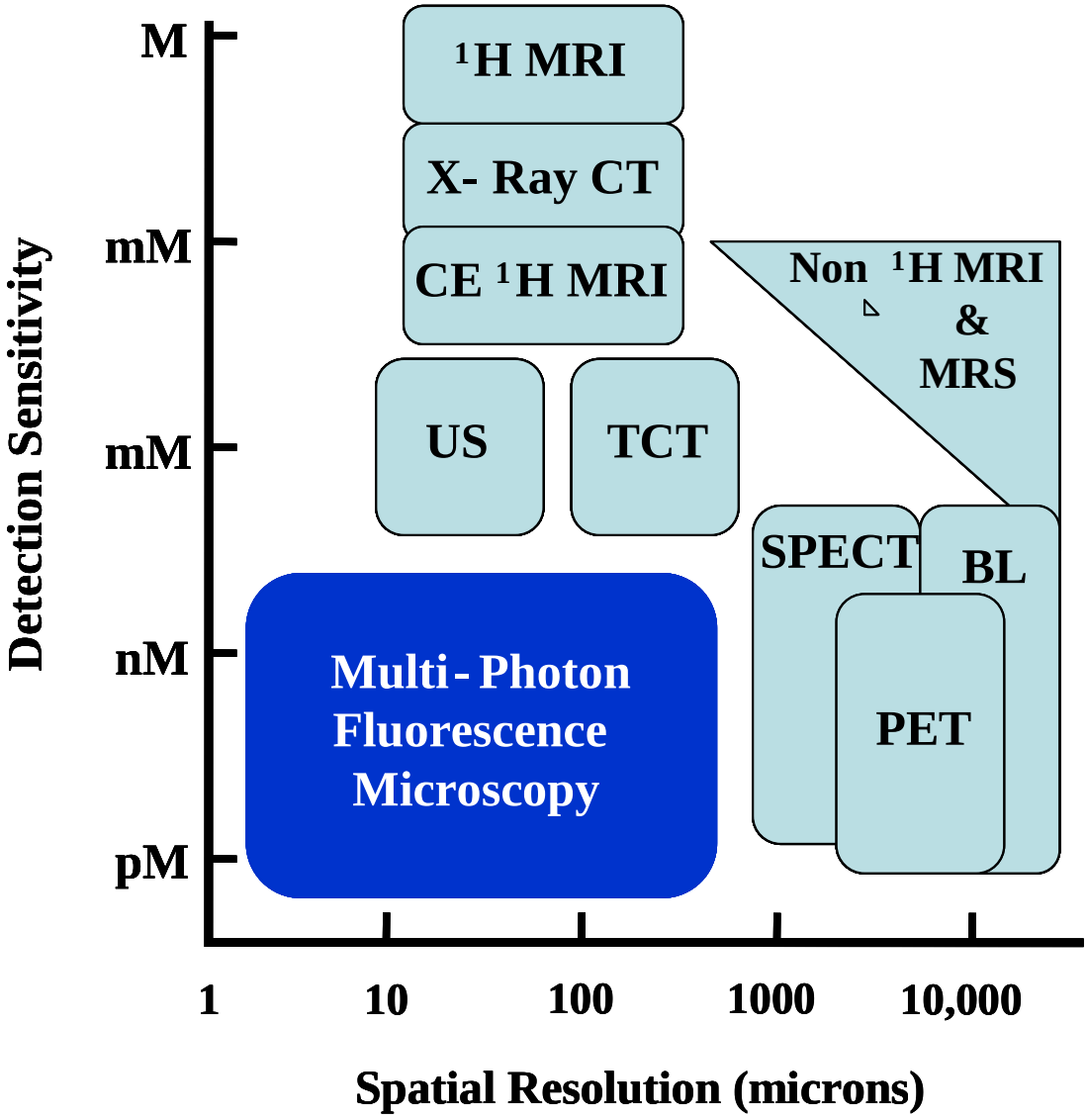

Figure 6. Spatial resolution and detection sensitivity of different imaging techniques. *MRI: Magnetic Resonance Imaging, CT: Computed Tomography, CE MRI: Contrast Enhancement MRI, US: Ultra Sound, TCT: Transmission CT, MRS: Magnetic Resonance Spectroscopy, SPECT: Single Photon Emission Computed Tomography, BL: Bioluminescence, PET: Positron Emission Tomography. Source of the image: (103).*

fluorophore, the probability for fluorescent emission from the fluorophores increases quadratically with the excitation intensity. Therefore, much more two-photon fluorescence is generated where the laser beam is tightly focused than where it is more diffuse. Effectively, fluorescence is observed in any appreciable amount in the focal

volume, resulting in a high degree of rejection of out-of-focus objects. The fluorescence from the sample is then collected by a high-sensitivity detector, such as a photomultiplier tube. This observed light intensity becomes one pixel in the eventual image; the focal point is scanned throughout a desired region of the sample to form all the pixels of the image.

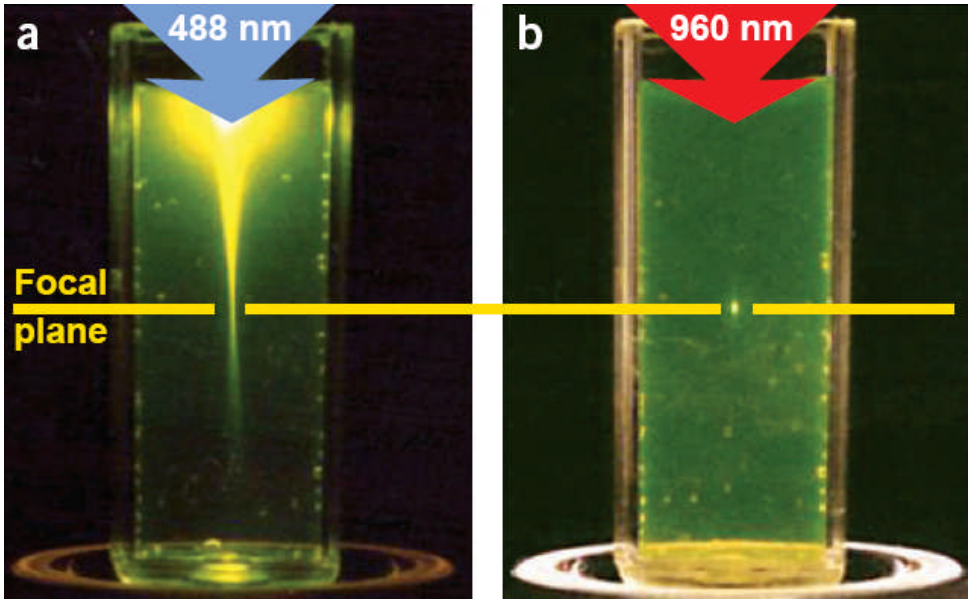

Figure 7. Excitation photobleaching pattern of single photon vs. multiphoton excitation*: dramatic difference between excitation modes in confocal (a) and multiphoton microscopy (b). During confocal excitation there is a huge out-of-focus absorption compared to single, punctuate pattern with no out-of-focus absorption observed in two photon excitation. Source of the image: (104).*

The use of infrared light to excite fluorophores in light-scattering tissue has additional benefits (105). Longer wavelengths are scattered to a lesser degree than shorter ones, which means greater portion of excitation light will reach the focal plane (figure 7.). In addition, these lower-energy photons are less likely to cause damage outside of the focal plane. There are several minor disadvantage in using two-photon microscopy: pulsed lasers are generally much more expensive, the microscope requires special optics to withstand the intense pulses, the two-photon absorption spectrum of a

molecule may vary significantly from its one-photon counterpart, and wavelengths greater than 1400 nm may be significantly absorbed by the water in living tissue.

3.1.2 Confocal- versus two-photon microscopy

In a confocal microscope (figure 8.), the excitation light is focused into the specimen, and the fluorescence from that focal spot is captured by the objective lens, passes cleanly through the pinhole, and reaches the detector. This fluorescence light is the desired signal, but some of it can be scattered as it passes back through the specimen. This scattered fluorescence does not pass through the pinhole, and is therefore lost and not detected. These losses greatly reduce the detected fluorescence signal. As the excitation light passes through the specimen, it may be absorbed or scattered before it reaches the focus. If it is absorbed, it can generate fluorescence. Since this fluorescence does not arise from the focal spot, it does not pass through the pinhole, so it is not efficiently detected. However, a small portion of out-of-focus fluorescence can be scattered into the pinhole, and then be detected. This fluorescence will create a background fog that will be roughly constant across the image. This fog reduces the dynamic range of the image, thus reducing the image contrast. Likewise, the scattered excitation can generate fluorescence, and this fluorescence can also contribute to the background fog.

In the two-photon excitation method (figure 8.) the excitation photons can be scattered as in the confocal system. However, the probability of two photons being scattered simultaneously to the same specimen location is essentially zero, and consequently, the background fog that plagues confocal imaging in thick specimens is not generated in two-photon excitation. In addition, a larger amount of the excitation light reaches the focal plane due to the reduced out-of-focus absorption and the decreased scattering of the longer-wavelength two-photon excitation light. Importantly, the generated fluorescence, even if scattered, has an increased likelihood of being detected by the photomultiplier tube because no pinhole is present to block it. This insensitivity to scattering effects and absence of out-of-focus absorption allow for the preservation of the full image contrast from considerable depth within specimens.

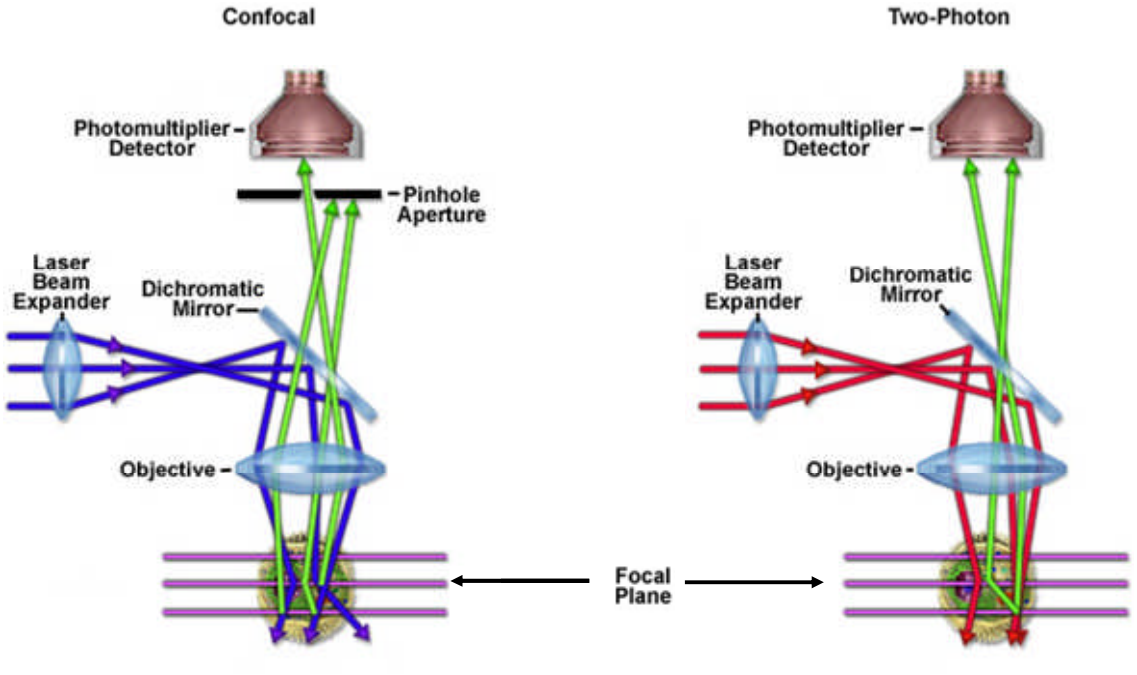

Figure 8. The scheme of the confocal- and the two-photon microscope. *Blue and red lines refer to the excitation lights in confocal- and two-photon microscope, respectively. While the emitted fluorescent light is shown in green.*

3.1.3 Application of the two-photon microscopy

The two-photon microscopy is offering not only the advantages of confocal microscopy, but is also capable visualizing intact living tissue with minimal phototoxicity and high, subcellular resolution (104). In combination with in vitro experimental models, both cortical and medullary structures freshly dissected from the rabbit kidney have been successfully visualized (106). Since multiphoton microscopy can section through an entire glomerulus (approximately 100 μm in diameter), it has been used with the isolated microperfused afferent arteriole (AA)–glomerulus technique to study dynamic processes of (juxta)glomerular structures (106-116). For more than a decade, multiphoton microscopy has been successfully used with various in vitro and in vivo experimental approaches to study many functions of different organs, including the kidney.

The first years after multiphoton microscopy became commercially available (around 1995) heralded the ‘awe’ period of in vivo organ imaging. The emphasis,

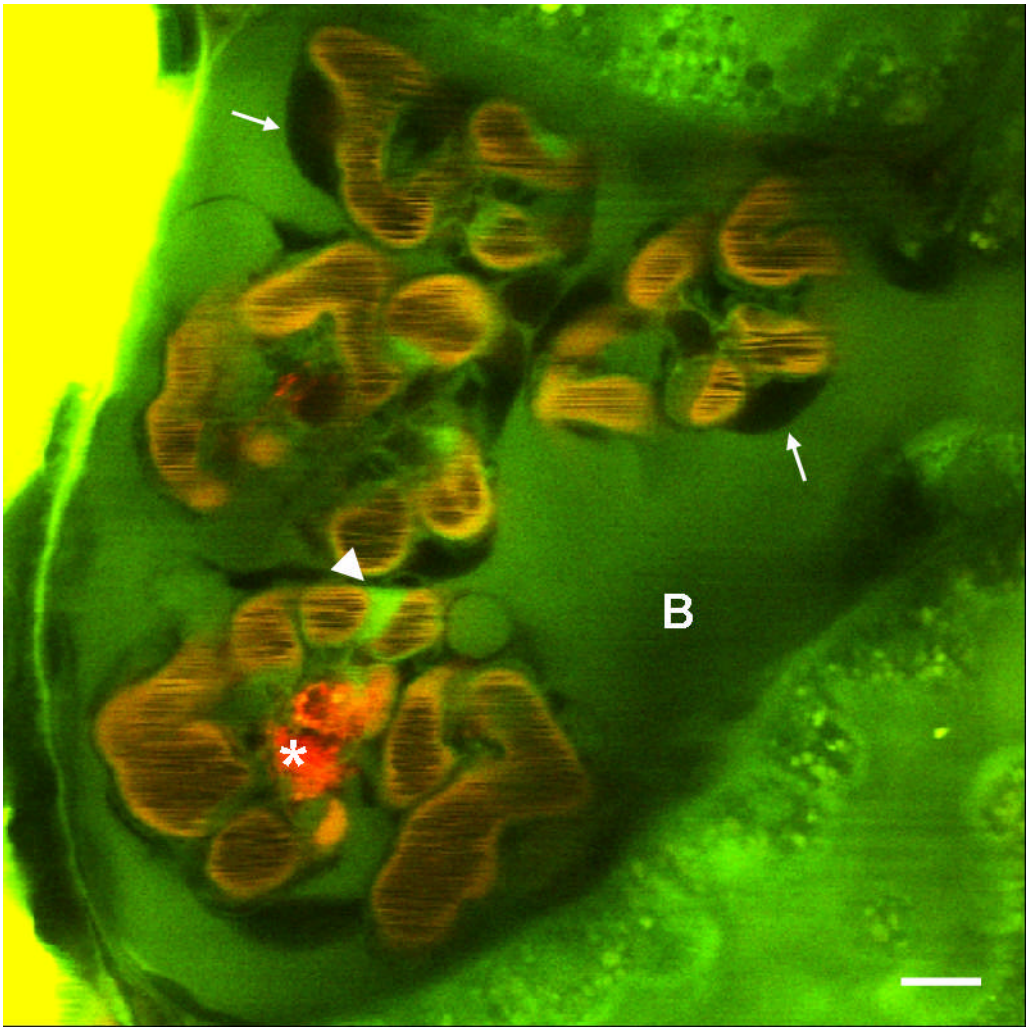

Figure 9. In vivo multiphoton image of a Munich-Wistar rat glomerulus. *The plasma was labeled by high molecular weight (70 kDa) dextran conjugated rhodamine (red). The black lines in the capillary loops are the streaming, unlabelled (black) red and white blood cells. B: Bowman-space that is labeled by of the fluid marker Lucifer Yellow. The arrows points at the unlabelled podocytes, the arrowhead shows the endothelial cell that is stained green due to the endocytosis of the Lucifer Yellow. * indicated the intraglomerular macrophages that have taken up the 70kDa dextran conjugated rhodamine. Scale is 10μm.*

however, soon shifted from generating aesthetic images to the development of quantitative imaging techniques for the evaluation of organ function. Studies aimed to establish new procedures or to extend existing methods in fluorescence imaging to directly observe and quantify basic physiological parameters of the kidney (107-109) including single-nephron glomerular filtration rate, glomerular permeability, blood flow, tubular flow, tubular reabsorption, urinary concentration/dilution, renin content and release, as well as more integrated and complex functions like the tubuloglomerular feedback mediated oscillations in glomerular filtration and tubular flow (107). Moreover, this technique is capable to visualize the ultrafine structure of organs in subcellular level in vivo (figure 9.): dynamic processes such as glomerular filtration (108, 109), proximal tubule endocytosis (110), apoptosis (108), microvascular function (108, 111), protein expression (112), and renal cysts (113) have been visualized and studied down to the subcellular resolution. A ratiometric intravital two-photon microscopy technique based on the generalized polarity concept has been recently applied to quantify glomerular filtration and tubular reabsorption (109). Yu et al. (114) also reported a new ratiometric measurement technique based on intravital fluorescence microscopy that allows rapid evaluations of renal function in rodent models. By using this technique, plasma clearance rates of a fluorescent GFR marker can be measured in less than 5 min after a bolus infusion of a fluorescent dye mixture into the blood stream. Intravital multiphoton imaging provided evidence for intense proximal tubular reabsorption of negatively charged macromolecules (albumin and dextran), which provided further explanation for their low content in the urine (111, 115).

Intravital multiphoton microscopy was used to directly visualize fenestrations of the AA endothelium in the renin-expressing segment first described by Rosivall (116) and bulk fluid flow in the JGA originating from the afferent arteriolar ultrafiltration of plasma into the JGA interstitium as well as the flow of glomerular filtrate in the Bowman’s space back into the extraglomerular mesangium (116). Labeling the AA endothelium by the endocytosis of the fluid marker Lucifer Yellow revealed the heterogeneity of the preglomerular vasculature (figure 10.).

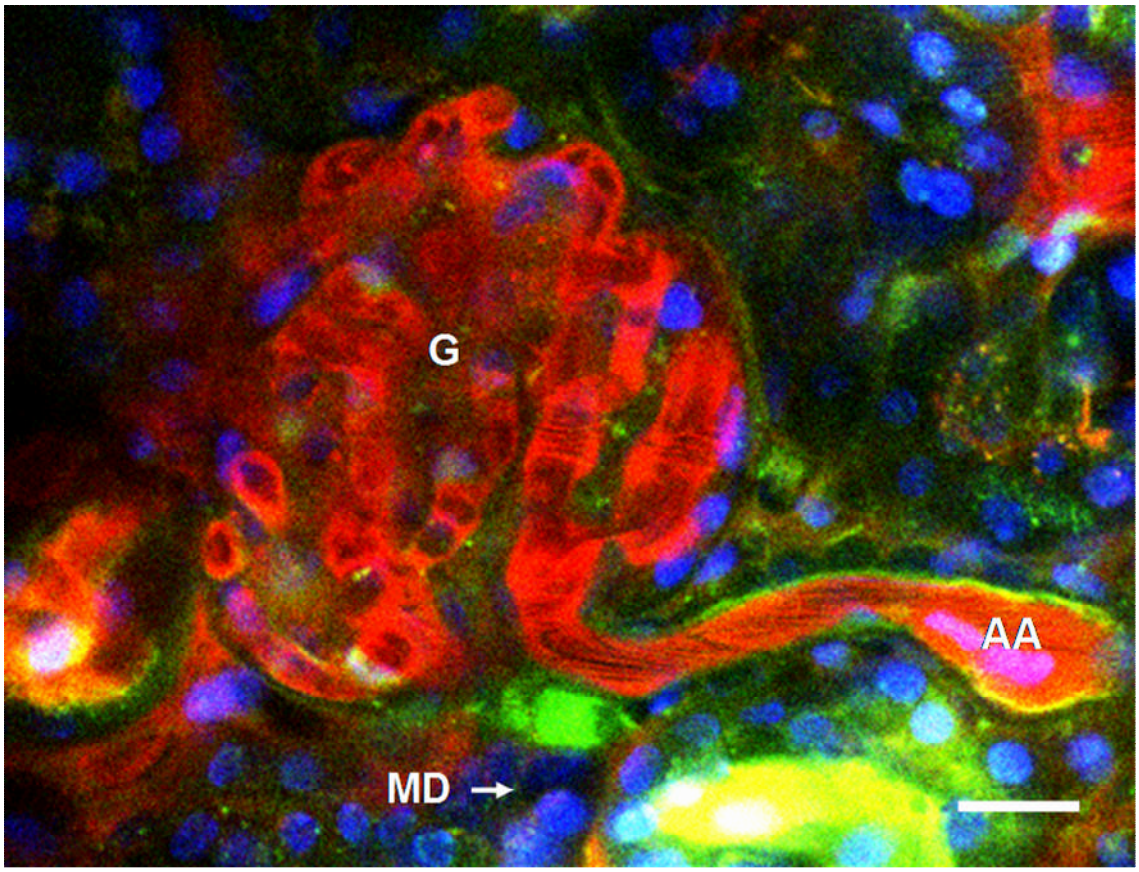

Figure 10. In vivo multiphoton image of a mouse glomerulus (G). *The endotelium of the afferent arteriole (AA) was labeled by the endocytosis of the fluid marker Lucifer Yellow. Note, the intense labeling of the proximal AA as opposed to the punctuate pattern at the juxtaglomerular segment of the AA: the intravascular space was labeled by high molecular weight (70 kDa) dextran-rhodamine B (red), the nuclei of the cells were stained by Hoechst 33342 (blue), the renin content of the AA by quinacrine (green). Scale is 10μm.*

Lucifer yellow stained the proximal and juxtaglomerular AA endothelium segments differently. In the proximal portion, the endothelium appeared as a solid and intensely fluorescent line, but it was weakly fluorescent with a discontinuous linear pattern in the juxtaglomerular segment (figure 10.). These observations, as a part of a bigger study, concluded that significant and dynamic fluid flow exists in the JGA, which may help filter the released renin into the renal interstitium (endocrine function).

It may also modulate TGF and renin signals in the JGA (hemodynamic function). These findings challenge the existing paradigm of the stable and isolated JGA environment.

3.2 TUBULOGLOMERULAR FEEDBACK

3.2.1 Animals

C57BL6 mice were bred and used in accordance with the Institutional Animal Care and Use Committee at the University of Southern California. For anesthesia 100mg/mL/100g bw. Inactin was used.

3.2.2 Immunohistochemistry

C57/BL6 mice were anesthetized with 100mg/mL Inactin. Animal was infused with PBS to wash the blood cells out of the circulation. Kidneys were fixed in situ by perfusion of 4% paraformaldehyde in PBS. The tissues were harvested and coronal kidney sections were then post-fixed overnight at 4°C in 4% paraformaldehyde and embedded in paraffin. Subsequently, 5-µm sections of the paraffin block were deparaffinized in toluene and rehydrated through graded ethanol. To retrieve antigens and enable immunostaining on paraformaldehyde-fixed paraffin-embedded tissue, the sections were heated in PBS in a microwave for 20 minutes and then allowed to cool in the PBS for 40 minutes. To reduce nonspecific binding, sections were blocked for 30 min with 20% normal goat serum in PBS. Monoclonal antibody against acetylated alpha tubulin (Sigma Aldrich, Saint Louis, Missouri) was used on paraffin-embedded mouse sections. Sections were subjected to microwave antigen retrieval (for 10 min) before staining and blocked for 1 hour with PBS-Tween containing 1% goat serum. Samples were incubated overnight at 4°C with 1:100 dilution of anti-acetylated alpha tubulin, 1:500 Alexa 594-conjugated secondary antibody (Invitrogen, Carlsbad, CA) for 1 hour, and Vectashield mounting medium containing DAPI for nuclear labeling (Vector Laboratories, Burlingame, CA).

3.2.3 In vitro isolated and microperfused glomerulus – JGA

Individual glomeruli with afferent arteriole and attached MD segment were freehand dissected from kidneys of C57/BL6 mice and perfused in vitro using similar

method described previously (117).Briefly, AA was canulated, stained with Fluo-4 (1 μM, 25˚C, 15 min.) for intracellular Ca^{2+} imaging and perfused with Ringer's solution in each experiment. In the first approach, the cTAL was removed so that the MD plaque remained intact and accessible from the bath (figure 13.), as opposed to the double perfusion model, in which the cTAL remained intact and attached to the glomerulus. Whenever the MD plaque was unable to be visualized or was damaged, causing strong vasoconstriction of the AA, those tissues were excluded from our study. Dissection solution was an isosmotic, low NaCl–containing Ringer's solution consisting of (in mM): 25 NaCl, 120 N-methyl-D-glucamine cyclamate (NMDG cyclamate), 5 KCl, 1 $MgSO_4$, 1.6 Na_2HPO_4, 0.4 NaH_2PO_4, 1.5 $CaCl_2$, 5 D-glucose, and 10 HEPES. Dissection was performed at 4°C. An individual glomerulus was transferred to a chamber mounted on an inverted fluorescent microscope (Zeiss Axiovert 200M). The tissue was bathed in Ringer's solution and the temperature was maintained at 37°C. TGF was induced by either of the following stimuli: (*A*) Laminar flow applied directly on the MD apical surface using different [NaCl] concentration solutions (0, 10, 80, 135mM [NaCl]). When removing NaCl from the solution, NaCl was isosmotically substituted with NMDG cyclamate, KCl with potassium gluconate, and $CaCl_2$ with calcium gluconate to achieve a [NaCl] of 0, 10 or 80mM. In separate groups, furosemide (100μM, 10min. incubation) was also added to 0mM NaCl–containing Ringer's solution to inhibit NKCC2; separately tempol (100μm, 10min incubation) to eliminate the flow-induced generation of reactive oxygen species; and finally suramin (50μM, 10min. incubation) to block the purinergic signaling. Fluid flow was 20nL/min. (*B*) Bending MD cilia directly with a glass micropipette under no-flow condition. Primary cilium of the MD cells were bended by moving a micropipette parallel with and close to the luminal membrane of the MD cells without touching the apical surface of the cells. (*C*) Perfusing the intact cTAL by different [NaCl] solutions (10, 80mM [NaCl]). In a separate group furosemide (100μM, 10min. incubation) was also added to 10mM NaCl–containing Ringer's solution. Fluid flow was 20nL/min.

In all approaches, TGF was observed as an elevation in the intracellular Ca^{2+} concentration of vascular smooth muscle cells (VSMC) of the AA, and as a consequence a reduction in the diameter of the AA. Data were collected in every 2 sec by Stallion imaging software (Intelligent Imaging Innovations, Inc.).

3.2.4 Data analysis

Numerical data are the mean ± s.e.m. Statistical significance was determined by using two-tailed Student's t-test. The α value was set at 0.05 for statistical significance.

3.3 PREGLOMERULAR SPHICTER

3.3.1 In vitro isolated and microperfused afferent arteriole-JGA-glomerulus

A superficial afferent arteriole with its glomerulus and attached distal tubule containing the MD was microdissected from kidneys of New Zealand white female rabbits (500 g, Harlan) as described before (54). All animal protocols have been approved by the Institutional Animal Care and Use Committee at the University of Southern California. Briefly, animals were randomly placed on low-salt (TD 90188, 0.01% NaCl), or regular (8630 Harlan Teklad, Madison, WI, USA, 0.3% NaCl) diet for one week. Animals had free access to tap water. Dissection and bath media were prepared from DMEM (DME mixture F-12; Sigma) with the addition of 1.2 g/l $NaHCO_3$. Before use, this solution was aerated with 95% O_2 – 5% CO_2 for 45 min, and pH was adjusted to 7.4. When used as a dissection medium, 3% fetal bovine serum (Hyclone) was added. The arteriole was perfused with a modified Krebs-Ringer-HCO_3 buffer containing (in mM) 115 NaCl, 5 KCl, 25 $NaHCO_3$, 0.96 NaH_2PO_4, 0.24 Na_2HPO_4, 1.2 $MgSO_4$, 1.2 $CaCl_2$, 5.5 D-glucose, and perfusion pressure was maintained at around 50 mmHg throughout the experiment. The tubular perfusate was an isosmotic, low NaCl containing Ringer's solution consisting of (in mM): 10 NaCl, 135 N-methyl-D-glucamine (NMDG) cyclamate, 5 KCl, 1 $MgSO_4$, 1.6 Na_2HPO_4, 0.4 NaH_2PO_4, 1.5 $CaCl_2$, 5 D-glucose, and 10 N -2-hydroxyethyl-piperazine-N' -2-ethanesulfonic acid (HEPES). TGF was initiated by switching to a similar Ringer's solution in which [NaCl] was increased from 10 to 80 mM. Isosmolality of this solution was maintained by reducing NMDG cyclamate to 65 mM. The tubule segment was cannulated and perfused at a baseline rate of 10 nl/min. The bath was identical to the arteriolar perfusate and was continuously aerated with 95% O_2 – 5% CO_2, and exchanged at a rate of 1 ml/min. The preparation was kept in the dissection solution and also, temperature was kept at 4˚C until cannulation of the arteriole and tubule was completed, and then gradually raised to 37˚C for the remainder of the experiment.

3.3.2 In vivo imaging of the kidney

Male Munich-Wistar rats (Irish Farms, Norco, CA) weighing 210–280 g were used for in vivo experiments. Under thiobutabarbital sodium anesthesia (Inactin, 100 mg/kg body wt, ip.), the right femoral vein was cannulated for fluorescent dye administration. From a dorsal incision, the kidney was exteriorized with intact blood flow and innervation. The animal was placed on the stage of an inverted microscope with the exposed kidney placed in a coverslip-bottomed heated chamber bathed in normal saline. The kidney was visualized from below as described by Dunn et al (108) (figure 11.).

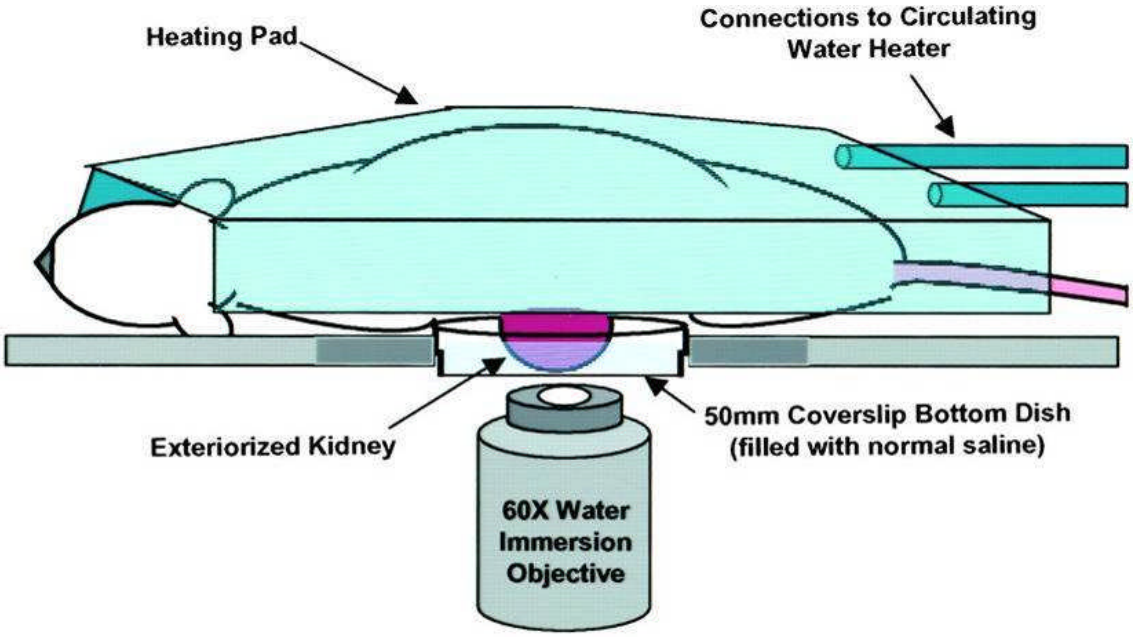

Figure 11. Model of the intravital imaging of live, intact rodent kidney. *After dorsal incision the left kidney was exteriorized and the animal was positioned on the stage of the inverted microscope, in a coverslip-bottomed, Krebs-Ringer solution bathed heated chamber. Also, the animal was wrapped in a heating blanket. Source if image: (108).*

3.3.3 Multiphoton confocal laser scanning fluorescence microscopy

Fluorescence imaging was performed using a Leica TCS SP2 AOBS MP confocal microscope system (Leica Microsystems, Heidelberg, Germany). A Leica DM IRE2 inverted microscope was powered by a wideband, fully automated, infrared (710-920nm) combined photo-diode pump laser and mode-locked titanium:sapphire laser

(Mai-Tai, Spectra-Physics, Mountain View, CA) for multiphoton excitation, and/or by orange (HeNe 594nm/2mW), green (HeNe 543nm/1.2mW) and blue (Ar 458nm/5mW; 476nm/5mW; 488nm/20mW; 514nm/20mW) lasers for conventional, one photon-excitation confocal microscopy. Images were collected in time-series (xyt) with Leica LCS imaging software. Several fluorophores were used to specifically label the structure of the afferent arteriole-glomerulus complex including Hoechst 33342 (3μM perfusate, Molecular Probes, Eugene, OR) to stain cell nuclei blue, Quinacrine (5μM perfusate) to selectively label individual renin granules of the terminal part of the afferent arteriole, and the cell membrane marker R-18 (2 μM, Molecular Probes).

For calcium imaging, the preparations were loaded via the arteriolar perfusate with Fluo-4 AM and Fura Red AM (10 μM each, Invitrogen) dissolved in dimethyl sulfoxide. Loading required ~15 min, after which fluorescent dyes were removed from both lumen. A ~20 min incubation of the preparation with the control perfusion solutions was allowed to permit stabilization of fluorescent signals. After experiments, Fluo-4/ Fura Red ratios were calculated.

For in vivo imaging, water-soluble fluorophores were used to tag renin secretory granules in the afferent arteriole (quinacrine, 100 μl of 25 mM stock per animal) and to label the circulating blood (serum) (rhodamine-conjugated 70,000 Da MW dextran, 100 μl of 10mg/ml stock per animal, Molecular Probes). Further technical details of imaging renin content of juxtaglomerular granular cells and renal tissues in vitro using this approach have been recently reviewed (54).

3.3.4 Materials

The following pharmacological agents were used in these experiments: 100 μM furosemide, a blocker of the Na:2Cl:K cotransporter; 50 μM of the non-selective purinergic receptor blocker suramin; 100 μM 8-cyclopentyl-1,3-dipropylxanthine (DPCPX), a selective adenosine A1 receptor blocker. Chemicals, if not indicated, were purchased from Sigma Chemical Co., St. Louis, MO, USA.

3.3.5 Immunohistochemistry

Sprague-Dawley rats (200g, Harlan, Madison, WI) were anesthetized with 100mg/mL Inactin and their kidneys were fixed in situ by perfusion of 4%

paraformaldehyde in PBS. Coronal kidney sections were then post-fixed overnight at 4°C in 4% paraformaldehyde and embedded in paraffin. Subsequently, 5-µm sections of the paraffin block were deparaffinized in toluene and rehydrated through graded ethanol. To retrieve antigens and enable immunostaining on paraformaldehyde-fixed paraffin-embedded tissue, the sections were heated in PBS in a microwave for 20 minutes and then allowed to cool in the PBS for 40 minutes. To reduce nonspecific binding, sections were blocked for 30 min with 20% normal goat serum in PBS. Sections were then incubated with a mouse monoclonal α-smooth muscle actin antibody (Sigma) at a 1:400 dilution for one hour and washed in PBS. Sections were labeled with an Alexa Fluor 594 conjugated goat anti-mouse antibody (Molecular Probes) for one hour at a dilution of 1:500 and again washed. Sections were counterstained with quinacrine (25mM) at a 1:700 dilution for 10 minutes. Following a wash step, sections were mounted with Vectashield mounting media containing the nuclear stain DAPI (Vector Laboratories) and examined with a Leica TCS SP2 confocal microscope.

3.3.6 Data Analysis

Numerical data are the mean ± s.e.m. Statistical significance was determined by using paired t-test and ANOVA. The α value was set at 0.05 for statistical significance.

3.4 CX30 – DISTAL NEPHRON ATP RELEASE

3.4.1 Animals

The $Cx30^{-/-}$ mouse model was established and described previously (118). Wild type and $Cx30^{-/-}$ mice (C57BL6 background) were bred at the University of Southern California. All animal protocols were approved by the Institutional Animal Care and Use Committee of USC. Genotype was confirmed by PCR of tail biopsies.

3.4.2 Immunohistochemistry

Rabbit polyclonal anti-Cx30 antibodies were purchased from Zymed Laboratories Inc. (San Francisco, CA) and used as described (59). Briefly, after fixation and blocking, wild type and $Cx30^{-/-}$ mouse kidney sections were incubated with Cx30 antibodies at a 1:50 dilution overnight and washed in PBS. Sections were then

incubated with horseradish peroxidase-conjugated goat anti-rabbit IgG and enhanced with Alexa Fluor 594 labeled tyramide signal amplification according to the instructions of the manufacturer (Molecular Probes, Eugene, OR). After a wash step, sections were mounted with Vectashield mounting media containing the nuclear stain DAPI (Vector Laboratories, Burlingame, OR) and examined with a Leica TCS SP2 confocal microscope (Leica Microsystems, Heidelberg, Germany).

3.4.3 Different approaches to detect ATP release

During the past two decades, several cell membrane receptors, which preferentially bind extracellular nucleotides and their analogs, have been identified. These receptors are known as nucleotide receptors or "purinergic" receptors. At the beginning the receptor characterization and the measurement of ATP release was difficult due to the fast ATP metabolism by ectonucleotidases (57), the generally high sensitivity of the receptors to several ATP metabolites. These obstacles made possible the coexistence of different ATP detection approaches:

● luciferin-luciferase assay: ATP is consumed immediately by the luciferase enzyme on a millisecond time scale. This ATP is the energy source for the following biochemical reaction:

luciferin + ATP → luciferyl adenylate + PPi
luciferyl adenylate + O_2 → oxyluciferin + AMP + 1 photon

This bioluminescence detection of ATP is equivalent to the consumption of ATP by luciferase: one photon collected for every molecule of ATP. However, this is a highly sensitive assay (capable of detection even nanomolar quantities of ATP) this approach has its own limitation: it is designed for cell culture application; ATP is consumed by other enzymes like ectonucleotidase which results in a 10-15% underestimation of the total ATP concentration (119).

● atomic force microscopy method: this technique uses atomic microscope tips coated with the myosin subfragment S1, which has a high affinity for ATP and changes shape on ATP hydrolysis. The myosin tips are placed next to a cell, bind the ATP as it is released, and the myosin in the tips responds by changing shape (120).

● biosensor technique: a single, non-excitable cell serves as an ATP detector. This cell sui generis or via transfection should express purinergic receptor(s). After loading the biosensor cell with intracellular Ca^{2+} indicator, the ATP release can be detected as a change in the fluorescence intensity, subsequently the Ca^{2+} influx. The strengths of this approach are the sensitivity in micromolar ATP concentration range, the easy application in cell culture or tissue models. The slight differences between each cell in responsiveness to ATP can be mentioned as potential pitfall of this technique (121).

In our experiment we chose the biosensor technique to measure ATP release due to the easy application in dissected tubular models and the adequate sensitivity. Although, we can confirm the concern of the variability caused by the difference in ATP sensitivity of the biosensor cell, however in our hand this problem seemed less critical.

3.4.4 ATP biosensor technique

Animals were anesthetized and after midline, abdominal incision one kidney was removed, placed into ice cold dissection solution containing DME mixture- F12, 1.2 g/L H_2CO_3, 3% FBS, and sliced into 2-4 mm slices. CCDs were free-hand dissected at 4˚C and partially split-open to provide access to the luminal cell surface, and placed into a temperature controlled chamber containing oxygenated Krebs-Ringer solution. Then, tubules were perfused in the 0 to 20 nl/min range (32) with a solution containing (in mM) 25 NaCl, 5 KCl, 1 $MgSO_4$, 1.6 $NaHPO_4$, 0.4 NaH_2PO_4, 5 D-Glu, 1.5 $CaCl_2$, 110 NMDG-cyclamate, 10 HEPES. In some experiments, bath osmolality was reduced from 300 to 270 mOsm/kg by adding 10% volume distilled water. Intercalated cells were labeled by 0.02 mg/mL Alexa Fluor594-peanut lectin (122), and principal cells by 25 μM quinacrine (123). Following cannulation and perfusion of a microdissected CCD, a small group of Fluo-4 and Fura Red (1 μM and 3 μM respectively , 25˚C, 15 min + 250 μM sulfinpyrazone) -loaded PC12 cells (ATCC) were gently positioned in direct contact with the apical surface of PCs or ICs. After positioning the biosensor cells, a short (10 min) equilibration period was given. These PC12 cells were used as biosensors of freshly released extracellular ATP based on changes in their $[Ca^{2+}]$ic as described before (28). Fluo-4 (excitation at 488 nm, emission at 520 ± 20 nm) and Fura Red

(excitation at 488 nm, emission at >600 nm) fluorescence were detected using a Leica TCS SP2 AOBS MP confocal microscope system (Leica Microsystems, Heidelberg, Germany) and fluorescence was calibrated to $[Ca^{2+}]$ic as described before (32). In some experiments PC12 cells were preincubated with the purinergic receptor blocker suramin (50 μM). Each perfused CCD was dissected from a different animal.

3.4.5 Pressure-natriuresis measurements

10-13 week old $Cx30^{+/+}$ mice (n=8) and $Cx30^{-/-}$ littermates (n=6) were anesthetized using the combination of Ketamine and Inactin (10 mg/100 g bw each). The surgery was carried out on a temperature controlled mouse operating pad (Vestavia Scientific, Birmingham, AL). Trachea was cannulated to facilitate breathing, and cannula were inserted into the carotid artery to perform continuous blood pressure measurements by BP-1 Blood Pressure Monitor (World Precision Instruments Inc, Sarasota, FL), and into the femoral vein for iv. infusion. The abdominal aorta (distal to the renal artery) and then the mesenteric artery were ligated in order to elevate blood pressure in a stepwise manner. A catheter was placed into the bladder to collect urine. The operation was followed by a 15-min equilibration period. Renal functions were then determined over three consecutive 20-min periods: (i) control, (ii) first elevation period in which the abdominal aorta was compressed, (iii) followed by the second elevation period in which the mesenteric artery was additionally ligated. In each period, urine and blood samples were collected to perform volume, Na^+ and K^+ measurements. Immediately after blood collection (70μL/sample), mice received an equivalent amount of donor mouse whole blood, collected a few hours prior to the experiment. A schematic drawing of the experimental setup is given in figure 12.

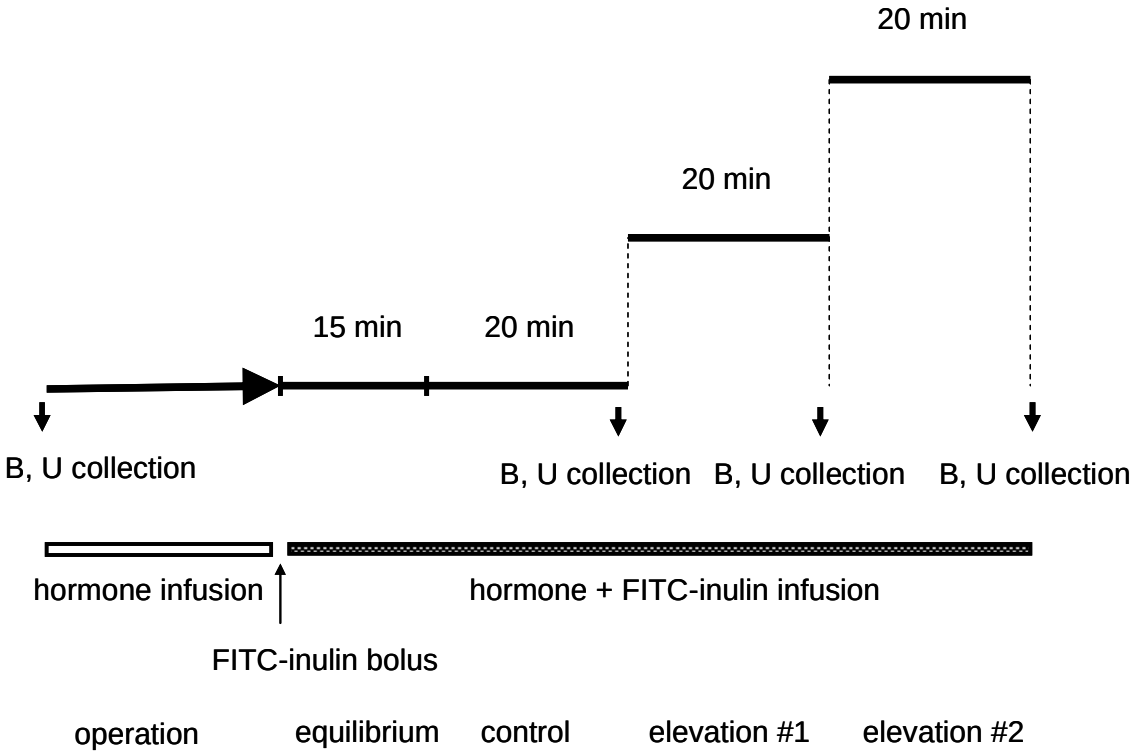

Figure 12. Experimental setup of the pressure-natriuresis in vivo study. *The operation and the subsequent 15-min. equilibrium were followed by 3 consecutive 20-min period. In the elevation #1 the abdominal aorta, in the elevation #2 the mesenteric arteries were ligated. B: blood, U: urine.*

3.4.6 Volumen supply

Animals had free access to drinking water till the day of experiment. After femoral vein cannulation, the animal was given a 0.35 μL/g bw/min continuous infusion containing 30mg/mL BSA, and a ”hormone cocktail” (1 μg/mL norepinephrine, 0.5 ng/mL arginine vasopressin, 0.2 mg/mL hydrocortisone and 0.2 μg/mL aldosterone), as described before (98). Throughout the experiment haematocrit was measured (Damon/IEC MB Centrifuge) to control the speed of the infusion (figure 12.).

3.4.7 GFR calculation

After surgery, mice were given a 1.75 μL/g bolus containing 5 mg/mL FITC-inulin, and a continuous 0.35 μL/g bw/min hormone infusion containing 5 mg/mL

FITC-inulin. FITC-inulin concentrations in blood and urine were determined by a cuvette-based PTI system (Photon Technology International), excitation at 480nm and emission at 530nm. GFR was calculated using the U*V/P equation (figure 12.).

3.4.8 Na^+, K^+, Cl^- and HCO_3^- measurements

Blood samples were centrifuged at 8 rpm for 8 min (Eppendorf Centrifuge 5415R). Serum was separated. The Na^+ and K^+ content of the serum were determined using a flame photometer (FLM 3 Radiometer Copenhagen) (figure 12.). Plasma Cl^- and HCO_3^- levels were measured in the USC Hospital clinical laboratory.

3.4.9 Plasma aldosterone and arginine-vasopressin measurement

After the equilibration period blood, before the animals received the hormone infusion, blood was collected for aldosterone, arginine-vasopressin and ion measurements. The plasma aldosterone level was determined using Aldosterone ELISA kit (Alpha Diagnostic, San Antonio, TX, USA), the plasma arginine-vasopressin level was measured by AVP EIA Kit (Cayman Chemical, Ann Arbor, MI, USA).

3.4.10 High salt diet

Wild type (n=19) and $Cx30^{-/-}$ (n=19) mice were kept on normal (0.3%) or high-salt (8% NaCl + 0.45% NaCl in drinking water) diet for two weeks. Some animals received benzamil (1.4mg/kg/day ip.), a selective inhibitor of the ENaC during the second week. Mice were anesthetized and blood pressure was measured through the cannulated carotid artery, as described above in Pressure-natriuresis measurements.

3.4.11 Western blot analysis of renal epithelial transporters expression

Manually dissected slices of kidney cortex was homogenized in a buffer containing 20 mM Tris-HCl, 1 mM EGTA, pH 7.0, and a protease inhibitor cocktail (BD Bioscience, San Jose, CA). 40 µg of protein was separated on a 4-20% SDS-PAGE and transferred onto PVDF membrane. The blots were blocked for a minimum of 1 hour with Odyssey Blocking Buffer (LI-COR Biosciences, Lincoln NE) at room temperature. This was followed by an incubation of the primary antibody (1:3000 αENaC, gift from Dr. Alicia McDonough, Los Angeles, CA) for 3 hrs at room temp, 1:250 NKCC2 (gift

from Carolyn Ecelbarger, Washington, DC) 4º C overnight, NHE3 1:750, (gift from Dr. Alicia McDonough, Los Angeles, CA) and NCC 1:500 overnight, (gift from Dr. David Ellison, Portland, OR) along with beta-Actin (1:5000, ABCam, Cambridge, MA) in 2.5mL 1x PBS (OmniPUR from VWR, San Dimas, CA), 2.5mL Odyssey Blocking Buffer (LI-COR Biosciences) and 5.0µL Tween 20 (Sigma Aldrich, St. Louis, MI) solution. After washing with PBS-T (1x PBS plus 1:1000 Tween 20), blots were incubated in 2.5 mL PBS, 2.5 mL Blocking Buffer, 5.0 µL Tween 20 and 5.0 µL 10% SDS, with either a goat anti-mouse or goat anti-rabbit secondary antibody (1:15000 LI-COR Biosciences), and visualized with Odyssey Infrared Imaging System, Western Blot Analysis (LI-COR Biosciences).

3.4.12 RT-PCR of purinergic receptors

Total RNA was purified from whole kidneys of $Cx30^{+/+}$ and $Cx30^{-/-}$ mice using a Total RNA Mini Kit (Biorad). RNA was quantified using spectrophotometry and reverse-transcribed to single-stranded cDNA using avian reverse-transcritpase and random hexamers according to the instructions of the manufacturer (Thermoscript RT-PCR system, Invitrogen). 2 µL of cDNA was amplified using a master mix containing Taq polymerase (Invitrogen) and the primers each at a final concentration of 100 µM. The primer sequences and expected band sizes for various Cx and ATP receptors were described before (59, 124, 125). The PCR reaction was carried out for 30 cycles of the following: 94°C for 30 seconds, 55.4°C for 30 seconds, and 72°C for 30 seconds. The PCR product was analyzed on a 2% agarose gel.

3.4.13 Data analysis

Numerical data are the mean ± s.e.m. Statistical significance was determined by using paired ANOVA and Bonferroni test for the pot hoc comparison. The α value was set at 0.05 for statistical significance.

4. RESULTS

4.1 TUBULOGLOMERULAT FEEDBACK

4.1.1 The flow induced feedback mechanism

In order to examine if MD cells are able to respond to changes in tubular fluid flow a single glomerulus with attached AA was dissected. The MD region was explored by removal of the adjacent cTAL parts. This way the MD cells become freely accessible from the bath. The MD cells were approached by a glass perfusion pipette (as shown in figure 13.) and solutions with different [NaCl] were applied with a constant 20nL/min flow rate. The feedback response was detected based on the elevation in the $[Ca^{2+}]$ic and the vasoconstriction of the AA. The $[Ca^{2+}]$ic of the VSMC was continuously monitored over the citoplasmic region of the cells. The flow induced significant $[Ca^{2+}]$ic elevation in the VSMCs (Fluo-4 F/Fo: 2.29±0.13, 2.21±0.10, 2.08±0.21, 2.15±0.13; [NaCl] in mM: 135, 80, 10, 0 respectively, in all cases $p<0.05$ – as opposed to the control where no flow stimulus happened 1.02±0.01) followed by a subsequent vasoconstriction of the AA. Interestingly, in some experiments it was possible to identify two separate responsive regions of the AA: a juxtaglomerular or proximal and a distal region. These two regions were connected by a vascular segment identified as the renin positive part of the AA based on the highly granulated morphology of the smooth muscle cells. After repeated flow stimuli the elevation in the $[Ca^{2+}]$ic of the VSMCs and the vasoconstriction did not show any sign of desensitization (figure 13.C).

TGF related $[Ca^{2+}]$ic elevations were also detected in the podocytes (Fluo-4 F/Fo: 1.28±0.02, $p<0.05$). The $[Ca^{2+}]$ic elevations in the podocytes were identical to that which has been observed in the AA VSMCs, in terms of the absence of desensitation. In addition to the involvement of the preglomerular artery and the podocytes in the flow-induced TGF, the whole mesangium responded to flow (figure 13.A-B). Simultaneously with the $[Ca^{2+}]$ic elevations the diameter of the whole glomerular tuft also reduced (figure 13.A-B).

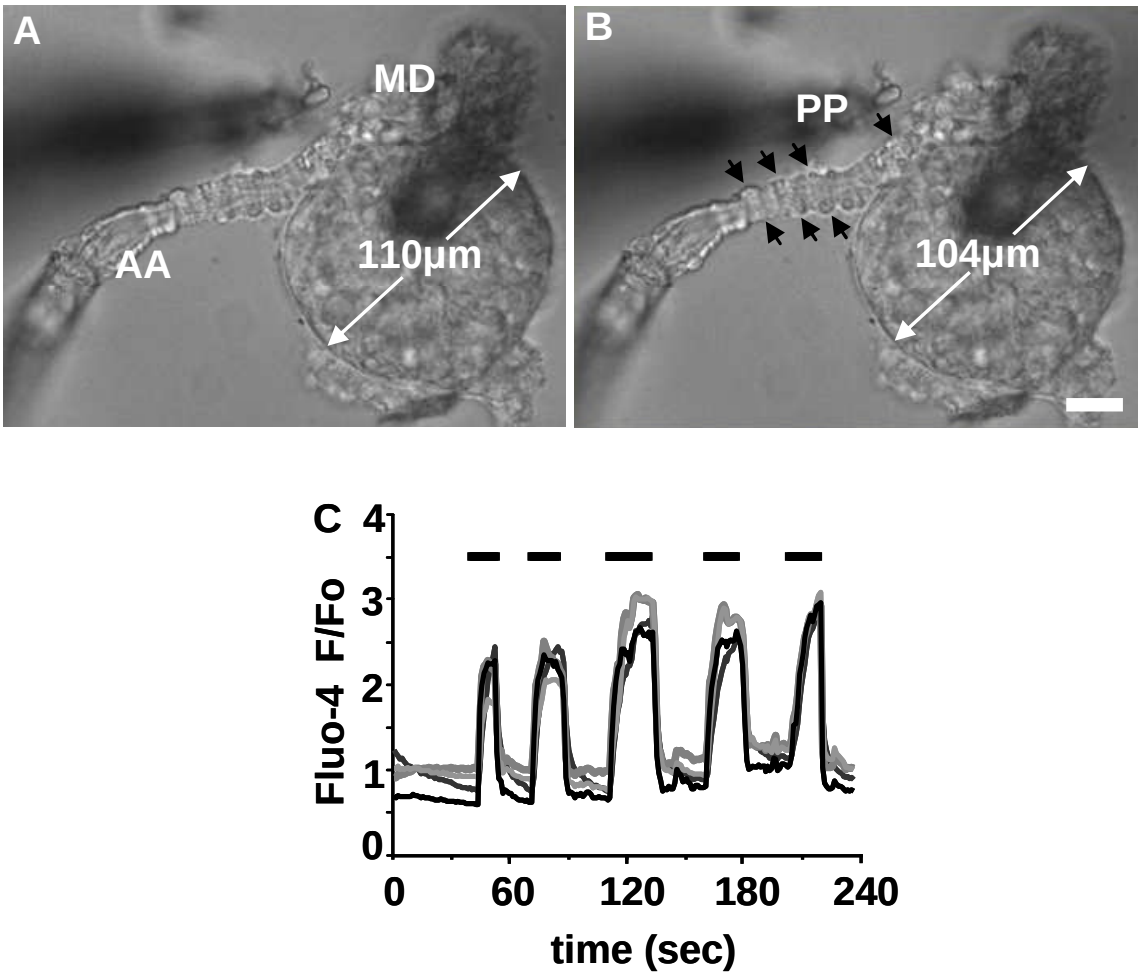

Figure 13. Direct stimulation of the macula densa (MD) by increased flow. *DIC image of an afferent arteriole (AA)-attached glomerulus preparation in which the tubule segments surrounding the MD were completely removed. The apical surface of MD cells was directly accessible from the bath with a perfusion pipette (PP). Compared to control (A), the application of laminar flow from the PP (0mM NaCl solution) directly to the MD apical surface (20 nl/min) produced vasoconstriction of the AA and elevations in VSMC [Ca^{2+}]ic (B). Arrows indicate the sites of vasoconstriction. Note that not only the AA but also the whole glomerulus contracts. AA: afferent arteriole, MD: macula densa. Scale is 20µm. Representative [Ca^{2+}]ic recordings of the VSMCs in the AA during flow-induced TGF. The flow stimulus (20 nl/min) was achieved by using 0mM NaCl solution. When the same maneuver was repeated 5 times within 4 min, the response showed no signs of desensitization.*

Applying fluid flow directly to the MD cells surface induced -the so far described- TGF regardless of the [NaCl] of the applied solution (figure 14.). As the [NaCl] of the perfusion solution was reduced the [Ca^{2+}]ic responses become slightly smaller, however statistically significant difference between the stimuli was not found ($p=0.52$ when response achieved by 135mM and 0mM [NaCl] solution was compared).

To further investigate the involvement of the NKCC2 cotransporter in the mechanism of the flow-induced TGF, furosemide (100μm) was applied. The inhibition of the NKCC2 cotransporter (0mM [NaCl] + furosemide) resulted in the same [Ca^{2+}]ic elevation of the VSMCs (Fluo-4 F/Fo: 1.99±0.04, $p>0.05$) as was achieved by the 0mM [NaCl] solution alone.

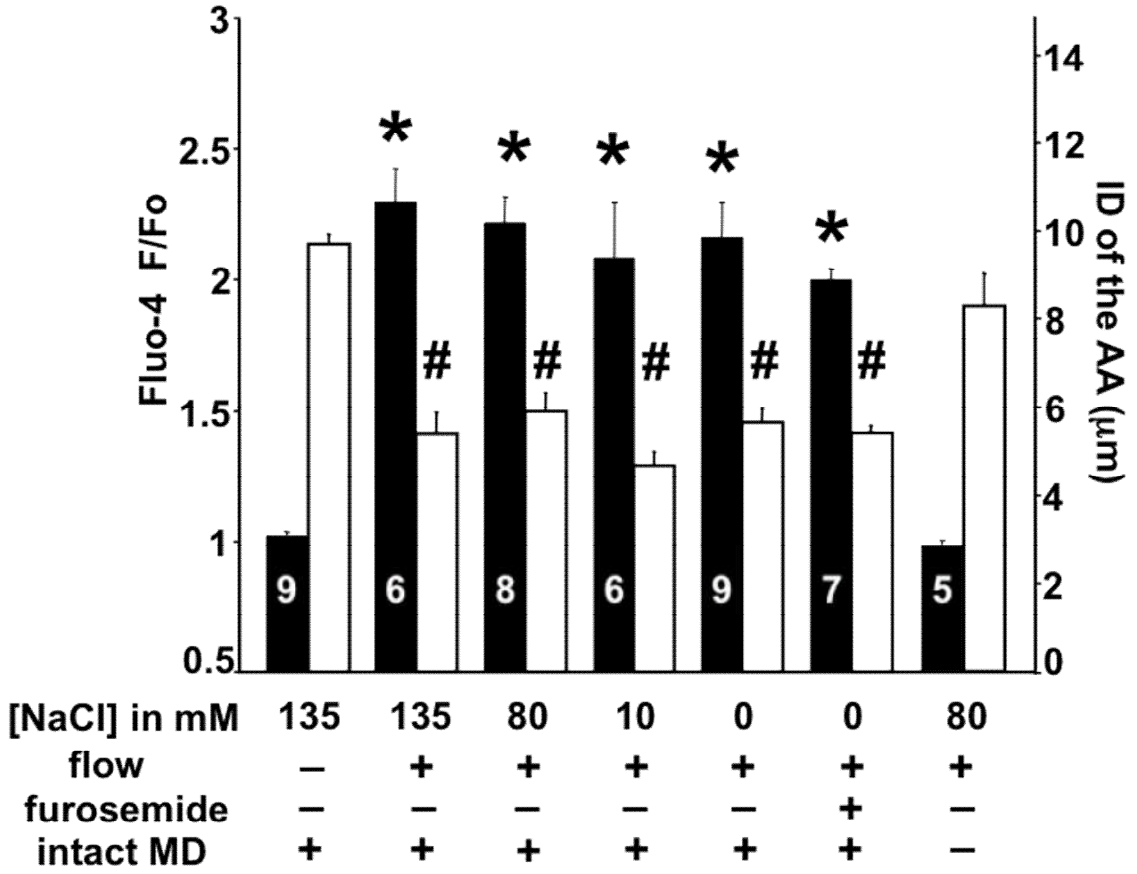

Figure 14. Summary of AA smooth muscle cell [Ca^{2+}]ic and the AA internal diameter changes during MD fluid flow-induced TGF using the open MD plaque preparation. *Flow rate at the MD was increased from zero to 20 nl/min. The tissue was bathed in 135 mM NaCl-containing Ringer's solution in all preparations. N numbers are shown*

*in each column. *: P<0.05 compared to no-flow baseline). A: Significant [Ca^{2+}]ic responses were observed regardless of the applied fluid [NaCl]. Parallel to the elevation in [Ca^{2+}]ic reduction (#:p<0.05 compared to no-flow baseline) in the AA internal diameter (ID) was detected. Even the application of 0mM [NaCl] perfusion solution containing 100μM furosemide (NKCC2 cotransport inhibitor) induced TGF. Flow stimulus after removal of the MD cells failed to induce TGF.*

4.1.2 Comparing the salt and the flow effect

Using the open MD approach (when parts of the cTAL were removed except for the MD) we showed that flow per se is capable to induce TGF. However, only slight, statistically non significant additional elevation in [Ca^{2+}]ic of VSMC was observed when [NaCl] was elevated in the perfusion solution (figure 14.). To clarify whether

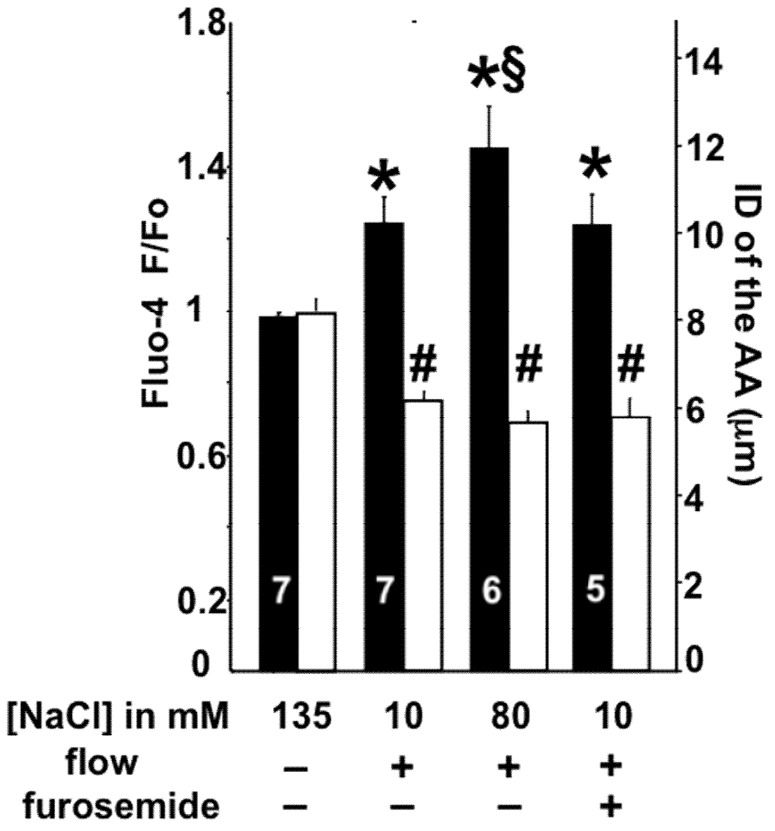

Figure 15. Summary of AA smooth muscle cell [Ca^{2+}]ic and the AA internal diameter changes during MD fluid flow-induced TGF using the intact cTAL-double perfusion model. *Using 10mM [NaCl] solution, the application of fluid flow evoked significant*

$[Ca^{2+}]$ic elevations and vasoconstriction in the AA VSMCs. When 80mM [NaCl] solution was used, significantly higher $[Ca^{2+}]$ic elevations were observed (§: P<0.05). Preincubation with 100μM tubular furosemide did not alter the magnitude of flow-induced TGF using 10mM [NaCl] solution.

elevated [NaCl] perfusion solution and tubular flow together has an additional effect we repeated the perfusion experiments using double perfusion model. Single glomerulus with attached AA and intact cTAL was dissected and both were perfused. When the cTAL was perfused with 80mM [NaCl] solution at flow rate of 20nL/min significant $[Ca^{2+}]$ic elevation in VSMCs (Fluo-4 F/Fo 1.45±0.11, $p<0.05$) and vasoconstriction was observed (figure 15.). If [NaCl] was reduced to 10mM and the same maneuver was repeated similar elevation in $[Ca^{2+}]$ic (Fluo-4 F/Fo 0.98±0.01 vs. 1.24±0.07, $p<0.05$) and reduction in the vessel diameter were observed. However, this response was significantly reduced ($p<0.05$) compared to that recorded using 80mM [NaCl] solution. Besides, when 10mM [NaCl] solution was supplemented with furosemide (100μm) the $[Ca^{2+}]$ic elevation in VSMCs was the same (Fluo-4 F/Fo: 1.23±0.08) compared to that achieved only with the application of the 10mM [NaCl] solution.

4.1.3 The identification of the flow sensor

As described earlier in mouse, rat and human tissue we wanted to confirm that the MD cells have cilia. Labeling mouse sections with α-tubulin, a ubiquitous component of the epithelial cilium, we also identified 5-8μm long cilia on the apical surface of the MD cells. Each MD cell possesses one, primary cilium (figure 16.).

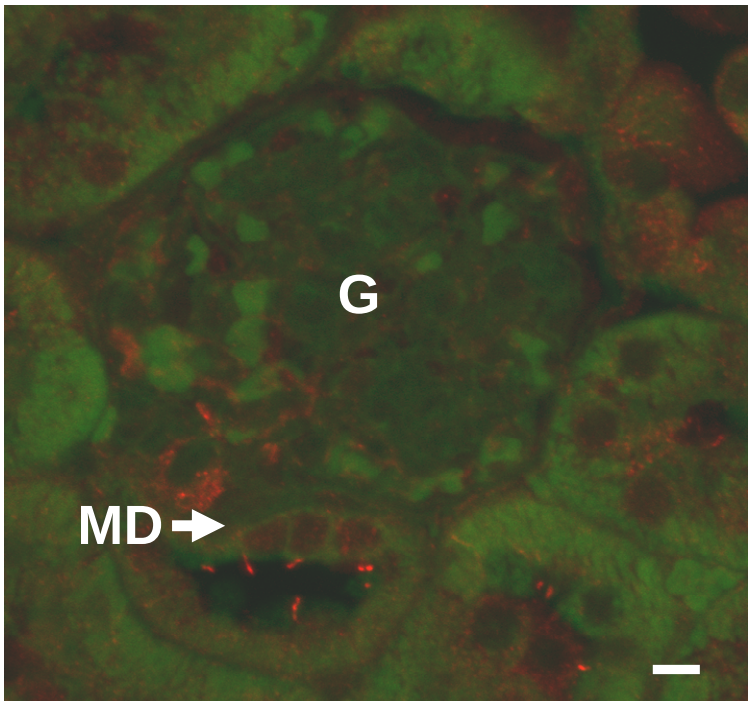

Figure 16. Immunofluorescence labeling of α-tubulin in the mouse kidney. *Each MD cell has one, 5-8μm long primary cilium (red) at the apical membrane. Autofluorescence (green) was used as a background to visualize tissue structure. G: glomerulus, MD: macula densa cells. Scale is 10 μm.*

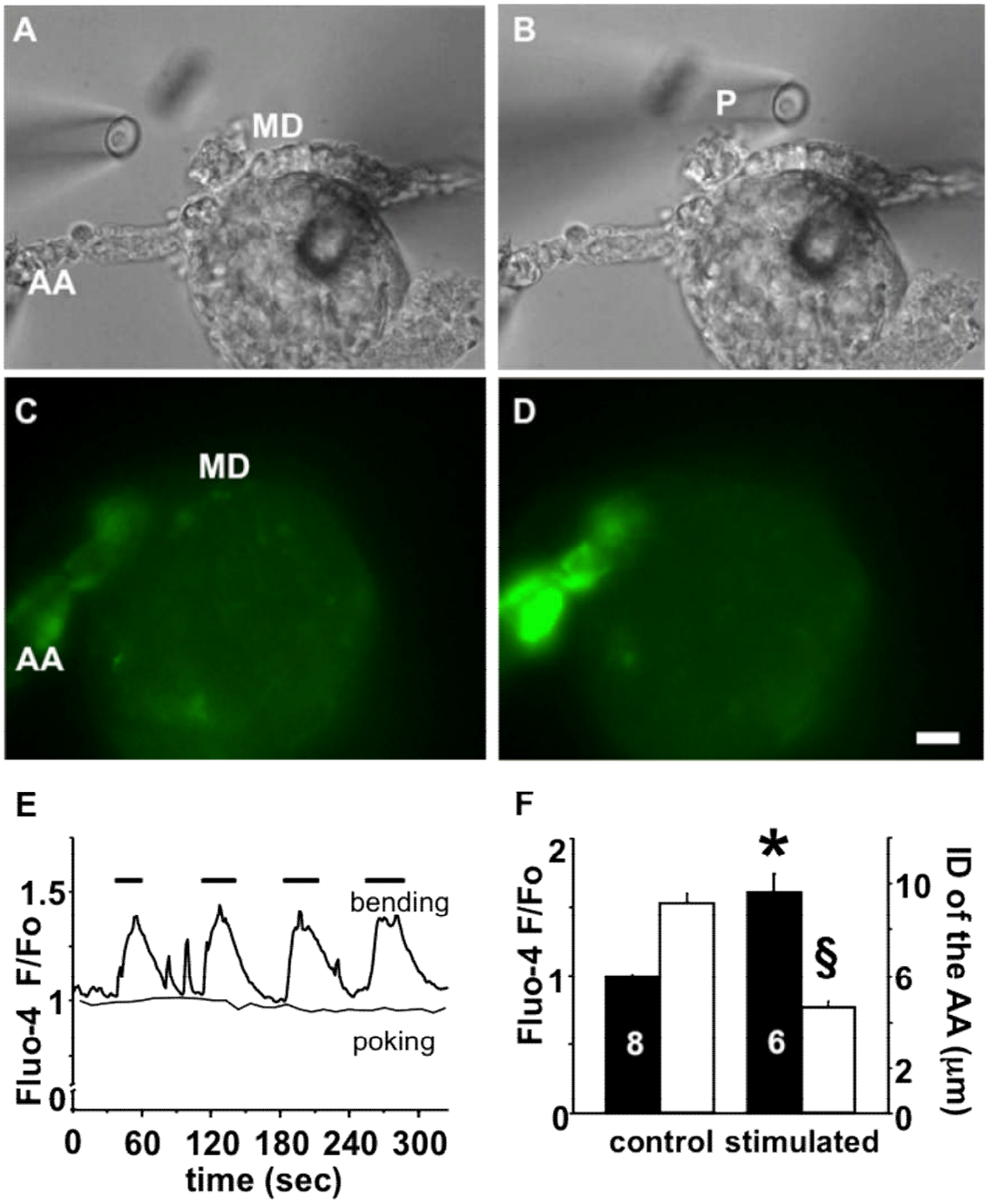

Figure 17. Stimulation of the macula densa (MD) by directly bending their apical cilia with a glass micropipette under no flow conditions. *Representative DIC (A-B) and fluorescent [Ca^{2+}]ic images (Fluo-4 labeling: green, C-D) before (A, C) and after (B, D) TGF was induced by moving the micropipette parallel with and close to the MD luminal membrane without touching the apical surface of the cells. E: Changes in Fluo-4 intensity in VSMCs of the afferent arteriole (AA) after repeated mechanical stimuli in*

the same preparation by cilia bending (as shown in A-B). In contrast, direct poking of MD cells with the pipette produced no changes in VSMC [Ca^{2+}]ic. F: Summary of the cilia bending data: [Ca^{2+}]ic elevations measured at the AA VSMCs (:p<0.001 compared to the control), and internal diameter changes measured in the AA (§: P<0.05 compared to the control). N numbers are shown in each column. P: micropipette. Scale is 20μm.*

4.1.4 Bending the cilium of the MD cell

In order to examine if the primary cilium is responsible for the flow-induced TGF the bending of the primary cilium of the MD cells was studied. Tissue was dissected in the same way as presented in the figure 13. MD cells were stimulated by the movement of a thin (5μm diameter) pipette. The pipette was moved parallel to the apical surface of the MD cells without touching the apical membrane of the cells (figure 17.A-B). This stimulus resulted in significant [Ca^{2+}]ic elevation in the AA VSMCs (Fluo-4 F/Fo: 1.00±0.02 vs. 1.60±0.12, p<0.001) and subsequent vasoconstriction of the AA (figure 17.C-D). This [Ca^{2+}]ic elevation in the VSMC was specific to this maneuver since direct mechanical stimulus (poking of the MD cells) did not produce any response. Repeating the stimulus did not result in desensitization (figure 17.E).

4.1.5 Signaling molecules in the TGF

Other studies have revealed that the superoxide anion also takes part in the TGF process (139, 140, 141). To further investigate this notion in the flow-induced TGF, superoxide anions were scavenged and the flow (20nL/min) application was repeated in the open MD approach. In our hands, tempol (100μm) failed to alter the [Ca^{2+}]ic elevation of the VSMCs achieved after the applications of 10mM (Fluo-4 F/Fo: 2.10±0.06 vs. 2.01±0.04, with vs. without tempol) or 80mM [NaCl] perfusion solution (Fluo-4 F/Fo: 2.24±0.04 vs. 2.25±0.08, with vs. without tempol) (figure 18.A). Besides the superoxide anion, the role of ATP in the flow-induced TGF was also studied. In the presence of the non-selective P2 purinergic blocker, suramin (100μM) the flow-induced responses were significantly blunted (80mM [NaCl] Fluo-4 F/Fo: 1.15±0.02 vs.

2.64±0.46 with or without suramin; 0mM [NaCl] Fluo-4 F/Fo: 1.26±0.06 vs. 2.21±0.06 with or without suramin) (figure 18.B).

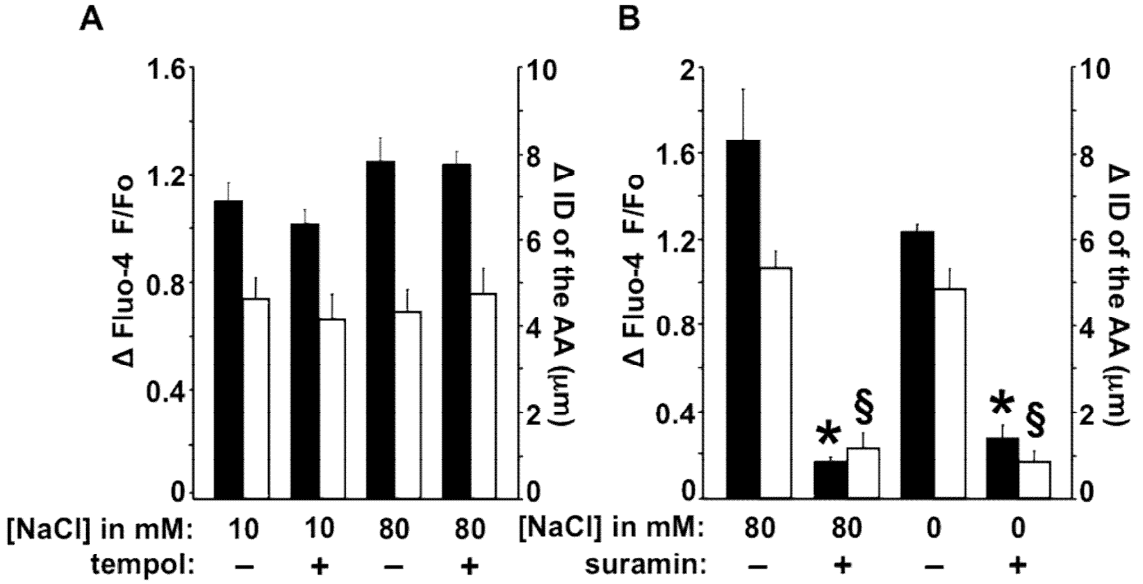

Figure 18. Signaling mechanisms of the flow-induced TGF. *Summary of the changes (Δ[Ca^{2+}]ic and ΔID) in AA VSMC [Ca^{2+}]ic and in the internal diameter (ID) of the AA during flow-induced TGF (increasing fluid flow rate from zero to 20 nl/min) using the open MD plaque preparation.* ***A:*** *The addition of tempol (100μM) to the bathing solution did not alter [Ca^{2+}]ic elevations and the AA vasoconstriction using either the 10 or 80mM [NaCl] solution, confirming that these results were independent of the flow-induced generation of reactive oxygen species.* ***B:*** *Evidence for the involvement of purinergic signaling in flow/salt induced TGF. The bath application of suramin (50 μM) significantly decreased the flow-induced [Ca^{2+}]ic elevations and vasoconstriction in AA VSMCs using either 10 or 80 mM [NaCl] perfusate. N numbers are shown in each column. *: P<0.001 and §: P<0.001 compared to non-suramin treated experiments.*

4.2 PREGLOMERULAR SHINCTER

4.2.1 Imaging the glomerular sphincter in vitro

The vascular morphology of the microperfused AA-attached glomerulus preparation was examined before and after the activation of the TGF mechanism by increasing tubular salt content at the MD from 10 to 80 mM. The summery is shown in figure 19 and a representative preparation in figure 20.

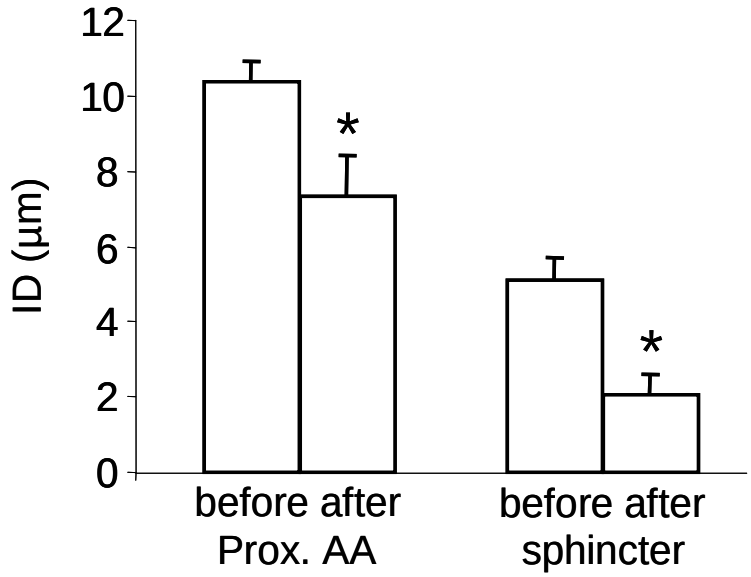

Figure 19. Internal diameter (ID) of the proximal and intraglomerular sphincter portions of the afferent arteriole (AA) before and after TGF activation. **: P<0.05 compared to ID before TGF.*

The internal diameter (ID) of the non-stimulated AA was uniform along the entire extraglomerular segment (10.4±0.5 µm, n=9), however, the ID of the terminal intraglomerular part was much smaller (5.1 ± 0.6 µm, n=9).

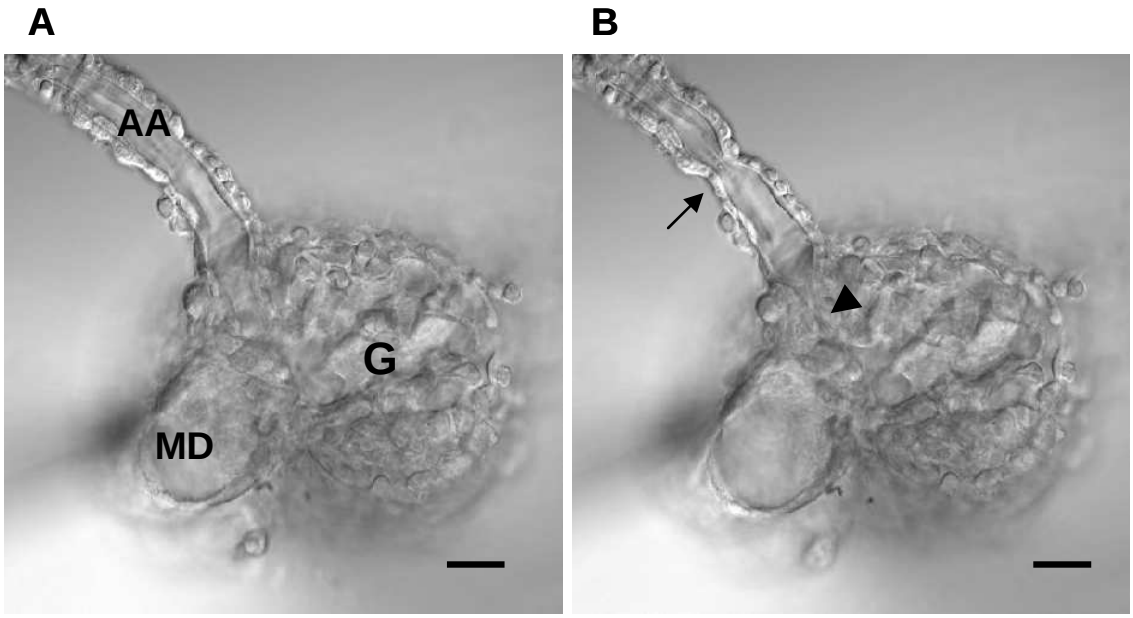

Figure 20. Differential interference contrast image of a representative in vitro microperfused preparation before (A) and after (B) TGF activation. *Compared to the modest vasoconstriction in the proximal segment of the afferent arteriole (AA, arrow) the intraglomerular AA, a "glomerular sphincter" (arrowhead) produced an almost complete closure of the AA. G: glomerulus, MD: macula densa. Scale is 20 µm.*

TGF activation resulted in a significant vasoconstriction in the proximal, extraglomerular AA. Vessel ID decreased by 34.2 ± 8.0 % at the most prominent constrictor site, approx. 60 µm from the glomerulus. However, TGF stimulation caused a proportionally larger increase in vascular resistance in the intraglomerular AA segment, approx. 25 µm in length; ID decreased by 69.3 ± 5.9 %.

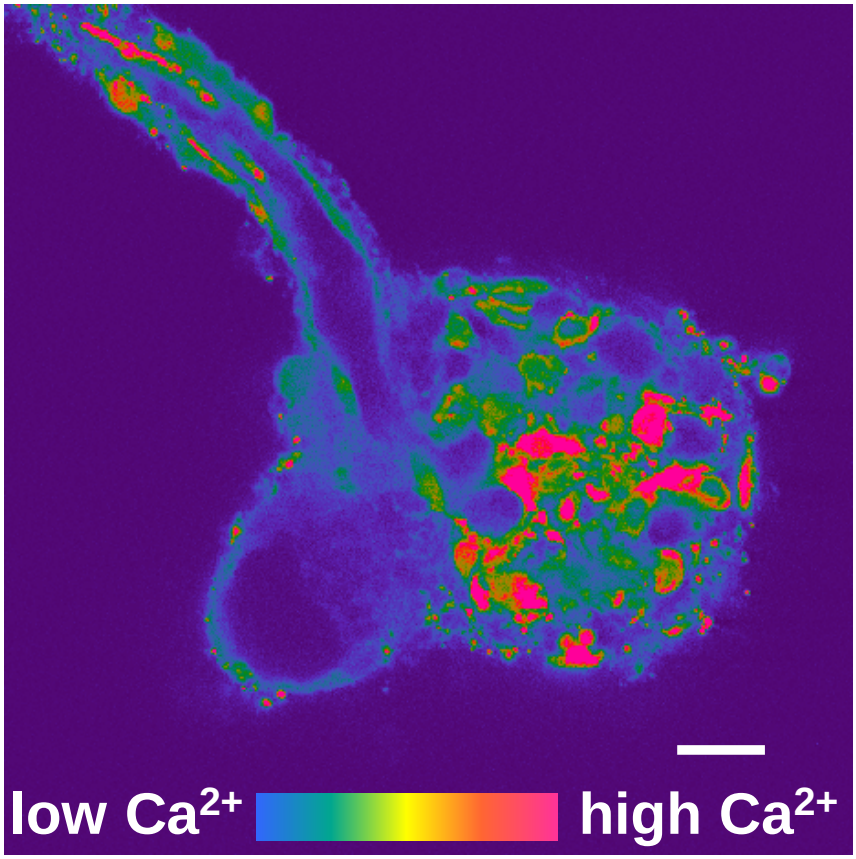

Figure 21. Calcium staining of the same preparation shown in figure 20. *Elevated cytosolic calcium levels are observed in both intraglomerular and extraglomerular mesangial cells after TGF activation. Scale is 20 µm.*

Morphological analysis on the cellular level revealed that renin granular cells in the wall of the intraglomerular sphincter did not produce any significant contraction during TGF. The area of individual granular cells on confocal sections changed from 90 ± 11 µm to 97 ± 5 µm (non-significant, n=10 cells from 9 different preparations) in response to TGF activation. However, calcium imaging (figure 21.) indicated a significant, 31.5 ± 8.8 % elevation in cytosolic [Ca^{2+}] in adjacent extraglomerular mesangial cells during TGF (n=7 from 7 different preparations).

In some preparation the efferent arteriole (EA) was cannulated and the glomerulus microperfused retrograde to examine the morphology of the intraglomerular EA during TGF. The ID of the intraglomerular EA was uniform and there was no sign

of a sphincter similar to the AA (figure 22.). The ID of the intraglomerular EA changed from 14.1 ± 1.0 µm to 13.9 ± 1.1 µm in response to TGF (non-significant, n=8).

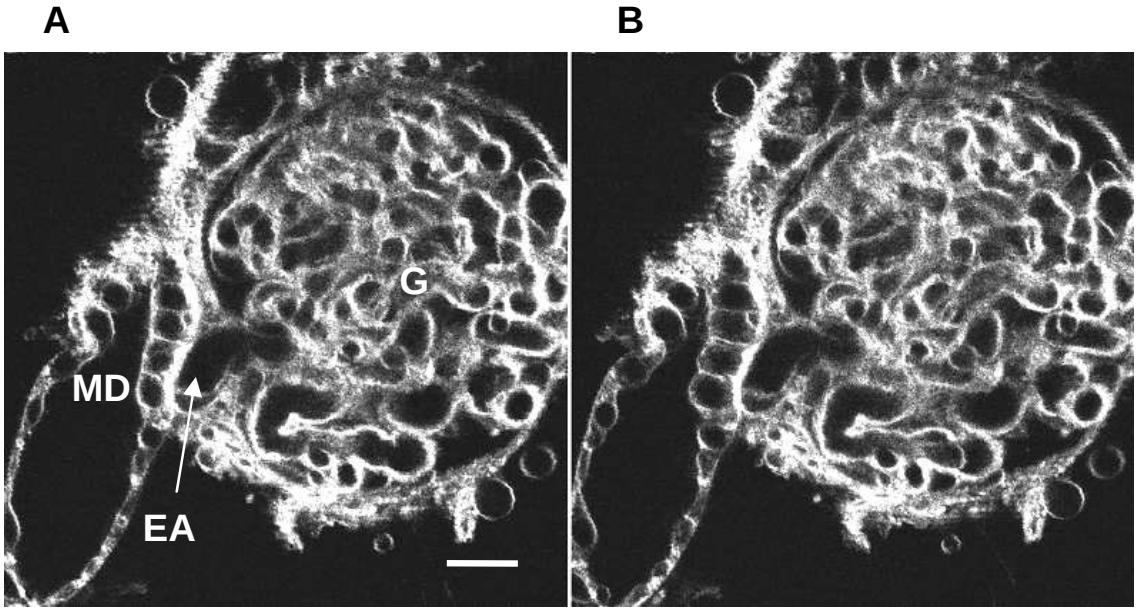

Figure 22. Fluorescence image of a representative in vitro microperfused efferent arteriole (EA)-glomerulus preparation before (A) and after (B) TGF activation. *The cell membrane marker R-18 was used to visualize morphology. Compared to the afferent arteriole, there was no sign of a sphincter-like structure in the intraglomerular EA. G: glomerulus, MD: macula densa. Scale is 20 µm.*

4.2.2 Imaging the glomerular sphincter in vivo

Two-photon imaging of the intact whole kidney was performed using Munich-Wistar rats to examine the morphology of the AA in vivo. Figure 23. exemplifies these studies conducted in five animals. As with the in vitro observations, there were segmental differences in the vascular diameter of proximal versus intraglomerular AA. The presence of a preglomerular sphincter was evident in all AAs observed. There was no correlation between the length of the sphincter and the renin-positive part of the AA.

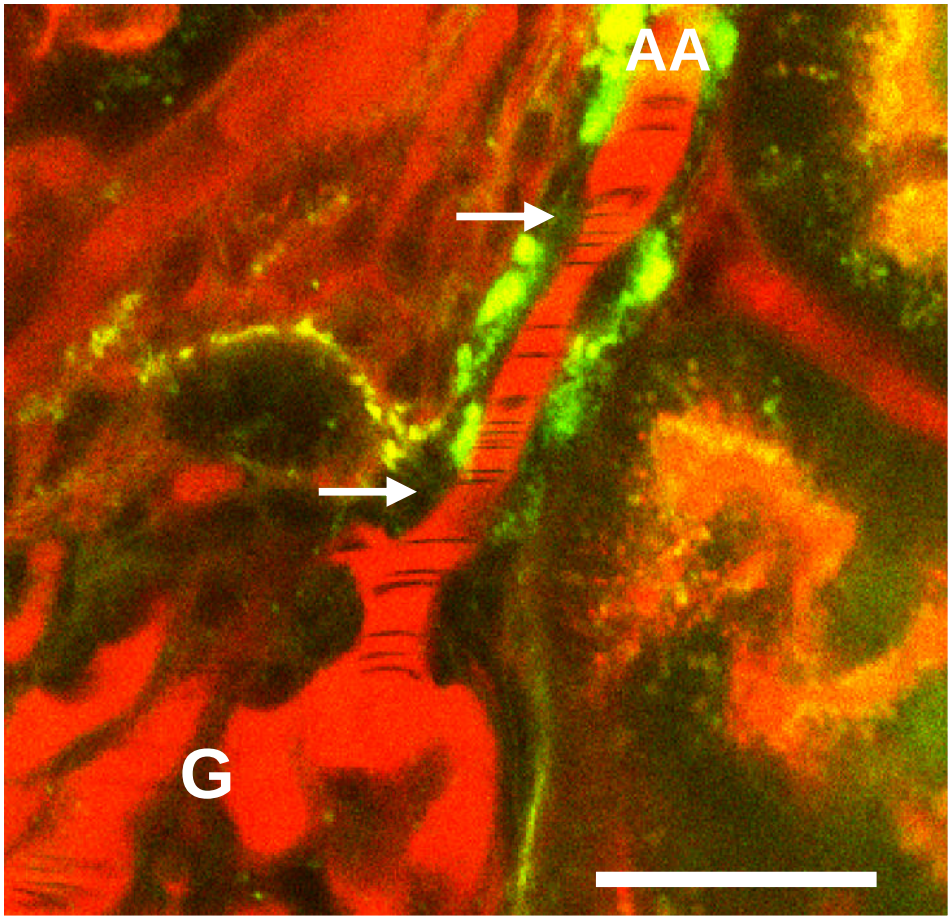

Figure 23. Presence of a precapillary glomerular sphincter in vivo in the intact kidney. *The circulating blood was labeled with a rhodamine-conjugated 70 kDa dextran (red) and the individual renin granules in the wall of the afferent arteriole (AA) with quinacrine (green). The dark, unstained objects in the red-colored plasma are circulating red blood cells. Note the significant narrowing of the terminal AA lumen (only between the arrows), but the entire length of the AA is renin-positive. G: glomerulus, scale is 25 µm.*

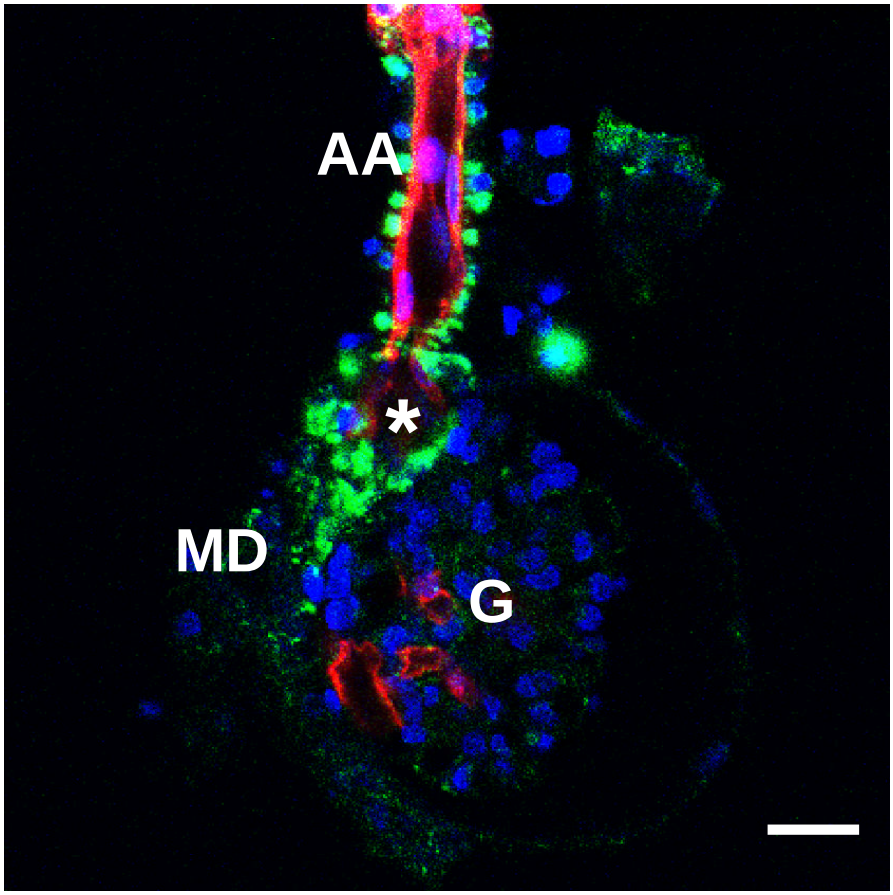

Figure 24. Multi-color labeling of the in vitro microperfused afferent arteriole (AA)-attached glomerulus (G) preparation containing the macula densa (MD). *Vascular endothelium of the AA and the glomerulus are labeled with R18 (red), renin granules with quinacrine (green), and cell nuclei with Hoechst 33342 (blue). The preparation is from a low salt diet treated rabbit. The entire length of the AA is renin-positive, however, the sphincter (*) is still confined to the intraglomerular segment. Scale is 25 µm.*

4.2.3 Effect of increased renin content

Animals were placed on low salt diet for one week to activate the renin-angiotensin system. Labeling individual renin granules in the in vitro microperfused AA-attached glomerulus preparations using quinacrine (figure 24.) confirmed that renin content was significantly up-regulated in these animals. The entire length of the AA

became renin-positive. However, regardless of the renin content, the glomerular sphincter was always confined to the terminal, intraglomerular part of the AA.

4.2.4 Immunohistochemistry

Immunohistochemical labeling of α-smooth muscle actin on rat kidney sections (figure 25.) identified the proximal, extraglomerular portion of the AA. The labeling was strong, throughout the cytoplasm in all vascular smooth muscle cells. In contrast, cells of the efferent arteriole were only weakly stained. No smooth muscle cells were found at the site of the glomerular sphincter, based on actin labeling. In renin granular cells, identified with quinacrine counterstaining, the actin labeling was at the limit of detection.

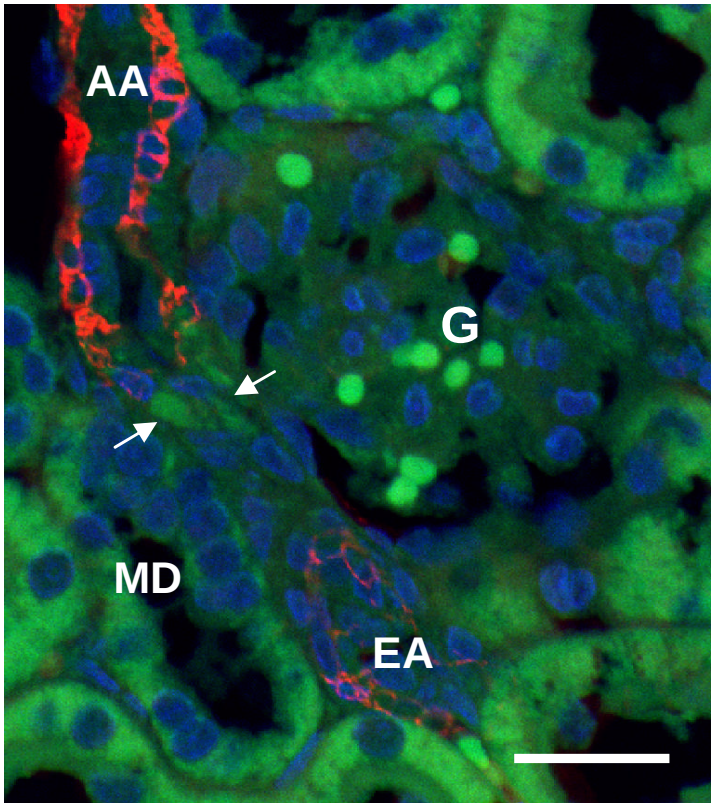

Figure 25. Immunohistochemical labeling of α-smooth muscle actin (red) in the rat kidney. *Tissue section was counterstained with quinacrine (green) to label renin granular cells (arrows) in the glomerular sphincter and with DAPI to label cell nuclei (blue). The sphincter portion lacks smooth muscle cells. AA: afferent arteriole, EA: efferent arteriole, G: glomerulus, MD: macula densa. Scale is 25 µm.*

4.2.5 Mechanism of the sphincter activation

Pharmacological experiments were performed using the in vitro microperfused experimental model to study the mechanism of the glomerular sphincter (figure 26.). The addition of 100 µM furosemide, a blocker of the Na:2Cl:K cotransporter, to the tubular perfusate completely abolished the TGF-mediated closure of the sphincter (control ID reduced by 2.4 ± 3.7 %, $P<0.05$ compared to control). Interestingly, the non-selective P2 purinergic receptor blocker suramin, added to the AA perfusate and bath not only prevented the TGF-induced vasoconstriction, but it caused a slight relaxation of the sphincter (control ID increased by 4.5 ± 4.9 %, $P<0.05$ compared to control). Addition of the adenosine A1 receptor inhibitor DCPCX to the arteriolar perfusate and bath had no effect on sphincter activity (control ID reduced by 46.8 ± 1.9 %, non-significant from control).

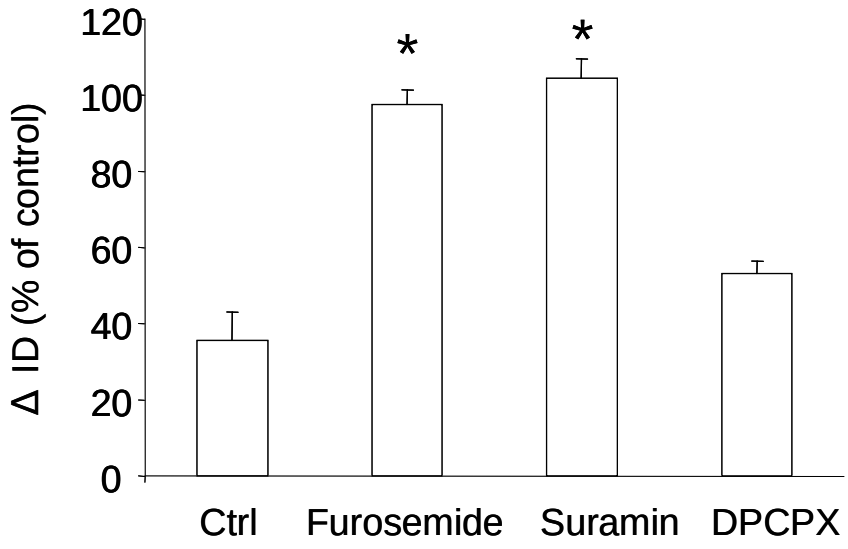

Figure 26. TGF-induced reductions in internal diameter (ID) of the intraglomerular sphincter portion of the afferent arteriole. *Effects of furosemide and purinergic blockers. *: P<0.05 compared to control.*

4.3 CX30 – DISTAL NEPHRON ATP RELEASE

4.3.1 Localization of Cx30 in the mouse kidney

Immunolocalization studies found intense Cx30 labeling in the luminal, non-junctional cell membrane of a select population of cells in the connecting tubule (CNT) and CCD (figure 27.A). Vascular structures or other tubule segments were devoid of Cx30 labeling. Previous studies identified the Cx30-positive cells in the CNT-CCD as intercalated cells and established that in the mouse kidney it is the only cell type that expresses Cx30 (59). No immunolabeling was found in $Cx30^{-/-}$ kidney sections confirming specificity of the Cx30 antibody (figure 27.B).

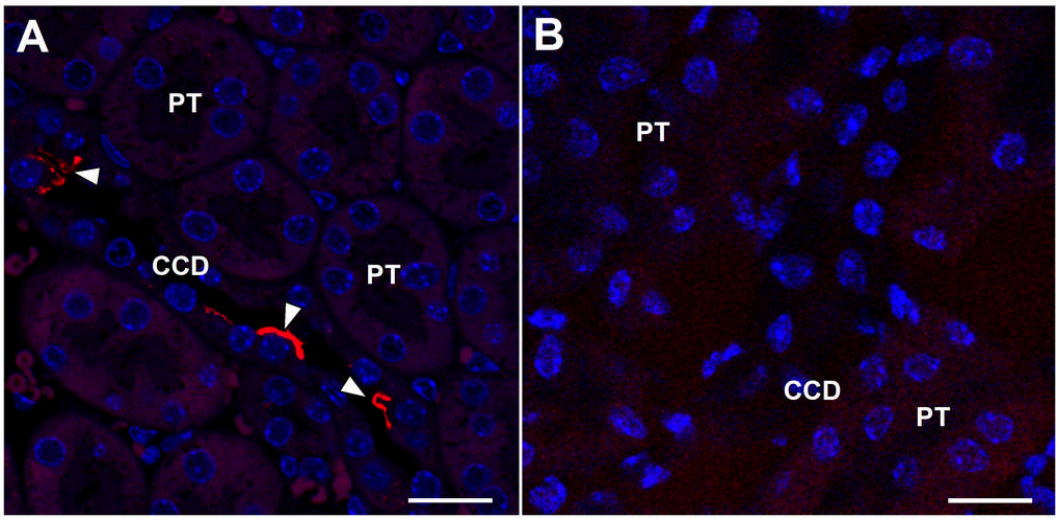

Figure 27. Immunofluorescence localization of Cx30 in the mouse kidney (red). A: *In the wild type kidney, intense Cx30 labeling (arrowheads) was found at the apical membrane of select cells in the cortical collecting duct (CCD) and the labeling showed a continuous linear pattern. Other structures including the proximal tubule (PT) were devoid of Cx30 labeling.* ***B:*** *No labeling was found in* $Cx30^{-/-}$ *kidneys. Cell nuclei were labeled with DAPI (blue). Bar is 20 µm.*

4.3.2 Luminal ATP release measurements

Since ATP release through Cx hemichannels has been established (126, 127, 58) and the unusual, nonjunctional membrane localization of Cx30 (figure 27.) suggested

hemichannel function, we measured Cx30-mediated ATP release into the tubular fluid using freshly dissected, in vitro microperfused CCDs from wild type and $Cx30^{-/-}$ mice and an established ATP biosensor technique (figure 28.) (28). Cell-specific fluorescent markers were used to identify intercalated (IC) and principal cells (PC), the two main cell types of the CCD (figure 28.A-B). As described before, the luminal surface of ICs was labeled using rhodamine-conjugated peanut-lectin (122) while quinacrine identified acidic vesicles in PCs (123). With the help of a glass micropipette, a single ATP-sensing PC12 cell loaded with calcium fluorophores was positioned through the opening of the CCD in direct contact with the apical surface of IC or PC cells (figure 28.B). In response to increasing tubular flow rate from 2 to 20 nl/min, the biosensor PC12 cells produced large elevations in $[Ca^{2+}]$ic when positioned next to ICs (Δ[Ca2+]ic = 432±14 nM, n=8), indicating ATP release from these cells (figure 28.C). Substantial, but significantly reduced flow-induced $[Ca^{2+}]$ic responses were observed when the biosensor cell was attached to PC cell's apical membrane ($\Delta[Ca^{2+}]$ic = 146±10 nM, n=7). Importantly, the ATP biosensor signal was almost completely abolished when ICs in preparations dissected from $Cx30^{-/-}$ mice were used (figure 28.C, F). Preincubation of the biosensor cells with the purinergic receptor inhibitor suramin served to ensure ATP specificity and it completely blocked the biosensor $[Ca^{2+}]$ic signal. Similarly, no response was detected when the biosensor PC12 cell was positioned at the exit of the open CCD without any direct cell membrane contact with either IC or PC cells.

Similar to the effect of increased tubular flow, reducing bath osmolality from 300 to 270 mOsm/kg (creating an interstitium-to-lumen pressure gradient) caused significant ATP release from ICs in a Cx30-dependent manner (figure 28.F). Analysis of the dose-response relationship of exogenous ATP-induced elevations in PC12 cells $[Ca^{2+}]$ic resulted in an EC_{50} value of 45.94μM (figure 28.D). Based on these measurements that translated biosensor cell $[Ca^{2+}]$ic responses to ATP levels, the relationship between tubular flow rate and luminal ATP release was established (figure 28E). The tubular flow rate with the half-maximal effect was 6.97 nl/min. The maximum luminal ATP release was in the 50μM range.

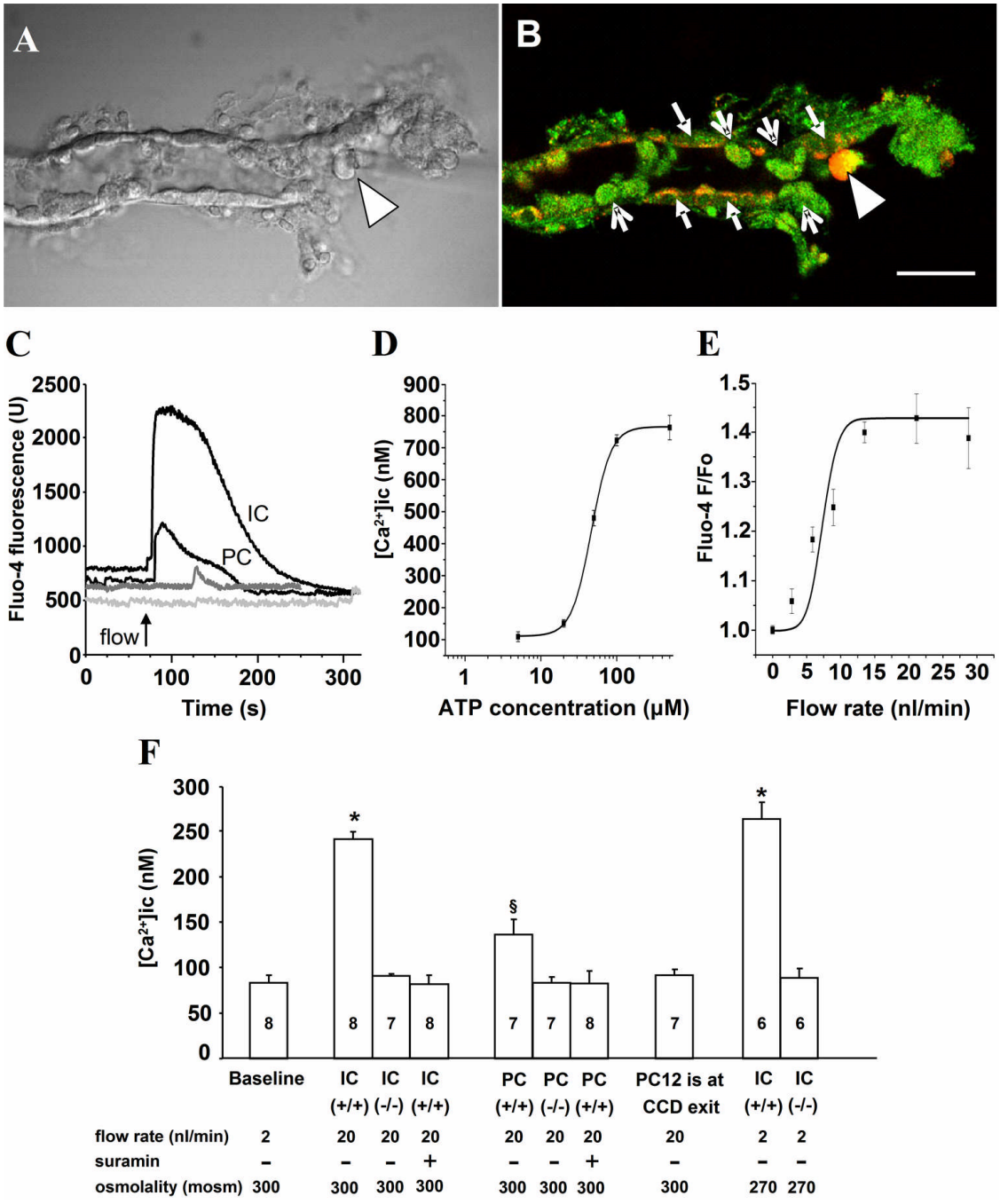

Figure 28. Detection of Cx30-mediated luminal ATP release in the isolated microperfused CCD. *Representative DIC (**A**) and fluorescence (**B**) images of the same in vitro microperfused, partially split-open mouse CCD. The luminal surface of intercalated cells (IC, red, block arrows) was labeled using rhodamine-conjugated peanut-lectin. Acidic granules in principal cells (PC) (green, open arrows) were labeled with quinacrine. A single ATP biosensor PC12 cell (arrowhead) loaded with Fluo-4/Fura Red (red in panel B) is shown positioned in the opening of the CCD against the*

apical surface of an IC (red) cell. Scale is 20μm. ***C:*** *Representative recordings from ATP biosensor experiments. After an increased tubular flow stimulus (time point indicated by an arrow) the biosensor PC12 cell produced a large elevation in $[Ca^{2+}]ic$ when positioned to the apical membrane of an IC cell indicating ATP release. This response was significantly reduced when the biosensor cell was attached to PC cell's apical membrane. Only a minimal response was observed in preparations dissected from Cx30-/- mice. The use of the purinergic receptor blocker suramin completely abolished the biosensor $[Ca^{2+}]ic$ signal.* ***D:*** *Dose-response curve of exogenous ATP-induced elevations in $[Ca^{2+}]ic$ in PC12 cells. The EC_{50} value was 45.94 μM.* ***E****: The relationship between tubular flow rate and luminal ATP release in the microperfused CCD. The ATP biosensor PC12 cells were positioned next to ICs. The tubular flow rate with the half-maximal effect was 6.97 nl/min.* ***F:*** *Summary of the changes in PC12 cell $[Ca^{2+}]ic$ in response to increased tubular flow and bath hypotonicity. *: $p<0.05$ compared to baseline; §: $p<0.05$ flow-stimulated IC vs. PC. No response was detected when the biosensor PC12 cell was positioned at the exit of the open CCD without any direct cell membrane contact with IC or PC cells. Values are mean ± SE. Numbers in the columns represent the number of preparations per group.*

4.3.3 Pressure natriuresis and diuresis in $Cx30^{-/-}$ mice

To test the significance of Cx30-mediated ATP release from the CCD in vivo, wild type and $Cx30^{-/-}$ mice were instrumented for pressure natriuresis measurements. This included the ligation of the distal aorta first and then the mesenteric and celiac arteries together that caused significant, two-step elevations in mean arterial pressure from the resting value of 115±4.5 mmHg to 131±4.1 mmHg, and then to 151±4.8 mmHg. There were no significant differences in blood pressure levels between $Cx30^{+/+}$ and $Cx30^{-/-}$ mice at any given time during these experiments (figure 29. and table 1.). The pressure natriuresis/kaliuresis/diuresis relationships are plotted in figures 29 A-C. As shown in figure 29 A. the increased renal perfusion pressure-induced natriuresis was significantly blunted in $Cx30^{-/-}$ mice ($Cx30^{+/+}$: 1.6±0.08, $Cx30^{-/-}$: 1.0±0.15 μEq/min during the highest pressure interval, $p<0.05$). There was no difference in pressure-induced kaliuresis in wild type and $Cx30^{-/-}$ mice (figure 29.B). Similar to natriuresis, the

urine output increased in response to elevations in renal perfusion pressure in both groups (figure 29.C), however the magnitude of pressure diuresis was markedly blunted in $Cx30^{-/-}$ mice ($Cx30^{+/+}$: 10.6±1.6, $Cx30^{-/-}$: 6.1±1.2µL/min during the highest pressure interval, $p<0.05$). GFR was maintained at a constant level during these studies and was not different between wild type and $Cx30^{-/-}$ animals (figure 29.D). Also, hematocrit did not change during these experiments indicating that fluid balance was generally well maintained in each experimental period (table 1).

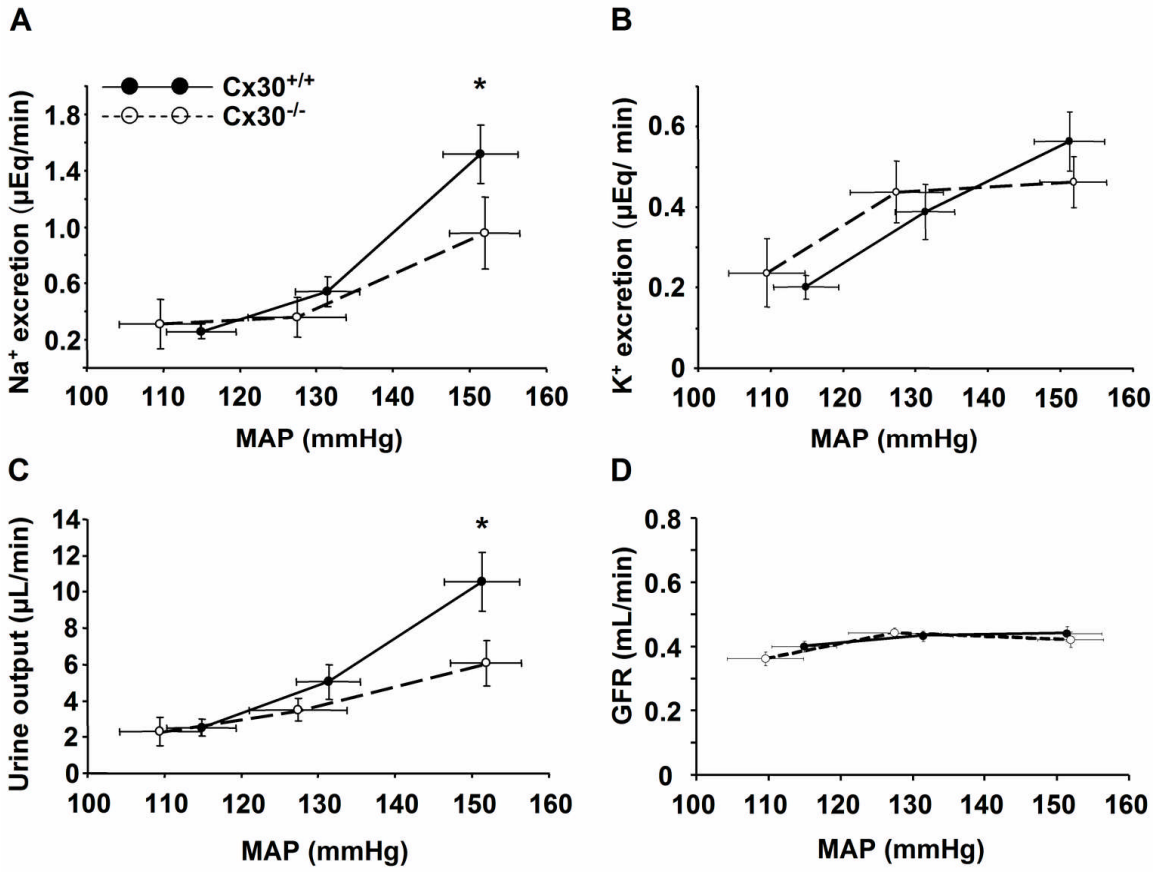

Figure 29. Pressure natriuresis (A), kaliuresis (B) and diuresis (C) in wild type and $Cx30^{-/-}$ mice. *In response to acute stepwise elevations in mean arterial blood pressure (MAP) caused by distal aorta and mesenteric and celiac artery ligations, significant elevations in Na^+ and K^+ excretion and urine output was observed. Compared to wild type (solid line and circles), $Cx30^{-/-}$ mice (dashed line, open circles) showed a reduced ability to excrete Na^+ and urinary fluid. No significant difference in kaliuresis was observed. Values are mean ± SE. *: $p<0.05$, $n=6$ for $Cx30^{+/+}$ and $n=8$ for $Cx30^{-/-}$ animals. D: Measurement of GFR during elevations in MAP. There was no significant change in GFR with elevations in blood pressure.*

	$Cx30^{+/+}$ n=8	$Cx30^{-/-}$ n=6
Age (day)	80 ± 2	78 ± 2
Body weight (g)	23.8 ± 4	25 ± 5.7
Plasma [Na^+] (mmol/L)	138 ± 11.5	139 ± 8
Plasma [K^+] (mmol/L)	4.9 ± 0.4	5.1 ± 0.4
Plasma [Cl^-] (mmol/L)	117 ± 2.4	116 ± 0.3
Plasma [HCO_3^-] (mmol/L)	16.2 ± 1.5	14.6 ± 0.9
Plasma [aldosterone] (pg/mL)	413 ± 71	405 ± 88
Plasma [arg-vasopressin] (pg/mL)	295 ± 31	307 ± 43
MAP (mmHg)	115 ± 4.5	110 ± 5.2
Hematocrit	0.4 ± 0.01	0.4 ± 0.03

Table 1. Systemic and renal parameters in $Cx30^{+/+}$ and $Cx30^{-/-}$ mice. **: $P<0.05$, n=8 ($Cx30^{+/+}$) and 6 ($Cx30^{-/-}$).*

4.3.4 Collecting duct specificity

To ascertain that the above described salt retention phenotype of $Cx30^{-/-}$ mice was due to the altered function of the CNT-CCD where Cx30 is exclusively expressed, mice were treated with benzamil, a selective inhibitor of the collecting duct-specific epithelial sodium channel (ENaC). Since there was no difference in blood pressures between wild type and $Cx30^{-/-}$ animals under normal conditions, mice were placed on high salt diet for two weeks. Blood pressure in the wild type (75±1.7 mmHg) did not change, however high salt diet caused a significant blood pressure elevation in $Cx30^{-/-}$ mice (103±2.4 mmHg, $p<0.0001$) (figure 30.). Administration of the ENaC blocker benzamil had no effect in $Cx30^{+/+}$ mice, but it returned blood pressure to normal levels in $Cx30^{-/-}$ mice on high salt diet (figure 30.).

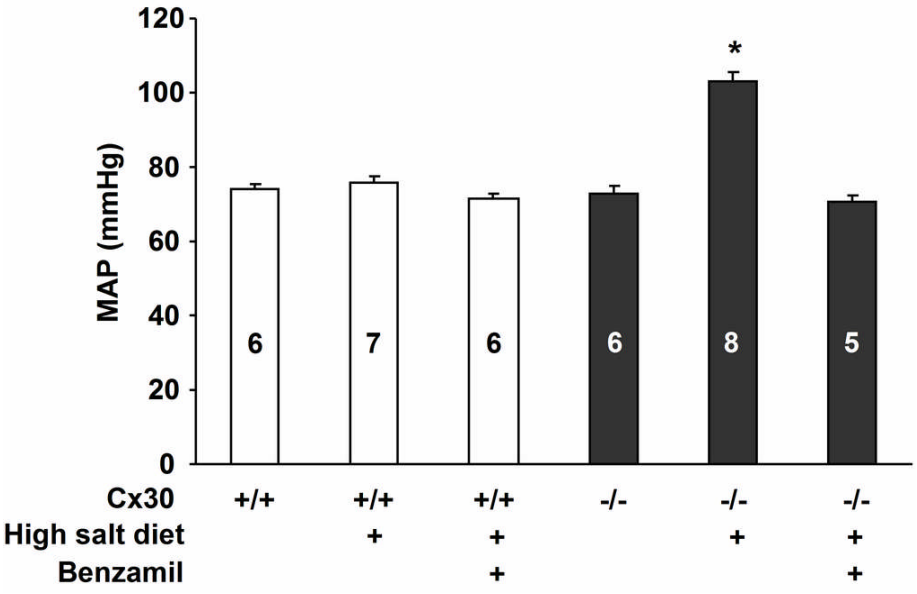

Figure 30. Effects of salt diet on mean arterial blood pressure (MAP) in wild type and Cx30$^{-/-}$ mice. *Animals on normal salt intake had no difference in blood pressure. When mice received high salt diet for two weeks, MAP in Cx30$^{-/-}$ mice increased in contrast to no change in the wild type (*: p<0.001). Administration of the selective epithelial sodium channel inhibitor benzamil had no effect on MAP in the wild type, but it returned the elevated MAP to normal levels in Cx30$^{-/-}$ mice on high salt diet. Numbers in the columns represent the numbers of animals per group.*

4.3.5 Expression of renal salt transporters and ENaC in Cx30$^{-/-}$ mice

The expression of the main renal salt transporters, Na^+:H^+ exchanger (NHE3), Na^+:2Cl^-:K^+ cotransporter (NKCC2), Na^+:Cl^- cotransporter (NCC), and the epithelial sodium channel (ENaC) was studied in wild type and Cx30$^{-/-}$ animals using immunoblotting of whole kidney homogenates as shown in figure 31. There was no statistically significant difference in the expression of these salt transporters or ENaC between Cx30$^{+/+}$ and Cx30$^{-/-}$ mice with the exception of NCC which was significantly less abundant (76±6% of that in the wild type) in kidneys of Cx30$^{-/-}$ mice (figure 31.).

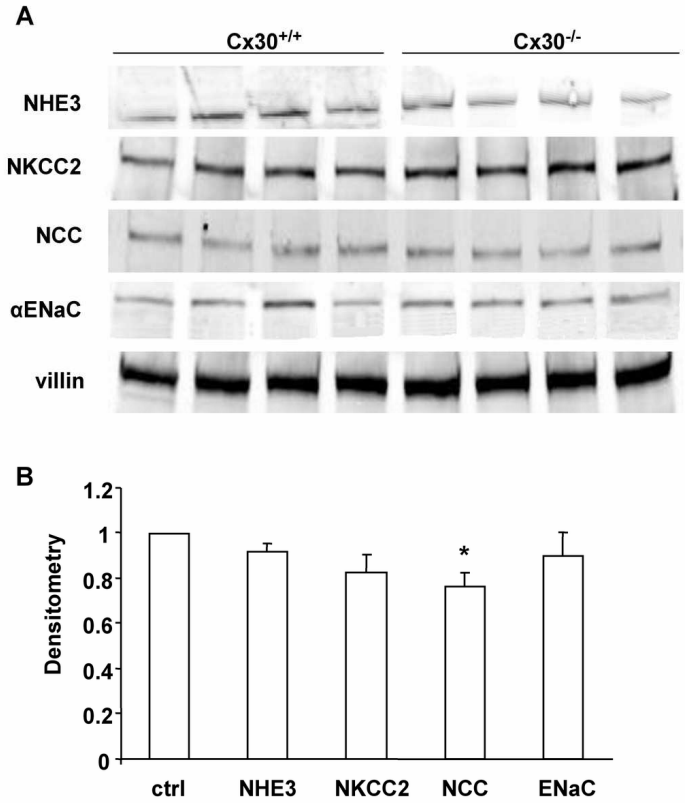

Figure 31. Expression of renal salt transporters in wild type and Cx30$^{-/-}$ mice. *Based on western blotting of whole kidney homogenates (**A**), all of the examined Na^+ transporters, the Na^+:H^+ exchanger NHE3, Na^+:2Cl^-:K^+ cotransporter (NKCC2), Na^+:Cl^- cotransporter (NCC), and epithelial sodium channel (ENaC) were equally abundant in kidneys of Cx30$^{+/+}$ and Cx30$^{-/-}$ animals except NCC which was lower in Cx30$^{-/-}$ mice. *: P<0.05, n=4 each.* ***B:*** *The ratio of densitometry values in Cx30$^{-/-}$ and wild type. Villin served as loading control.*

4.3.6 Connexin and purinergic receptor expression profile in Cx30$^{-/-}$ mice

The expression profile of well established renal connexin isoforms in kidneys of Cx30$^{+/+}$ and Cx30$^{-/-}$ mice were compared using RT-PCR of whole kidney samples as shown in figure 32 A. Expression of Cx30.3, Cx37, Cx40, Cx43 and Cx45 were found in both wild type and Cx30$^{-/-}$ animals with the exception that Cx30$^{-/-}$ mice were Cx30-deficient as expected (figure 32.A). Similarly, a variety of P2X and P2Y purinergic receptors, including the main luminal membrane isoform P2Y2 appeared to be expressed in kidneys of both Cx30$^{+/+}$ and Cx30$^{-/-}$ mice (figure 32.B).

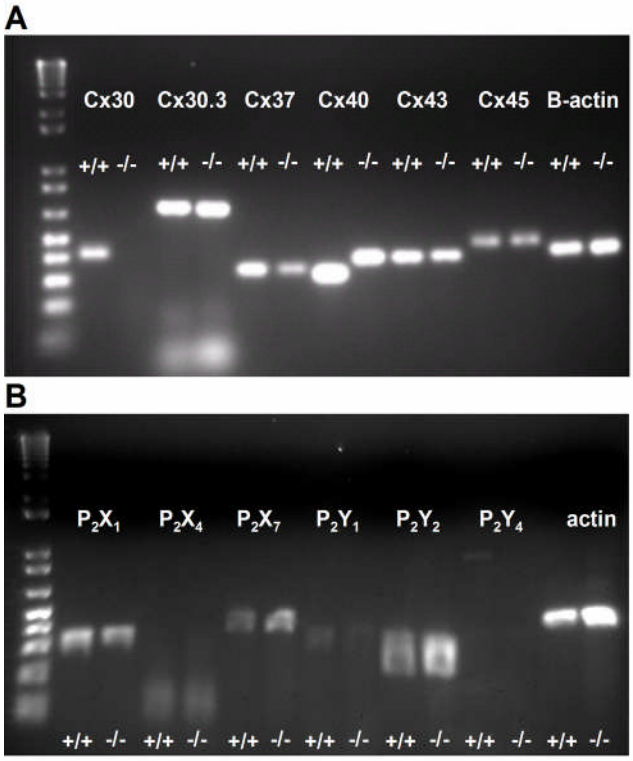

Figure 32. Expression profile of connexin (A) and purinergic receptor (B) isoforms in kidneys of Cx30$^{+/+}$ and Cx30$^{-/-}$ animals. *As expected, Cx30 was not present in kidneys of Cx30$^{-/-}$ mice, but all other examined connexin isoforms and a variety of P2X and P2Y receptors were expressed in kidneys of Cx30$^{+/+}$ and Cx30$^{-/-}$ animals.*

4.3.7 Other systemic and renal parameters in Cx30$^{-/-}$ mice

All animals were age-matched and body weight was not different between Cx30$^{+/+}$ and Cx30$^{-/-}$ groups (table 1.). Also, plasma electrolyte levels were the same. Since Cx30 hemichannels were localized to the apical membrane of IC cells which regulate pH homeostasis, plasma [Cl^-] and [HCO_3^-] were measured but did not show any difference between the two groups (table 1). Plasma aldosterone and vasopressin levels were not different between Cx30$^{+/+}$ and Cx30$^{-/-}$ mice (table 1.).

5. DISCUSSION

5.1 TUBULOGLOMERULAR FEEDBACK

This study aimed to investigate weather tubular flow elevation per se can activate the TGF feedback and if so what is the sensor to detect the flow changes. We confirmed that the MD cells possess one, apical primary cilium. Applying fluid flow to the MD apical surface or bending the primary cilia directly induces TGF regardless of the [NaCl] of the applied solution. The feedback mechanism evoked by these maneuvers involves the vascular smooth muscle cells of the afferent artery, the podocytes and the whole glomerular tuft as well. Even repeated stimuli did not result in desensitization. To identify the signaling mechanism that is responsible for conducting the flow-effect reactive oxygen species was scavenged though it has no effect on flow-induced TGF. However, inhibition of the P2 purinergic receptors significantly reduced the TGF response. Our data suggest that the primary cilium of the MD cell act as a flow sensor. Additionally to the tubular salt sensing mechanisms, MD cells are equipped with a tubular flow sensing mechanism which may contribute to MD cell function and TGF.

The studies on nature of the tubulo-arteriolar communication represent one of the classical and most interesting fields of the renal physiology. During the 60s major physiologist argued on the factor that initializes the TGF. It was proposed (128) that beside of [NaCl], changes in the osmolality, solute delivery as well as flow of the distal nephron regulate glomerular filtration. Although our knowledge on the MD cells has significantly developed, the exact mechanism of the TGF is still debated (129, 130, 131, 132). Elevation in tubular salt at the MD (1), which is concomitant with parallel increase in tubular fluid flow rate, is well accepted stimulus of TGF (30, 133, 10, 134). This phenomenon was extensively studied during the golden age of the micropuncture era. The micropuncture evidences made a huge contribution to our understanding of the transport processes taken place in the nephron (135, 136). Nowadays, the recent technical advances provided exceptional, previously unavailable high special and temporal resolution to re-approach even classic physiological mechanisms (137).

Using a cTAL – afferent arteriole double perfusion model it has been demonstrated that tubular flow elevation can stimulate TGF (32). Interestingly, elevated

tubular flow rate resulted in a more pronounced TGF response compared to that evoked by the application of high [NaCl] to the MD (32). To examine the role of the flow in triggering of the TGF a single AA-attached glomerulus with a MD plaque was dissected in which the tubule segment, surrounding the MD cells, was removed. This way the apical surface of the MD cells was directly assessable from the bath with a perfusion pipette. Tubular distension is also believed to contribute to the overall TGF respond (138). Using this approach we were able to test the flow effect without any distension of the surrounding tubule. The flow rate was calibrated (32) and applied at the range (2-20 nl/min) in which TGF respond is to be the most responsive (135). After flow elevation a rapid Ca^{2+} mediated vasoconstriction of the afferent arteriole was recorded. The most pronounced reduction in the vessel diameter occurred at the juxtaglomerular portion of the AA though as the Ca^{2+} wave propagated upwards in the AA, a minor response at the proximal part of the vessel was also observed. In addition, Ca^{2+} elevations simultaneously with the TGF were also found in the intraglomerular podocytes. Latter can also contribute to the contraction of the whole glomerular tuft observed during the TGF. The flow-induced TGF was reproducible several times without any sing of desensitization.

To further investigate the nature of the flow-induced TGF, the effect of different salt concentration solution was tested, as well as furosemide was applied directly to the cTAL. Neither of the low tubular [NaCl] nor the furosemide eliminated the flow-induced TGF indicating a NKCC2 independent signaling pathway. Intensive efforts focused on the involvement of the superoxide anion in the TGF (139, 140, 141). In these studies it has been discovered that the activation of both NKCC2 cotransporter and Na/H exchanger leads to increased superoxide production (142). Our results suggest that the NKCC2 contransporter is not involved in the flow-induced TGF. In accordance with this, scavenging the superoxide anions did not alter the flow-induced TGF, demonstrating that our results were independent of the flow-induced generation of reactive oxygen species. So we speculate that there should be a different sensor and possibly a different pathway in the MD cells which makes these cells capable of responding to the tubular flow elevation.

Two laboratories demonstrated independently of each other that like almost every vertebrate cell, the MD cell is also equipped with cell surface projection called

primary cilium (93, 94). Though this morphological finding was described more than three decades ago, it remained unnoticed and as a consequence the role of the primary cilium of MD cell received negligible attention. Recently, Pretorius et al. reported that cultured MDCK cells produce a Ca^{2+}-coupled intracellular signaling after flow stimuli (95, 143, 144, 145). The author demonstrated that this response was due to the bending of the primary cilium of the cells. In support of these observation we hypothesize that the MD cells primary cilium can also act as a mechanosensor as described in case of the MDCK cells. Using immunofluorescence labeling of α-tubulin in mouse kidney we confirmed that MD cells possess a 5-8 μm long primary cilium. In functional experiment, under no flow condition, bending of these cilia results in TGF response. In these functional experiments, there was only weak evidence for the sensitiveness of the direction towards the cilium is bended, namely bending the cilium opposite to the direction which induced Ca^{2+} influx resulted in reduction and even complete inhibition of both the Ca^{2+} influx and TGF in some experiments. However, it appears to us that the unsuited experimental approach and the limited number of observations require further efforts to determine the relationship between the direction of the cilia bending and the MD cell function.

To test the signaling pathway responsible for the flow-induced TGF, experiments were performed in the presence of P2 purinergic receptor blocker. Inhibiting the effect of ATP resulted in a reduced TGF regardless of the [NaCl] of the applied solution. This result indicates that ATP is involved in the signaling pathway of the flow-effect. However, we should emphasize that the inhibition of the P2 purinergic receptors did not diminish the entire flow-induced TGF, since the increase in the $[Ca^{2+}]$ic of the AA VSMCs achieved in the presence of purinergic blockade is still higher than the control level. This evidence indicates that though ATP seems the major transmitter of the flow-induced TGF but is not solely accountable for it. Other observations also indicate the importance of adenosine in TGF (146, 147). Based on these results, we supposed that ATP may be released and hydrolyzed immediately to adenosine which in turn may be responsible for the remaining respond after P2 purinergic receptor inhibitions.

MD cells have a reduced ability to control their cell volume (102, 138). Changes in luminal [NaCl] and osmolality will produce alteration in the MD cell volume as well.

Thus the MD cell volume will reflect the changes of the tubular content and it may play an important role in the function of the MD cell. In terms of the primary cilium, it also might be possible that changes in the cell volume will be reflected in the flow-induced response: if the MD cells swell the lumen of the tubule will reduce resulting in higher flow at the area, and moreover the cilium will most likely be positioned closer to the center of the lumen where they are exposed to higher tubular flow. Thus, the elevation in the [NaCl] initiates not only the TGF but also sets the sensitivity of the "flow-sensor machinery". Though this hypothetical model seems to reflect several, so far not included components meantime giving a more complex view of TGF, it needs more evidence and verification.

In conclusion, our data suggest that the primary cilia of MD cells act as a flow sensor. In addition to tubular salt sensing mechanisms, MD cells are equipped with a tubular flow sensing mechanism which may contribute to MD cell function and TGF.

5.2 PREGLOMERULAR SPHINCTER

These studies describe the morphology, function, and mechanism of the terminal AA, an intraglomerular precapillary sphincter. The results confirm previous preliminary data (43,102,54) that the principal effector site of TGF-mediated increase in vascular resistance occurs in the area of this glomerular sphincter. For the first time, imaging techniques with high temporal and spatial resolution provided real-time observation of the sphincter activity during TGF using the in vitro microperfused JGA preparation. Surrounding extraglomerular mesangial cells, and not renin granular cells, contracting in concert with the entire intraglomerular mesangium appear to be responsible for the generation of sphincter activity. Also a novelty in these studies is the first-time demonstration of a functional glomerular sphincter in the intact rat kidney, using two-photon microscopy. Moreover, the exciting finding that MD control of sphincter activity was purely ATP-mediated provides further support that ATP is directly involved in TGF, and not only through its breakdown to adenosine (52, 148, 149).

Preliminary reports from our laboratory (102, 54) provided images of this glomerular sphincter, and an almost complete closure of the terminal AA was suggested during TGF activation. Measurements of the sphincter ID in the present studies found that the vascular lumen constricted to only about 2 μm. This remarkable magnitude of

TGF-mediated vasoconstriction and vascular resistance further supports that this area of the AA functions as a precapillary sphincter. Taken the fourth power relationship between vessel diameter and vascular resistance, this glomerular sphincter constitutes a very high resistance to flow. However, as demonstrated in figure 20, this relatively short segment of AA is only one of several, serially connected constrictions on the entire AA, and the average vascular resistance must be lower than at this site alone. Nevertheless, changes in vascular diameter at the sphincter and in more proximal, extraglomerular segments of the AA were disproportional, with the sphincter being the principal effector site of TGF-mediated vasoconstriction. Consistent with the strong sphincter activity, real-time imaging of the kidney in vivo (still image is shown in figure 23.) revealed that velocity of the circulating red blood cells reduces at the sphincter and the cells change their orientation when passing through.

In contrast to previous speculations regarding the effector cell type (43, 54), the present studies identified the extraglomerular mesangial cells surrounding the renin granular cells, as the cell type responsible for the sphincter activity. In the sphincter area, significant elevations in cytosolic calcium during TGF were detected in extraglomerular mesangial cells which cell type produces calcium-mediated constrictions (150). Real-time observations and calcium imaging (figure 21.) suggested that extraglomerular mesangial cells in the glomerular sphincter contracted almost simultaneously with the entire intraglomerular mesangium. In fact, these two mesangial areas are continuous, connected by a dense gap junctional network and act as a functional syncytium (151). In contrast, renin granular cells did not produce significant changes in cell shape during TGF. Although, juxtaglomerular granular cells contain a low amount of contractile myofilaments such as α-smooth muscle actin (figure 25.) in sub-plasma membrane areas, they probably function in renin exocytosis (152).

Consistent with the extraglomerular mesangial cells constituting the sphincter, we found that increased renin content does not change the length or site of the sphincter. Low salt diet for one week significantly increased the length of the renin-positive segment of the AA (figure 24.). However, the glomerular sphincter was still localized in intraglomerular part.

Since the extraglomerular mesangium plays a key role in the sphincter activity, we studied the intraglomerular part of the efferent arteriole whether a similar structure

exists in that vessel. However, we found no evidence for a sphincter-like segment in the efferent arteriole (figure 22.). As opposed to the AA, the efferent arteriole begins deep inside the glomerulus and contains genuine vascular smooth muscle cells expressing different ion channels and receptors than those in the AA (153). These morphological and functional differences may explain why the contracting mesangium has no effect on the efferent arteriole. The present studies found no changes in the vascular diameter of this vessel during TGF in contrast to earlier findings (154). However, we studied only the intraglomerular part of the efferent arteriole.

MD control of sphincter activity appeared to be purely ATP-mediated in the present studies using rabbit tissue. This is an interesting finding taken that adenosine is considered the mediator of TGF (155). ATP is released from MD cells into the JGA interstitium (28), is degraded to adenosine (149), and adenosine acts on afferent arteriole vascular smooth muscle cells (48, 49, 155) causing vasoconstriction. However, several studies support the importance of both ATP and adenosine in JGA function. P2X1 purinergic receptor deficient mice have impaired autoregulatory responses (52), while adenosine A1 receptor knockout mice lack TGF responses (48, 49). Also, very recent work (149) that found impairment of TGF in ecto-5'-nucleotidase/CD73-deficient mice and also with pharmacological inhibition of the enzyme (154) further support the existence of a functionally active ATP dephosphorylating enzyme cascade in the JGA and the mediator role of adenosine in TGF. However, localization of the ecto-5'-nucleotidase enzyme may explain why this intraglomerular sphincter is purely ATP-mediated. Immunolocalization of this ATP degrading enzyme found all components of the JGA devoid of staining (156). Also, the extraglomerular mesangium showed no, or only weak staining in several species (157) while cortical interstitial cells, immediately adjacent to the smooth muscle cells of the AA and continuing along the Bowman's capsule labeled very intensely. Therefore, we speculate that the area of the intraglomerular sphincter is isolated and protected from this final ATP hydrolyzing enzyme. This may explain why ATP can directly act on P2 purinergic receptors in the sphincter area.

In summary, the intraglomerular precapillary sphincter formed and controlled by extraglomerular mesangial cells is the principal effector site of TGF-mediated increase in vascular resistance. MD control of sphincter activity is purely ATP-mediated, which

mechanism is clearly different from the adenosine-mediated vasoconstrictions in more proximal AA segments.

Vascular resistance and the mechanism of vasoconstriction of the terminal, intraglomerular part of the AA is different than in proximal, extraglomerular segments which may have therapeutic significance.

5.3 CX30 – DISTAL NEPHRON ATP RELEASE

This study identified functional Cx30 hemichannels in the intact kidney tissue as an important source of luminally released ATP in the collecting duct. Cx30 hemichannel opening at the luminal cell membrane of the CCD was triggered mechanically by elevations in tubular fluid flow rate or an interstitium-to-lumen osmotic pressure gradient, resulting in significant amounts of released ATP (up to 50μM) in the luminal microenvironment. Physiological significance of the Cx30-mediated luminal ATP release was confirmed in vivo in a mouse model of pressure natriuresis, an important renal physiological mechanism that maintains body fluid and electrolyte balance and blood pressure. $Cx30^{-/-}$ mice expressed a salt retention phenotype indicated by their reduced ability to excrete urinary salt and water in response to acute elevations in blood pressure. This was due to the dysfunction of the Cx30-expressing collecting duct since high salt diet-induced elevations in blood pressure (in $Cx30^{-/-}$ mice) were prevented by pharmacological inhibition of salt reabsorption in the CCD. This report describes a mechanically-induced ATP releasing mechanism in the intact CCD and its partial involvement in the pressure-natriuresis phenomenon. Also, this paper further emphasizes the in vivo physiological significance of purinergic regulation of renal tubular salt and water reabsorption.

The present studies were inspired by our laboratory's recent localization of Cx30 in cells of the distal nephron in the mouse, rat and rabbit kidney (59). High expression of Cx30 was found at the luminal membrane of the medullary and cortical thick ascending limbs, distal tubule, and the cortical and medullary collecting ducts (59). As shown in figure 27.A and discussed previously (59), among these species the mouse kidney has the lowest level of renal Cx30 expression, where it is restricted to IC cells of the CNT-CCD. In contrast, in the rat kidney Cx30 was found in PCs of the CCD as well (59). This cell-specific expression of Cx30 in the mouse kidney allowed us to detect

Cx30-mediated ATP release from ICs of the intact, in vitro microperfused CCD using a biosensor approach (figure 28.). PCs served as control and consistent with Cx30 expression, significantly reduced biosensor cell responses were detected from these cells (figure 28.C, F). ATP specificity of the biosensor technique was confirmed using purinergic receptor inhibition as previously established (28). In the $Cx30^{-/-}$ tissue, ATP biosensor responses were almost completely abolished suggesting that Cx30 hemichannel activity is a major ATP releasing pathway in the tubular lumen. Significantly reduced or absent ATP levels around PCs and at the open exit of the CCD, respectively (figure 28.F), indicate rapid ATP degradation after release. This is consistent with the high levels of ATP degrading enzymes co-localizing with Cx30 at the luminal membrane of ICs in the CCD and in other nephron segments (157, 158). It should be mentioned that another Cx isoform, Cx30.3 was recently localized also at the nonjunctional luminal membrane of select renal epithelial cells, partially overlapping with Cx30 (124). It is not known if Cx30.3 plays a similar, ATP releasing hemichannel function or if Cx30 and Cx30.3 form heteromeric hemichannels, a well-known feature of several Cx isoforms (126). Nevertheless, luminal Cx30 hemichannel-mediated ATP release is likely not an isolated and CCD-specific phenomenon as it is expected to be present in other nephron segments and may involve other Cx isoforms as well.

It is well established that elevations in tubular flow triggers ATP release through both luminal and basolateral cell membranes of the CCD (159, 160, 161) and that the released ATP binds to a variety of P2X and P2Y purinergic receptors (57, 162) that regulate renal salt and water reabsorption and K^+-secretion (163, 55, 164, 165, 166, 167, 168, 169, 159, 170, 171). The present study provides further mechanistic details of the renal tubular purinergic signaling system by identifying Cx30 hemichannels as a major releasing mechanism of luminal ATP. Since Cx30 hemichannel activity was triggered by mechanical stimulation of the apical cell membrane (increased tubular flow rate or an interstitium-to-lumen osmotic pressure gradient), in subsequent in vivo experiments we applied the pressure-natriuresis model which also involves mechanical factors (172, 90, 88, 173). We speculate that high blood pressure-induced elevations in intrarenal interstitial hydrostatic pressure, similar to the interstitium-to-lumen osmotic pressure gradient applied in the in vitro experiments (figure 27.F) initiated the Cx30-mediated release of ATP in vivo. Purinergic inhibition of tubular salt and water reabsorption then

caused elevations in CCD fluid flow rate leading to more ATP release and augmentation of pressure natriuresis. It is also possible that upstream, proximal tubular mechanisms (89, 174) initiated the elevations in CCD flow rate that were further augmented by triggering Cx30-mediated ATP release in the CD system. The 40% reduced pressure natriuresis and diuresis in $Cx30^{-/-}$ mice (figure 29.C) may represent the Cx30-dependent collecting duct component of this phenomenon.

The tubular fluid flow rates applied in vitro (2-20 nl/min, figure 28.) are in the range of previously established free-flow collections from early distal tubules in vivo (174). Interestingly, the earlier in vivo data in control (7.5 nl/min) and in acute hypertension (8.3 nl/min) (174) well correspond to the most sensitive range of the tubular flow rate-ATP release relationship established in the present study (6.97 nl/min, figure 28.E).

The development of a salt retention phenotype in $Cx30^{-/-}$ mice that lack luminal ATP release in the CCD is also in agreement with the phenotype in mice deficient in the main luminal ATP receptor of the nephron, P2Y2 (55). Therefore, the similar phenotype of Cx30 and P2Y2 knockout mice emphasizes the physiological importance of renal tubular ATP (see the summarizing scheme in figure 33.). Also, the mechanosensitive, Cx30-mediated ATP release and subsequent purinergic calcium signaling in the nephron (160, 161) fit with the previously identified downstream signaling steps of pressure natriuresis. These steps involve calcium-dependent synthesis of arachidonic acid metabolites (172-88), NO, and cGMP (173) and ultimately the reduced salt reabsorption in both proximal and distal nephron segments (172-174, 98). The fact that pressure-kaliuresis was not different between wild type and $Cx30^{-/-}$ mice (figure 29.B) may suggest the involvement of ATP-insensitive K^+-secretion pathways, for example the maxi-K^+ (or BK) channel rather than the low conductance ROMK channel (159-171).

To connect further these in vivo findings to the Cx30-expressing CCD segment, and to emphasize the importance of Cx30-mediated ATP release in blood pressure control, mice were placed on high salt diet for two weeks. Systemic blood pressure was significantly elevated in $Cx30^{-/-}$ versus wild type mice, which was corrected by the administration of a pharmacological inhibitor of ENaC, a CCD-specific ion channel that reabsorbs sodium (figure 30.). The reduced expression of the Na:Cl cotransporter

(figure 31) is most likely a compensatory change due to the increased ENaC-mediated salt retention in $Cx30^{-/-}$ mice, which is reminiscent of the findings in mineralocorticoid escape (175). $Cx30^{-/-}$ mice on normal salt intake were normotensive which may be explained by the effects of anesthesia or downregulation of NCC expression. Importantly, the impaired pressure natriuresis and diuresis in $Cx30^{-/-}$ mice were not attributed to alterations in other renal Cxs or purinergic receptors since the expression of these genes, at least on the mRNA level, was preserved and appeared to be similar between the two groups (figure 32.). Likewise, there was no difference in systemic parameters including aldosterone and vasopressin levels (table 1.) that could have influenced renal salt and water reabsorption.

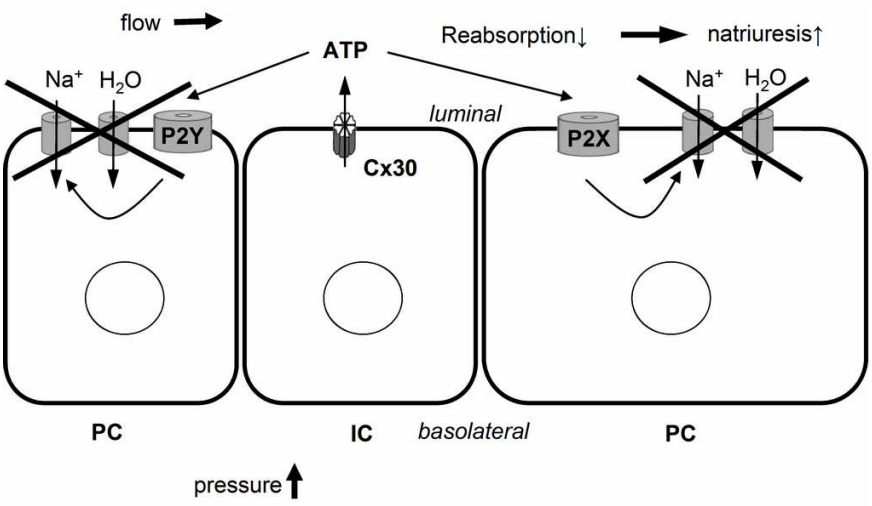

Figure 33. Schematic illustration of mechanically induced, Cx30-mediated ATP release into the tubular lumen in the CCD and its effects on salt and water reabsorption, natriuresis and diuresis. *Increases in intra-renal pressure and/or tubular flow rate that accompany blood pressure elevations result in the opening of Cx30 hemichannels at the luminal membrane of CCD intercalated cells and the release of ATP. Stimulation of luminal purinergic receptors (mainly P2Y2) results in the inhibition of salt and water reabsorption and increased natriuresis and diuresis. This inhibitory mechanism is absent in $Cx30^{-/-}$ mice resulting in a salt retention phenotype.*

Tubular flow-dependent [Ca^{2+}]ic elevations in the CCD have been demonstrated both in vitro (160, 161) and in vivo (137) and importantly, in both principal and intercalated cells (160). Since it is well established that cells of the CCD lack direct coupling through gap junctions (161), based on the present data we propose both autocrine (on ICs) and paracrine effects (on PCs) of luminal ATP released through Cx30 hemichannels, at least in the mouse kidney (figure 33.). As stated above, the expression of luminal membrane Cx30 hemichannels is more ubiquitous in the distal nephron in other species (59) suggesting their generalized role in luminal ATP release and salt and water reabsorption. Also, the hemichannel function may help resolve the apparent controversy that cells of the CCD express various Cx isoforms (59, 124) even though they lack direct cell-to-cell coupling through gap junctions (161). Furthermore, we speculate that Cx30 hemichannel opening induced by mechanical stimulation (interstitial pressure, tubular flow) may involve primary cilia (in PCs) and microvilli (in ICs) that are well established sensors of shear and hydrodynamic impulses (160) at the Cx30-expressing apical membrane. Supporting this hypothesis is the recent finding that the loss of apical monocilia on collecting duct principal cells impairs ATP secretion across the apical cell surface (176).

It should be mentioned that as established earlier (118), Cx30-/- mice are deaf due to dysfunction of the inner ear. We find it intriguing that the present studies identified another phenotype in these mice, namely renal salt retention due to dysfunction of the collecting duct system. Similarities in regulatory mechanism and common ion transporters in the renal collecting duct and the inner ear are well-known (177) and very recently, a genetic link between Bartter syndrome (dysfunction of the Cx30-expressing nephron segment) and sensorineural deafness in humans has been established (178). This suggests that Cx30-mediated ATP release is an important physiological regulatory mechanism in many organs and species, including humans. ATP release mediated by other hemichannels and their role in various organ functions have been described in many other cell types including the glomerular endothelium (125), red blood cells (179), osteocytes (180), and taste buds (181).

In summary, this is the first report on the expression of functional Cx30 hemichannels in renal tubules that release ATP into the tubular fluid in response to mechanical stimulation. Autocrine/paracrine effects of luminal ATP released via Cx30

hemichannels involve inhibition of renal salt and water reabsorption and this novel mechanism appears to be connected to at least one part (the distal nephron-collecting duct component) of pressure natriuresis and diuresis.

6. ABSTRACT

Using two-photon microscopy of the in vitro microperfused juxtaglomerular apparatus and intact Munich-Wistar rat kidney, we aimed to determine if MD cells can detect variations in tubular flow per se. Increasing cortical thick ascending limb flow rate from 2 to 20 nl/min (constant 10 mM [NaCl]) produced a significant elevation in $[Ca^{2+}]$ic in afferent arteriole (AA) smooth muscle cells (Fluo-4 F/Fo:2.08±0.21). Application of laminar flow directly to the MD apical surface produced the same results even using 10mM salt solutions. Acetylated α-tubulin immunohistochemistry identified single primary cilia in each MD cells. Under no flow conditions, bending MD cilia directly with a micropipette rapidly caused significant elevations in AA smooth muscle $[Ca^{2+}]$ic (Fluo-4 F/Fo:1.60±0.12). Scavenging the superoxide production did not alter the flow-induced tubuloglomerular feedback (TGF), however purinergic blockade (suramin) significantly reduced the response. TGF activation constricted the preglomerular sphincter lumen by 69.3 ± 5.9%, as opposed to modest changes in proximal AA segments. Extraglomerular mesangial cells increase $[Ca^{2+}]$ic, and contract in concert with the entire intraglomerular mesangium to generate sphincter activity. Suramin, but not the adenosine A1 receptor inhibitor DCPCX, completely abolished the TGF-induced sphincter activation. In conclusion, MD cells are equipped with a tubular flow sensing mechanism which may contribute to MD cell function and TGF. Preglomerular sphincter is the principal effector site of TGF that is controlled by ATP and P2 purinergic receptors.

ATP and metabolites are present in the renal tubular and interstitial fluid and are involved in the regulation of salt and water reabsorption. Several connexin (Cx) isoforms form ATP-permeable hemichannels. We localized Cx30 in the apical membrane of renal epithelial cells suggesting a possible release function. The aim of these studies was to test if Cx30 hemichannels release ATP and are involved in the regulation of tubular electrolyte and water transport. WT and Cx30 KO mice cortical collecting ducts were dissected, partially slit-open and microperfused in vitro. Using the biosensor technique we showed that ATP release, triggered by an increase in tubular flow, is significantly higher from intercalated cells than from principal cells and were abolished by suramin or in KO tissue. Next, mice were surgically instrumented for clearance and pressure natriuresis measurements. After stepwise increases in BP, urine flow increased 4.2-fold in WT vs. 2.6-fold in KO animals. Fractional urinary Na^+ excretion increased 5.1-fold in WT vs. 2.8-fold in KO animals. This is the first study suggesting that distal tubular Cx30 hemichannels release ATP which inhibits renal salt and water reabsorption causing pressure natriuresis.

7. MAGYAR NYELVŰ ÖSSZEFOGLALÓ

Juxtaglomerularis apparatus (JGA) a renin–angiotensin rendszer központi eleme, meghatározó a vese só és vízhátartás szabályozásában, ill. a vérnyomás beállításában. Kísérleteink célja a következő volt: in vitro, mikroperfundált JGA és in vivo, intakt patkány vesében two-photon mikroszkóppal megvizsgáljuk, hogy a tubuloglomerularis feedback (TGF) kiváltható-e a tubuláris folyadékáramlás (FÁ) változtatásával. Distalis tubulusban a FÁ-t 2-20nl/min változtatva szignifikáns [Ca^{2+}]ic emelkedést tapasztaltunk az afferens arteriola (AA) simaizomsejtjeiben (Fluo-4 F/Fo:2.08±0.21). Immunohisztokémiai vizsgálataink igazolták, hogy minden macula densa (MD) sejt rendelkezik egy primer ciliummal az apikális membránján. FÁ megváltozatása nélkül mikropipettával megdöntöttük a MD sejtek primer ciliumát, ami szignifikáns [Ca^{2+}]ic emelkedést (Fluo-4 F/Fo:1.60±0.12) idézett elő az AA simaizomsejtjeiben. A szuperoxid anion termelését gátolva a FÁ megváltozatásával előidézett TGF nem változott, míg a purinerg P2 receptor blokkoló suramin teljesen meggátolta azt. TGF során, a proximális AA területén csupán enyhe vasokonstrikciót, ellenben a preglomeruláris sphincter területén 69.3 ± 5.9%-os érátmérőcsökkenést mértünk. Extra- és intraglomeruláris mesangiális sejtek [Ca^{2+}]ic-ja szinkronizáltan emelkedett a TGF során, ami a sphincter összehúzódását eredményzte. Adenosine A1 receptor blokkoló DCPCX-szel ellentétben suramin megakadályozta a sphincter működését a TGF alatt. Eredményeink arra utalnak, hogy a MD sejtekek képesek érzékelni a tubuláris FÁ változásait. Ez a tulajdonságuk hozzájárul a TGF folyamatához. A TGF fő effectora a preglomeruláris sphincter, ami ATP és P2 purinerg mediált jelátvitel szabályozása alatt áll.

A tubularis és intersticialis folyadékban jelenlévő ATP és bomlástermékei részt vesznek a tubuláris só- és vízvisszaszívás szabályozásában. Számos Connexin(Cx) molekula alkot ATP áteresztő csatornát. Immunohisztokémiával Cx30 csatornákat vese gyűjtőcsatorna apikális membránján lokalizáltuk. Célunk az volt, hogy megvizsgáljuk a Cx30 csatorna képes-e ATP-t áteresztetni, és részt vesz-e a tubularis elektrolit és víztranszport szabályozásában. Cx30 WT és KO egerek gyűjtőcsatornáit kiboncoltuk, és in vitro mikroperfundáltuk. Bioszenzor technikával kimutattuk: tubularis flow emelésével stimulált ATP szekréció szignifikánsan nagyobb interkalált sejtekből, mint principális sejtekből. ATP elválasztás Cx30 KO szövetben, ill. suramin hatására jelentősen csökken. Cx30 egerérben a vérnyomás lépcsőzetes emelésével a vizeletelválasztás 4.2x-esere növekedett WT, míg 2.6x-osára KO állatokban. A frakcionális Na^+ kiválasztás 5.1x-esére növekedett WT, míg 2.8x-ára KO állatokban. Eredményeink bizonyítják, hogy a distalis tubulus Cx30 csatornái képesek ATP-t áteresztetni, és gátolva a só- és vízvisszaszívást nyomásdiurezishez vezetnek.

8. ACKNOWLEDGEMENT

I am deeply indebted to my supervisors Prof. Laszlo Rosivall and Janos Peti-Peterdi for the continuous support during my PhD studies (Institute of Pathophysiology, Semmelweis University, Budapest). Prof. Rosivall is a real scientist and a great man with a constant oasis of ideas and passion in science which exceptionally inspired me during the couple months that I had a chance to closely work with him. I greatly acknowledge Janos Peti-Peterdi for his advice, supervision and contribution which made him the backbone of this research.

I would like to thank the technical assistance of Fiona Hanner, Sarah Vargas and Anush Gevorgyan at the University of Southern California. Also I thank for the help, valuable suggestions and cheering of my colleagues Ildiko Toma, Ken-ichi Manabe, Fiona Hanner, Julie Kang, Elliott Meer, Eric Bansal and John Koo. I greatly appreciated the work of the administrative team at the Zilka Neurogenetic Institute at the University of Southern California. In addition, I thank for Judit Liptak at the Semmelweis University for assisting me with the administrative tasks necessary for completing my doctoral program.

I am very grateful to my first mentor, Csilla Hably, a gracious tutor who planted in me the seeds of science and provided me with an excellent atmosphere for doing research. Also, I thank for Prof Andras Spät who let me experience what high standards means in scientific research.

Special thanks for the support, the encouragement and the love of my wife and our families that guided my efforts during the years of my doctoral studies.

My work at the University of Southern California was supported by the American Heart Western States Postdoctoral Fellowship.

9. LIST OF PUBLICATIONS

Publications related to present thesis:

1. **Sipos A**, Vargas SL, Toma I, Hanner F, Willecke K, Peti-Peterdi J. Connexin 30 deficiency impairs renal tubular ATP release and pressure natriuresis. J Am Soc Nephrol 20: 1724-32, 2009. (PMID: 19478095) IF: 7.111.

2. **Sipos A,** Toma I, Kang JJ, Rosivall L, Peti-Peterdi J. Advances in renal (patho)physiology using multiphoton microscopy. Kidney Int 72:1188-91, 2007. (PMID: 17667980), IF: 4.922.

3. Kang JJ, Toma I, **Sipos A**, McCulloch F, Peti-Peterdi J. Imaging the renin-angiotensin system: An important target of anti-hypertensive therapy. Adv Drug Deliv Rev 58:824-33, 2006. (PMID: 16979787) IF: 7.977.

4. Rosivall L, Mirzahosseini S, Toma I, **Sipos A**, Peti-Peterdi J. Fluid flow in the juxtaglomerular interstitium visualized in vivo. Am J Physiol Renal Physiol 291:F1241-7, 2006. (PMID: 16868308) IF: 4.199.

5. Kang JJ, Toma I, **Sipos A**, McCulloch F, Peti-Peterdi J. Quantitative imaging of basic functions in renal (patho)physiology. Am J Physiol Renal Physiol 291:F495-502, 2006. (PMID: 16609147) IF: 4.199.

Book chapter:

1. Kang JJ, Toma I, **Sipos A**, Peti-Peterdi J. From in vitro to in vivo: imaging from the single cell to the whole organism. Curr Protoc Cytom. Edited by JP Robinson, Z Darzynkiewicz, R Hoffman, JP Nolan, A Orfao, PS Rabinovitch, S Watkins, T Downey; John Wiley & Sons Inc. 44: 12.12.1-12.12.26, 2008. (PMID: 18770644)

Other publications in peer-reviwed journals:

1. Wilkinson L, Gilbert T, **Sipos A,** Toma I, Pennisi D, Peti-Peterdi J, Little M. Loss of renal microvascular integrity in postnatal Crim1 hypomorphic transgenetic mice. Kidney Int. 2009, Doi: 10.1038/ki.2009.345. IF: 6.418.

2. Peti-Peterdi J, Toma I, **Sipos A**, Vargas SL. Multiphoton Imaging of Renal Regulatory Mechanisms. Physiology 24:88-96, 2009. IF: 6.954.

3. Toma I, Kang JJ, **Sipos A**, Vargas S, Bansal E, Hanner F, Meer E, Peti-Peterdi J. Succinate receptor GPR91 provides a direct link between high glucose levels and renin release in murine and rabbit kidney. J Clin Invest. 118:2526-34, 2008. (PMID: 18535668) IF: 16.915.

4. Hanner F, von Maltzahn J, Maxeiner S, Toma I, **Sipos A**, Krüger O, Willecke K, Peti-Peterdi J. Connexin45 is expressed in the juxtaglomerular apparatus and is involved in the regulation of renin secretion and blood pressure. Am J Physiol Regul Integr Comp Physiol 295:R371-80, 2008. (PMID: 18579650) IF: 3.661.

5. Kang JJ, Toma I, **Sipos A**, Meer EJ, Vargas SL, Peti-Peterdi J. The collecting duct is the major source of prorenin in diabetes. Hypertension. 51:1597-604, 2008. (PMID: 18413493) IF: 7.194.

6. Salmon AH, Toma I, **Sipos A**, Muston PR, Harper SJ, Bates DO, Neal CR, Peti-Peterdi J. Evidence for restriction of fluid and solute movement across the glomerular capillary wall by the subpodocyte space. Am J Physiol Renal Physio. 293:F1777-86, 2007. (PMID: 17804486) IF: 4.416.

Cover images:

1. Kidney International, Nature publishing group, 72 (10) November, 2007 from publication **Sipos A**, Toma I, Kang JJ, Rosivall L, Peti-Peterdi J. Advances in renal (patho)physiology using multiphoton microscopy. Kidney Int 72:1188-91, 2007. (PMID: 17667980) IF: 4.922

2. Hypertension, 51 (6) June, 2008 from publication Kang JJ, Toma I, **Sipos A**, Meer EJ, Vargas SL, Peti-Peterdi J. The collecting duct is the major source of prorenin in diabetes. Hypertension. 51:1597-604, 2008. (PMID: 18413493) IF: 7.194

3. Advanced Drug Delivery Reviews 58 (7) September, 2006 from publication Kang JJ, Toma I, **Sipos A**, McCulloch F, Peti-Peterdi J. Imaging the renin-angiotensin system: An important target of anti-hypertensive therapy. Adv Drug Deliv Rev 58:824-33, 2006. (PMID: 16979787) IF: 7.977

Abstracts:

1. Svenningsen P, **Sipos A,** Peti-PeterdiJ ATP releasing Connexin 30 hemichannels mediate flow-induced calcium signaling in the collecting duct JASN 2009.
2. Hanner F, **Sipos A**, Vargas S, Toma I, Peti-Peterdi J. Expression of pannexin 1 hemichannels in renal tubules Gap Junction Conference, 2009.
3. **Sipos A**, Vargas SL, Peti-Peterdi J. Connexin 30 knockout mice develop salt sensitivity JASN (19): 159A, 2008.
4. **Sipos A**, Toma I, Vargas SL, Peti-Peterdi J. Direct demonstration of tubular fluid flow sensing by macula densa cells FASEB Journal 22:761.28, 2008.
5. Hanner FP, Toma I, **Sipos A**, Vargas S, Peti-Peterdi J. Localization and function of connexin 45 in the renal cortical vasculature FASEB Journal 22:761.9, 2008.
6. **Sipos A**, Toma I, Vargas SL, McCulloch F, Peti-Peterdi J. Impaired luminal ATP release and pressure natriuresis in connexin 30 knockout mice FASEB Summer conference 2007.
7. Toma I, Kang JJ, Bansal E, **Sipos A**, McCulloch F, Peti-Peterdi J. GPR91 triggers paracrine signaling in the JGA FASEB Journal 21:595.4, 2007.
8. Kang JJ, Toma I, **Sipos A**, Bansal E, Peti-Peterdi J. Uric acid triggers renin release and causes glomerular hyperfiltration FASEB Journal 21:595.22, 2007.
9. McCullock F, Toma I, **Sipos A**, Peti-Peterdi J. Localization of connexin 45 in the kidney FASEB Journal 21:937.29, 2007.
10. **Sipos A**, McCulloch F, Toma I, Peti-Peterdi J. Impaired renal Na^+ and water reabsorption and K^+ secretion in mice lacking connexin 30 JASN (17): 472A, 2006.
11. Toma I, **Sipos A**, McCulloch F, Peti-Peterdi J. In vivo imaging of the kidney in early diabetes FASEB Journal 20:A1170, 2006.
12. Ambrus B, Hably Cs, Vág J, Kerémi B, Csillag M, **Sipos A**, Bartha J. The role of nitric oxide, α1-adrenergic and AT1 receptors in the regulation of blood flow of adrenal gland. Acta Physiologica Hungarica (89): 61, 2002.

13. Hably Cs, Vág J, Kerémi B, Csillag M, Ambrus B, **Sipos A**, Bartha J. AT1 but not α1-receptor blockade increases the nitric oxide synthesis in working and resting skeletal muscle. Acta Physiologica Hungarica (89): 62, 2002.

14. Kerémi B, Vág J, Csillag M, Hably Cs, **Sipos A**, Ambrus B, Bartha J, Fazekas Á. Candesartan treatment increases the vasoconstrictor effect of L-NAME in rat submandibular gland. Acta Physiologica Hungarica (89): 95, 2002.

15. **Sipos A**, Hably Cs, Vág J, Kerémi B, Csillag M, Ambrus B, Bartha J. Role of AT1 receptors in the L-NAME evoked hypertension and renal vasoconstriction: effect of dietary salt. Acta Physiologica Hungarica 89 (1-3) i-xii, 60, 2002.

16. **Sipos A**, Kiss I, Hably Cs, Vág J, Bartha J. Extracellular space, sodium and water turnover in rats: effect of NOS inhibition and dietary salt. Nephrol Dial Transplant 16(6):A4, 2001.

10. REFERENCES

1 Thurau K, Schnermann J. The sodium concentration in the macula densa cells as a regulating factor for glomerular filtration (micropuncture experiments) Klin Wochenschr. 15;43:410-3, 1965.

2 Navar LG, Inscho EW, Majid SA, Imig JD, Harrison-Bernard LM, Mitchell KD. Paracrine regulation of the renal microcirculation. Physiol. Rev. 76:425–536, 1996.

3 Barajas L. Anatomy of the juxtaglomerular apparatus. Am. J. Physiol. Renal Physiol. 7:F333–F43, 1979.

4 Navar LG, Ploth DW, Bell PD. Distal tubular feedback control of renal hemodynamics and autoregulation. Annu. Rev. Physiol. 49:557–71, 1980.

5 Schnermann J, Traylor T, Yang T, Arend L, Huang YG, et al. Tubuloglomerular feedback: new concepts and developments. Kidney Int. 54:S40–S45, 1998.

6 LaPointe J-Y, Laamarti A, Bell PD. Ionic transport in macula densa cells. Kidney Int. 54:S58–S64, 1998.

7 Yang T, Huand YG, Singh I, Schnermann J, Briggs JP. Localization of bumetanide- and thiazide-sensitive Na-KCl cotransporters along the rat nephron. Am. J. Physiol. Renal Physiol. 271: F931–F39, 1996.

8 Plata C, Meade P,V´azquez N, Herbert SC, Gamba G. Functional properties of the apical Na+-K+-2Cl- cotransporter isoforms. J. Biol. Chem. 277: 11001–12, 2002.

9 Giménez I, Isenring P, Forbush B. Spatially distributed alternative splice variants of the renal Na-K-Cl cotransporter exhibit dramatically different affinities for the transported ions. J. Biol. Chem. 277: 8767–70, 2002.

10 LaPointe J-Y, Bell PD, Cardinal J. Direct evidence for an apical Na:2Cl:K co-transport in macula densa cells. Am. J. Physiol. Renal Physiol. 258:F1466–F69, 1990.

11 Fowler, B.C., Chang, Y.S., Laamarti, A., Higdon, M., Lapointe, J.Y. & Bell, P.D. Evidence for apical sodium proton exchange in macula densa cells. Kidney Int 47, 746–751, 1995.

12 Peti-Peterdi, J., Chambrey, R., Bebok, Z. et al. Macula densa Na(+)/H(+) exchange activities mediated by apical NHE2 and basolateral NHE4 isoforms. Am J Physiol Renal Physiol 278, F452–F463, 2000.

13 Briggs JP, Schnermann J. The tubuloglomerular feedback mechanism: functional and biochemical aspects. Annu. Rev. Physiol. 49:251–73, 1987.

14 Peti-Peterdi J, Bebok Z, LaPointe J-Y, Bell PD. Cytosolic [NaC] regulation in macula densa cells: novel role for an apical H:K ATPase. Am. J. Physiol. Renal Physiol. 282:F324–F29, 2002.

15 Codina M, Pressley TA, DuBose TD. The colonic H, K-ATPase functions as a Na-dependent K (NH4)-ATPase in apical membranes from rat distal colon. J. Biol. Chem. 274:19693–98, 1999.

16 CougnonM,BouyerP, Planelles G, Jaisser F. Does the colonicH,KATPase also act as a Na,K-ATPase? Proc. Natl. Acad. Sci. USA 95:6516–20, 1998.

17 Wetzel RK, Sweadner KJ. Immunocytochemical localization of Na-KATPase and subunits in rat kidney. Am. J. Physiol. Renal Physiol. 281:F531, 2001.

18 Hurst, A.M., Lapointe, J.Y., Laamarti, A. & Bell, P.D. Basic properties and potential regulators of the apical K+ channel in macula densa cells. J Gen Physiol 103, 1055–1070, 1994.

19 Ren Y, Yu H, Wang H, Carretero OA, Garvin JL. Nystatin and valinomycin induce tubuloglomerular feedback. Am J. Physiol. Renal Physiol. 281:F1102–F8, 2001.

20 Vallon V, Osswald H, Blantz RC, Thomson S. Potential role of luminal potassium in tubuloglomerular feedback. J. Am. Soc. Nephrol. 8:1831–37, 1997.

21 Vallon V, Osswald H, Blantz RC, Thomson S. Luminal signal in tubuloglomerular feedback: what about potassium? Kidney Int. Suppl. 67:S177–79, 1998.

22 Schnermann J. Effects of barium ions on tubuloglomerular feedback. Am. J. Physiol. Renal Physiol. 268:F960–F66, 1995.

23 Xu, J.Z., Hall, A.E., Peterson, L.N., Bienkowski, M.J., Eessalu, T.E. & Hebert, S.C. Localization of the ROMK protein on apical membranes of rat kidney nephron segments. Am J Physiol 273, F739–F748, 1997.

24 Lapointe, J.Y., Bell, P.D., Hurst, A.M. & Cardinal, J. Basolateral ionic permeabilities of macula densa cells. Am J Physiol 260, F856–F860, 1991.

25 Bell PD, LaPointe J-Y, Cardinal J. Direct measurement of basolateral membrane potential in cells of the macula densa. Am. J. Physiol. Renal Physiol. 257:F463–F68, 1989.

26 Lapointe J-Y, Bell PD, Sabirov R, Okada Y. Calcium-activated non-selective cation channel in macula densa cells Am. J. Physiol. Renal Physiol. 285:F275-80, 2003.

27 Mitchell, K.D. & Navar, L.G. Modulation of tubuloglomerular feedback responsiveness by extracellular ATP. Am J Physiol 264, F458–F466, 1993.

28 Bell PD, Lapointe JY, Sabirov R, Hayashi S, Peti-Peterdi J, Manabe K, Kovacs G, Okada Y: Macula densa cell signaling involves ATP release through a maxi anion channel. Proc Natl Acad Sci USA 100: 4322-7, 2003.

29 Dev, B., Drescher, C. & Schnermann, J. Resetting of tubulo-glomerular feedback sensitivity by dietary salt intake. Pflugers Arch 346, 263–277, 1974.

30 Wright, F.S. & Schnermann, J. Interference with feedback control of glomerular filtration rate by furosemide, triflocin, and cyanide. J Clin Invest 53, 1695–1708, 1974.

31 Komlosi, P., Peti-Peterdi, J., Fuson, A.L., Fintha, A., Rosivall, L. & Bell, P.D. Macula densa basolateral ATP release is regulated by luminal [NaCl] and dietary salt intake. Am J Physiol Renal Physiol 286, F1054–F1058, 2004.

32 Peti-Peterdi J. Calcium wave of tubuloglomerular feedback. Am J Physiol Renal Physiol. 291(2):F473-80, 2006.

33 Harris, R.C., McKanna, J.A., Akai, Y., Jacobson, H.R., Dubois, R.N. & Breyer, M.D. Cyclooxygenase-2 is associated with the macula densa of rat kidney and increases with salt restriction. J Clin Invest 94, 2504–2510, 1994.

34 Campean, V., Theilig, F., Paliege, A., Breyer, M. & Bachmann, S. Key enzymes for renal prostaglandin synthesis: site-specific expression in rodent kidney (rat, mouse). Am J Physiol Renal Physiol 285, F19–F32, 2003.

35 Fuson, A.L., Komlosi, P., Unlap, T.M., Bell, P.D. & Peti- Peterdi, J. Immunolocalization of a microsomal prostaglandin E synthase in rabbit kidney. Am J Physiol Renal Physiol 285, F558–F564, 2003.

36 Peti-Peterdi, J., Komlosi, P., Fuson, A.L. et al. Luminal NaCl delivery regulates basolateral PGE2 release from macula densa cells. J Clin Invest 112, 76–82, 2003.

37 Jensen BL, Mann B, Skott O, and Kurtz A. Differential regulation of renal prostaglandin receptor mRNAs by dietary salt intake in the rat. Kidney Int 56: 528–537, 1999.

38 Wilcox, C.S., Welch, W.J., Murad, F. et al. Nitric oxide synthase in macula densa regulates glomerular capillary pressure. Proc Natl Acad Sci U S A 89, 11993–11997, 1992.

39 Toma I, Kang JJ, Sipos A, Vargas S, Bansal E, Hanner F, Meer E, Peti-Peterdi J. Succinate receptor GPR91 provides a direct link between high glucose levels and renin release in murine and rabbit kidney. J Clin Invest. 118(7):2526-34, 2008.

40 Liu, R., Pittner, J. & Persson, A.E. Changes of cell volume and nitric oxide concentration in macula densa cells caused by changes in luminal NaCl concentration. J Am Soc Nephrol 13, 2688–2696, 2002.

41 Kovacs, G., Komlosi, P., Fuson, A., Peti-Peterdi, J., Rosivall, L. & Bell, P.D. Neuronal nitric oxide synthase: its role and regulation in macula densa cells. J Am Soc Nephrol 14, 2475–2483, 2003.

42 Gorren, A.C., Schrammel, A., Schmidt, K. & Mayer, B. Effects of pH on the structure and function of neuronal nitric oxide synthase. Biochem J 331 (Pt 3), 801–807, 1998.

43 Moore LC, Casellas D, Persson AE, Muller-Suur R, Morsing P. Renal hemodynamic regulation by the renin-secreting segment of the afferent arteriole. Kidney Int Suppl. 30:S65-8, 1990.

44 Steinhausen M, Blum M, Fleming JT, Holz FG, Parekh N, Wiegman DL. Visualization of renal autoregulation in the split hydronephrotic kidney of rats. Kidney Int. 35(5):1151-60, 1989.

45 Edwards RM. Segmental effects of norepinephrine and angiotensin II on isolated renal microvessels. Am J Physiol. 244(5):F526-34, 1983.

46 Weihprecht H, Lorenz JN, Briggs JP, Schnermann J. Vasomotor effects of purinergic agonists in isolated rabbit afferent arterioles. Am J Physiol. 263(6 Pt 2):F1026-33, 1992.

47 Weihprecht H, Lorenz JN, Briggs JP, Schnermann J. Synergistic effects of angiotensin and adenosine in the renal microvasculature. Am J Physiol. 266(2 Pt 2):F227-39, 1994.

48 Sun D, Samuelson LC, Yang T, Huang Y, Paliege A, Saunders T, Briggs J, Schnermann J. Mediation of tubuloglomerular feedback by adenosine: evidence from mice lacking adenosine 1 receptors. Proc Natl Acad Sci U S A. 14;98(17):9983-8, 2001.

49 Brown R, Ollerstam A, Johansson B, Skott O, Gebre-Medhin S, Fredholm B, Persson AE. Abolished tubuloglomerular feedback and increased plasma renin in adenosine A1 receptor-deficient mice. Am J Physiol Regul Integr Comp Physiol. 281(5):R1362-7, 2001.

50 Hall JE, Granger JP, Hester RL. Interactions between adenosine and angiotensin II in controlling glomerular filtration Am. J. Physiol. Renal Physiol. 248:F340–F46, 1985.

51 Hall JE, Granger JP. Adenosine alters glomerular filtration control by angiotensin II. Am. J. Physiol. Renal Physiol. 250:F917–F23, 1986.

52 Inscho EW, Cook AK, Imig JD, Vial C, Evans RJ. Physiological role for P2X1 receptors in renal microvascular autoregulatory behavior. J Clin Invest 112:1895-905, 2003.

53 Taugner R, Rosivall L, Buhrle CP, Groschel-Stewart U. Myosin content and vasoconstrictive ability of the proximal and distal (renin-positive) segments of the preglomerular arteriole. Cell Tissue Res. 248(3):579-88, 1987.

54 Peti-Peterdi J. Multiphoton imaging of renal tissues in vitro. Am J Physiol Renal Physiol. 288(6):F1079-83, 2005.

55 Rieg T, Bundey RA, Chen Y, Deschenes G, Junger W, Insel PA, Vallon V. Mice lacking P2Y2 receptors have salt-resistant hypertension and facilitated renal Na+ and water reabsorption. FASEB J. 21(13):3717-26, 2007.

56 Wildman SS, Chraibi A, Horisberger J-D, King BF, Unwin RJ Downstream regulation of ENaC by ATP-gated P2X receptors. J Am Soc Nephrol 14 : SA-FC165, 2003.

57 Schwiebert EM, Kishore BK. Extracellular nucleotide signaling along the renal epithelium. Am J Physiol Renal Physiol. 280(6):F945-63, 2001.

58 Cotrina ML, Lin JH, Alves-Rodrigues A, Liu S, Li J, Azmi-Ghadimi H, Kang J, Naus CC, Nedergaard M. Connexins regulate calcium signaling by controlling ATP release. Proc Natl Acad Sci U S A. 22;95(26):15735-40, 1998.

59 McCulloch F, Chambrey R, Eladari D, Peti-Peterdi J. Localization of connexin 30 in the luminal membrane of cells in the distal nephron. Am J Physiol Renal Physiol. 289(6):F1304-12, 2005.

60 Schild L, Kellenberger S: Structure function relationships of ENaC and its role in sodium handling. Adv Exp Med Biol 502: 305–314, 2001.

61 Schafer JA Abnormal regulation of ENaC: syndromes of salt retention and salt wasting by the collecting duct. Am J Physiol Renal Physiol 283: F221–F235, 2002.

62 Hummler E, Horisberger J-D: Genetic disorders of membrane transport. The epithelial sodium channel and its implications in human diseases. Am J Physiol 276: G567–G571, 1999.

63 Garty, H. and Palmer, L. G. Epithelial sodium channels : function, structure and regulation. Physiol. Rev. 77, 359–396, 1997.

64 Canessa CM, Horisberger JD, Rossier BC. Epithelial sodium channel related to proteins involved in neurodegeneration Nature. 361(6411):467-70, 1993.

65 Canessa CM, Schild L, Buell G, Thorens B, Gautschi I, Horisberger JD, Rossier BC. Amiloride-sensitive epithelial Na+ channel is made of three homologous subunits. Nature. 367(6462):463-7, 1994.

66 Sheng S, Li J, McNulty KA, Kieber-Emmons T, Kleyman TR Epithelial sodium channel pore region J. Biol. Chem. 276 (2), 1326-1334, 2001.

67 Firsov D, Gautschi I, Merillat AM, Rossier BC, Schild L. The heterotetrameric architecture of the epithelial sodium channel (ENaC). EMBO J.17(2):344-52, 1998.

68 Kosari F, Sheng S, Li J, Mak DO, Foskett JK, Kleyman TR. Subunit stoichiometry of the epithelial sodium channel. J Biol Chem. 29;273(22):13469-74, 1998.

69 Snyder PM, Cheng C, Prince LS, Rogers JC, Welsh MJ. Electrophysiological and biochemical evidence that DEG/ENaC cation channels are composed of nine subunits. J Biol Chem. 273(2):681-4, 1998.

70 Eskandari S, Snyder PM, Kreman M, Zampighi GA, Welsh MJ, Wright EM. Number of subunits comprising the epithelial sodium channel. J Biol Chem. 274(38):27281-6, 1999.

71 Canessa CM, Merillat AM, Rossier BC. Membrane topology of the epithelial sodium channel in intact cells. Am J Physiol. 267(6 Pt 1):C1682-90, 1994.

72 Snyder PM, McDonald FJ, Stokes JB, Welsh MJ. Membrane topology of the amiloride-sensitive epithelial sodium channel. J Biol Chem. 269(39):24379-83, 1994.

73 Yan W, Spruce L, Rosenblatt MM, Kleyman TR, Rubenstein RC. Intracellular trafficking of a polymorphism in the COOH terminus of the alpha-subunit of the human epithelial sodium channel is modulated by casein kinase 1 Am J Physiol Renal Physiol. 293(3):F868-76, 2007.

74 Niisato N, Taruno A, Marunaka Y. Aldosterone-induced modification of osmoregulated ENaC trafficking Biochem Biophys Res Commun. 361(1):162-8, 2007.

75 Snyder PM Minireview: Regulation of Epithelial Na+ Channel Trafficking Endocrinology 146 (12) 5079-5085, 2005.

76 Lifton RP, Wilson FH, Choate KA, Geller DS Salt and blood pressure: new insight from human genetic studies. Cold Spring Harb Symp Quant Biol 67:445–450, 2002.

77 Fredholm BB, IJzerman AP, Jacobson KA, Klotz KN, Linden J. International Union of Pharmacology. XXV. Nomenclature and Classification of Adenosine Receptors Pharmacol reviews 53 (4), 527-552, 2001.

78 Abbracchio MP, Burnstock G, Boeynaems JM, Barnard EA, Boyer JL, Kennedy C, Knight GE, Fumagalli M, Gachet C, Jacobson KA, Weisman GA. International Union of Pharmacology LVIII: update on the P2Y G protein-coupled nucleotide receptors: from molecular mechanisms and pathophysiology to therapy. Pharmacol Rev. 58(3):281-341, 2006.

79 North RA. Molecular Physiology of P2X Receptors Physiol. Rev. 82: 1013-1067, 2002.

80 Gever JR, Cockayne DA, Dillon MP, Burnstock G, Ford A Pharmacology of P2X channels Pfugers Arch. 452: 513-537, 2006.

81 Hilgemann DW, Feng S, Nasuhoglu C: The complex and intriguing lives of PIP2 with ion channels and transporters. Sci STKE 111: RE19, 2001.

82 Hilgemann DW: Cytoplasmic AT: P-dependent regulation of ion transporters and channels: Mechanisms and messengers. Annu Rev Physiol 59: 193–220, 1997.

83 Blazer-Yost BL, Paunescu TG, Helman SI, Lee KD, Vlahos CJ: Phosphoinositide 3-kinase is required for aldosteroneregulated sodium reabsorption. Am J Physiol 277: C531–C536, 1999.

84 Poulsen AN, Klausen TL, Pedersen PS, Willumsen NJ, Frederiksen O. Regulation of ion transport via apical purinergic receptors in intact rabbit airway epithelium. Pflugers Arch. 450(4):227-35, 2005.

85 Wildman SS, Marks J, Churchill LJ, Peppiatt CM, Chraibi A, Shirley DG, Horisberger JD, King BF, Unwin RJ. Regulatory interdependence of cloned epithelial Na+ channels and P2X receptors J Am Soc Nephrol. 16(9):2586-97. 2005.

86 Ma HP, Eaton DC. Acute Regulation of Epithelial Sodium Channel by Anionic Phospholipids J Am Soc Nephrol 16:3182-3187, 2005.

87 Hall JE, Guyton AC, Coleman TG, Mizelle HL, Woods LL. Regulation of arterial pressure: Role of pressure natriuresis and diuresis. Fed. Proc. 45: 2897–903, 1986.

88 Navar LG, Paul RV, Carmines PK, Chou CL, Marsh DJ. Intrarenal mechanisms mediating pressure natriuresis: role of angiotensin and prostaglandins. Fed Proc. 45(13):2885-91, 1986.

89 Zhang Y, Mircheff AK, Hensley CB, Magyar CE, Warnock DG, Chambrey R, Yip KP, Marsh DJ, Holstein-Rathlou NH, McDonough AA. Rapid redistribution and inhibition of renal sodium transporters during acute pressure natriuresis. Am J Physiol. 270(6 Pt 2):F1004-14, 1996.

90 Williams JM, Sarkis A, Lopez B, Ryan RP, Flasch AK, Roman RJ. Elevations in renal interstitial hydrostatic pressure and 20-hydroxyeicosatetraenoic acid contribute to pressure natriuresis. Hypertension. 49(3):687-94, 2007.

91 Messer-Létienne I, Bernard N, Roman RJ, Sassard J, Benzoni D. 20-Hydroxyeicosatetraenoic acid and renal function in Lyon hypertensive rats. Eur J Pharmacol. 378(3):291-7, 1999.

92 Oyekan AO. Cytochrome p450-dependent metabolites of arachidonic acid and renal function in the rat. Clin Exp Pharmacol Physiol. 27(8):581-6, 2000.

93 Sottiurai V, Malvin LR The demonstration of cilia in canine macula densa cells. Am. J. Anat. 135(2): 281-286, 1972.

94 Webber WA, Lee J, Fine structure of mammalian renal cilia. Anat. Record 182:339-344, 1975.

95 Praetorius HA, Spring KR. Bending the MDCK cell primary cilium increases intracellular calcium. J Membr Biol. 184(1):71-9, 2001.

96 Stout CE, Costantin JL, Naus CC, Charles AC. Intercellular calcium signaling in astrocytes via ATP release through connexin hemichannels. J Biol Chem. 22;277(12):10482-8, 2002.

97 Takenaka T, Inoue T, Kanno Y, Okada H, Hill CE, Suzuki H. Connexins 37 and 40 transduce purinergic signals mediating renal autoregulation. Am J Physiol Regul Integr Comp Physiol. In press 2007.

98 Roman RJ, Cowley AW Jr. Characterization of a new model for the study of pressure-natriuresis in the rat. Am J Physiol. 248(2 Pt 2):F190-8, 1985.

99 Zhang Y, Magyar CE, Norian JM, Holstein-Rathlou NH, Mircheff AK, McDonough AA. Reversible effects of acute hypertension on proximal tubule sodium transporters. Am J Physiol. 274:C1090-100, 1998.

100 Göppert-Mayer M. Über Elementarakte mit zwei Quantensprüngen Ann Phys 9: 273–95, 1931.

101 Denk W, Strickler J, Webb W. Two-photon laser scanning fluorescence microscopy Science 248 (4951): 73-6, 1990.

102 Peti-Peterdi J, Morishima S, Bell PD et al. Two-photon excitation fluorescence imaging of the living juxtaglomerular apparatus. Am J Physiol Renal Physiol 283: F197–F201, 2002.

103 Herget-Rosenthal S, Molitoris BA. Advances in the imaging the kidney and cellular processes. Nephron Exp Neprol 103:e31-32, 2006.

104 Zipfel WR, Williams RM, Webb WW. Nonlinear magic: multiphoton microscopy in the biosciences. Nature Biotechnology 21, 1369 – 1377, 2003.

105 Helmchen F, Denk W Deep tissue two-photon microscopy Nat Methods 2 (12): 932-40, 2005.

106 Peti-Peterdi J. Multiphoton imaging of renal tissues in vitro. Am J Physiol Renal Physiol 288: F1079–F1083, 2005.

107 Kang JJ, Toma I, Sipos A et al. Quantitative imaging of basic functions in renal (patho)physiology. Am J Physiol Renal Physiol 291: F495–F502, 2006.

108 Dunn KW, Sandoval RM, Kelly KJ et al. Functional studies of the kidney of living animals using multicolor two-photon microscopy. Am J Physiol Cell Physiol 283: C905–C916, 2002.

109 Yu W, Sandoval RM, Molitoris BA. Quantitative intravital microscopy using a generalized polarity concept for kidney studies. Am J Physiol Cell Physiol 289: C1197–C1208, 2005.

110 Sandoval RM, Kennedy MD, Low PS et al. Uptake and trafficking of fluorescent conjugates of folic acid in intact kidney determined using intravital two-photon microscopy. Am J Physiol Cell Physiol 287: C517–C526, 2004.

111 Molitoris BA, Sandoval RM. Intravital multiphoton microscopy of dynamic renal processes. Am J Physiol Renal Physiol 288: F1084–F1089, 2005.

112 Tanner GA, Sandoval RM, Molitoris BA et al. Micropuncture gene delivery and intravital two-photon visualization of protein expression in rat kidney. Am J Physiol Renal Physiol 289: F638–F643, 2005.

113 Tanner GA, Sandoval RM, Dunn KW. Two-photon in vivo microscopy of sulfonefluorescein secretion in normal and cystic rat kidneys. Am J Physiol Renal Physiol 286: F152–F160, 2004.

114 Yu W, Sandoval RM, Molitoris BA. Rapid determination of renal filtration function using an optical ratiometric imaging approach. Am J Physiol Renal Physiol 292: F1873–F1880, 2007.

115 Russo LM, Sandoval RM, McKee M et al. The normal kidney filters nephrotic levels of albumin retrieved by proximal tubule cells: retrieval is disrupted in nephrotic states. Kidney Int 71: 504–513, 2007.

116 Rosivall L, Mirzahosseini S, Toma I et al. Fluid flow in the juxtaglomerular interstitium visualized in vivo. Am J Physiol Renal Physiol 291: F1241–F1247, 2006.

117 Peti-Peterdi J, et al. Macula densa Na:H exchange activities mediated by apical NHE2 and basolateral NHE4 isoforms. Am. J. Physiol. 278:F452–F463, 2000.

118 Teubner B, Michel V, Pesch J, Lautermann J, Cohen-Salmon M, Söhl G, Jahnke K, Winterhager E, Herberhold C, Hardelin JP, Petit C, Willecke K: Connexin30 (Gjb6)-deficiency causes severe hearing impairment and lack of endocochlear potential. Hum Mol Genet 12: 13-21, 2003.

119 Taylor AL, Kudlow BA, Marrs KL, Gruenert DC, Guggino WB, Schwiebert EM Bioluminescence detection of ATP release mechanisms in epithelia Am J Physiol Cell Physiol 275:1391-1406, 1998.

120 Schneider SW, Egan ME, Jena BP, Guggino WB, Oberleitner H, and Geibel JP. Continuous detection of extracellular ATP on living cells by using atomic force microscopy. Proc Natl Acad Sci USA 96: 12180–12185, 1999.

121 Hazama A, Hayashi S, and Okada Y. Cell surface measurement of ATP release from single pancreatic b cells using a novel biosensor technique. Pflügers Arch 437: 31–35, 1998.

122 Komlosi P, Fuson AL, Fintha A, Peti-Peterdi J, Rosivall L, Warnock DG, Bell PD: Angiotensin I conversion to angiotensin II stimulates cortical collecting duct sodium transport. Hypertension 42: 195-9, 2003.

123 Kang JJ, Toma I, Sipos A, Meer EJ, Vargas SL, Peti-Peterdi J: The collecting duct is the major source of prorenin in diabetes. Hypertension 51: 1597-604, 2008.

124 Hanner F, Schnichels M, Zheng-Fischhöfer Q, Yang LE, Toma I, Willecke K, McDonough AA, Peti-Peterdi J: Connexin 30.3 is expressed in the kidney but not regulated by dietary salt or high blood pressure. Cell Commun Adhes 15: 219-30, 2008.

125 Toma I, Bansal E, Meer EJ, Kang JJ, Vargas SL, Peti-Peterdi J: Connexin 40 and ATP-dependent intercellular calcium wave in renal glomerular endothelial cells. Am J Physiol Regul Integr Comp Physiol 294: R1769-76, 2008.

126 Ebihara L: New roles for connexins. News Physiol Sci 18: 100-103, 2003.

127 Bao L, Sachs F, Dahl G: Connexins are mechanosensitive. Am J Physiol Cell Physiol 287: C1389-95, 2004.

128 Guyton AC, Langston JB, Navar G. Theory for renal autoregulation by feedback at the juxtaglomerular apparatus. Circ Res. 15:suppl:187-97, 1964.

129 Schnermann J and Briggs JP. Function of the juxtaglomerular apparatus: control of glomerular hemodynamics and renin secretion. In: The Kidney Physiology and Pathophysiology, edited by Seldin DW and Giebisch G.. Philadelphia: Elsevier Inc. p. 589–626, 2008.

130 Komlosi P, Bell PD, Zhang ZR. Tubuloglomerular feedback mechanisms in nephron segments beyond the macula densa. Curr Opin Nephrol Hypertens. 18(1):57-62, 2009.

131 Castrop H. Mediators of tubuloglomerular feedback regulation of glomerular filtration: ATP and adenosine. Acta Physiol (Oxf). 189(1):3-14, 2007.

132 Komlosi P, Fintha A, Bell PD Current mechanisms of macula densa cell signalling. Acta Physiol Scand. 181(4):463-9, 2004.

133 Schlatter E, Salomonsson M, Persson AE, Greger R. Macula densa cells sense luminal NaCl concentration via furosemide sensitive Na+2Cl-K+ cotransport. Pflugers Arch. 414(3):286-90, 1989.

134 Lapointe JY, Laamarti A, Hurst AM, Fowler BC, Bell PD. Activation of Na:2Cl:K cotransport by luminal chloride in macula densa cells. Kidney Int. 47(3):752-7, 1995.

135 Briggs J, Schubert G, Schnermann J. Further evidence for an inverse relationship between macula densa NaCl concentration and filtration rate. Pflugers Arch. 392(4):372-8, 1982.

136 Schnermann J, Briggs J, Schubert G. In situ studies of the distal convoluted tubule in the rat. I. Evidence for NaCl secretion. Am J Physiol. 243(2):F160-6, 1982.

137 Sipos A, Toma I, Kang JJ, Rosivall L, Peti-Peterdi J. Advances in renal (patho)physiology using multiphoton microscopy. Kidney Int. 72(10):1188-91, 2007.

138 Komlosi P, Fintha A, Bell PD. Unraveling the relationship between macula densa cell volume and luminal solute concentration/osmolality. Kidney Int. 70(5):865-71, 2006.

139 Wilcox CS, Welch WJ. Interaction between nitric oxide and oxygen radicals in regulation of tubuloglomerular feedback. Acta Physiol Scand. 168(1):119-24, 2000.

140 Ren Y, Carretero OA, Garvin JL. Mechanism by which superoxide potentiates tubuloglomerular feedback. Hypertension. 39(2 Pt 2):624-8, 2002.

141 Carlström M, Persson AE. Important role of NAD(P)H oxidase 2 in the regulation of the tubuloglomerular feedback. Hypertension. 53(3):456-7, 2009.

142 Liu R, Garvin JL, Ren Y, Pagano PJ, Carretero OA. Depolarization of the macula densa induces superoxide production via NAD(P)H oxidase. Am J Physiol Renal Physiol. 292(6):F1867-72, 2007.

143 Praetorius HA, Spring KR. Removal of the MDCK cell primary cilium abolishes flow sensing. J Membr Biol. 191(1):69-76, 2003.

144 Praetorius HA, Frokiaer J, Nielsen S, Spring KR. Bending the primary cilium opens Ca2+-sensitive intermediate-conductance K+ channels in MDCK cells. J Membr Biol. 191(3):193-200, 2003.

145 Praetorius HA, Spring KR. The renal cell primary cilium functions as a flow sensor. Curr Opin Nephrol Hypertens. 12(5):517-20, 2003.

146 Schnermann J, Osswald H, Hermle M. Inhibitory effect of methylxanthines on feedback control of glomerular filtration rate in the rat kidney. Pflugers Arch. 369(1):39-48, 1977.

147 Vallon V, Mühlbauer B, Osswald H. Adenosine and kidney function. Physiol Rev. 86(3):901-40, 2006.

148 Inscho EW, Cook AK, Imig JD, Vial C, Evans RJ. Renal autoregulation in P2X1 knockout mice. Acta Physiol Scand. 181(4):445-53, 2004.

149 Castrop H, Huang Y, Hashimoto S, Mizel D, Hansen P, Theilig F, Bachmann S, Deng C, Briggs J, Schnermann J. Impairment of tubuloglomerular feedback regulation of GFR in ecto-5'-nucleotidase/CD73-deficient mice. J Clin Invest 114:634-42, 2004.

150 Ma R, Pluznick JL, Sansom SC. Ion channels in mesangial cells: function, malfunction, or fiction. Physiology (Bethesda). 20:102-11, 2005.

151 Moore LC, Iijima K, Rich A, Casellas D, Goligorsky MS. Communication of the tubuloglomerular feedback signal in the JGA. Kidney Int Suppl 32:S45-50, 1991.

152 Sequeira Lopez ML, Pentz ES, Nomasa T, Smithies O, GomezR A. Renin cells are precursors for multiple cell types that switch to the renin phenotype when homeostasis is threatened. Dev Cell 6:719-28, 2004.

153 Ito S, Abe K. Contractile properties of afferent and efferent arterioles. Clin Exp Pharmacol Physiol. 24(7):532-5, 1997.

154 Ren Y, Garvin JL, Carretero OA. Efferent arteriole tubuloglomerular feedback in the renal nephron. Kidney Int. 59(1):222-9, 2001.

155 Schnermann J, Levine DZ. Paracrine factors in tubuloglomerular feedback: adenosine, ATP, and nitric oxide. Annu Rev Physiol.65:501-29, 2003.

156 Gandhi R, Le Hir M, Kaissling B. Immunolocalization of ecto-5'-nucleotidase in the kidney by a monoclonal antibody. Histochemistry.95(2):165-74, 1990.

157 Le Hir M, Kaissling B. Distribution and regulation of renal ecto-5'-nucleotidase: implications for physiological functions of adenosine. Am J Physiol. 264(3 Pt 2):F377-87, 1993.

158 Kishore BK, Isaac J, Fausther M, Tripp SR, Shi H, Gill PS, Braun N, Zimmermann H, Sévigny J, Robson SC: Expression of NTPDase1 and NTPDase2 in murine kidney: relevance to regulation of P2 receptor signaling. Am J Physiol Renal Physiol 288: F1032-43, 2005.

159 Satlin LM, Carattino MD, Liu W, Kleyman TR: Regulation of cation transport in the distal nephron by mechanical forces. Am J Physiol Renal Physiol 291: F923-31, 2006.

160 Liu W, Xu S, Woda C, Kim P, Weinbaum S, Satlin LM: Effect of flow and stretch on the [Ca2+]i response of principal and intercalated cells in cortical collecting duct. Am J Physiol Renal Physiol 285: F998-F1012, 2003.

161 Woda CB, Leite M, Jr, Rohatgi R, Satlin LM: Effects of luminal flow and nucleotides on [Ca2+]i in rabbit cortical collecting duct. Am J Physiol Renal Physiol 283: F437 - F446, 2002.

162 Unwin RJ, Bailey MA, Burnstock G: Purinergic Signaling Along the Renal Tubule: The Current State of Play. Physiology 18: 237-241, 2003.

163 Shirley DG, Bailey MA, Unwin RJ: In vivo stimulation of apical P2 receptors in collecting ducts: evidence for inhibition of sodium reabsorption. Am J Physiol Renal Physiol 288: F1243-8, 2005.

164 Leipziger J: Control of epithelial transport via luminal P2 receptors. Am J Physiol Renal Physiol 284: F419-32, 2003.

165 Lehrmann H, Thomas J, Kim SJ, Jacobi C, Leipziger J: Luminal P2Y2 receptor-mediated inhibition of Na+ absorption in isolated perfused mouse CCD. J Am Soc Nephrol 13: 10-8, 2002.

166 Wildman SS, Marks J, Turner CM, Yew-Booth L, Peppiatt-Wildman CM, King BF, Shirley DG, Wang W, Unwin RJ: Sodium-dependent regulation of renal amiloride-sensitive currents by apical P2 receptors. J Am Soc Nephrol 19: 731-42, 2008.

167 Pochynyuk O, Bugaj V, Vandewalle A, Stockand JD: Purinergic control of apical plasma membrane PI(4,5)P2 levels sets ENaC activity in principal cells. Am J Physiol Renal Physiol 294: F38-46, 2008.

168 Kishore BK, Chou CL, Knepper MA: Extracellular nucleotide receptor inhibits AVP-stimulated water permeability in inner medullary collecting duct. Am J Physiol 269: F863–F869, 1995.

169 Vallon V: P2 receptors in the regulation of renal transport mechanisms. Am J Physiol Renal Physiol 294: F10 - F27, 2008.

170 Lu M, MacGregor GG, Wang W, Giebisch G: Extracellular ATP inhibits the small-conductance K channel on the apical membrane of the cortical collecting duct from mouse kidney. J Gen Physiol 116: 299-310, 2000.

171 Liu W, Morimoto T, Woda C, Kleyman TR, Satlin LM: Ca2+ dependence of flow-stimulated K secretion in the mammalian cortical collecting duct. Am J Physiol Renal Physiol 293: F227-35, 2007.

172 Granger JP, Alexander BT, Llinas M: Mechanisms of pressure natriuresis. Curr Hypertens Rep 4: 152-9, 2002.

173 Ahmed F, Kemp BA, Howell NL, Siragy HM, Carey RM: Extracellular renal guanosine cyclic 3'5'-monophosphate modulates nitric oxide and pressure-induced natriuresis. Hypertension 50: 958-63, 2007.

174 Chou CL, Marsh DJ: Role of proximal convoluted tubule in pressure diuresis in the rat. Am J Physiol 251: F283-9, 1986.

175 Wang XY, Masilamani S, Nielsen J, Kwon TH, Brooks HL, Nielsen S, Knepper MA: The renal thiazide-sensitive Na-Cl cotransporter as mediator of the aldosterone-escape phenomenon. J Clin Invest 108: 215-22, 2001.

176 Hovater MB, Olteanu D, Hanson EL, Cheng NL, Siroky B, Fintha A, Komlosi P, Liu W, Satlin LM, Bell PD, Yoder BK, Schwiebert EM: Loss of apical monocilia on collecting duct principal cells impairs ATP secretion across the apical cell surface and ATP-dependent and flow-induced calcium signals. Purinergic Signal 4: 155-70, 2008.

177 Lang F, Vallon V, Knipper M, Wangemann P: Functional significance of channels and transporters expressed in the inner ear and kidney. Am J Physiol Cell Physiol 293: C1187-208, 2007.

178 Nozu K, Inagaki T, Fu XJ, Nozu Y, Kaito H, Kanda K, Sekine T, Igarashi T, Nakanishi K, Yoshikawa N, Iijima K, Matsuo M: Molecular analysis of digenic inheritance in Bartter syndrome with sensorineural deafness. J Med Genet 45: 182-186, 2008.

179 Locovei S, Bao L, Dahl G: Pannexin 1 in erythrocytes: function without a gap. Proc Natl Acad Sci USA 103: 7655-9, 2006.

180 Genetos DC, Kephart CJ, Zhang Y, Yellowley CE, Donahue HJ: Oscillating fluid flow activation of gap junction hemichannels induces ATP release from MLO-Y4 osteocytes. J Cell Physiol 212: 207-14, 2007.

181 Huang YJ, Maruyama Y, Dvoryanchikov G, Pereira E, Chaudhari N, Roper SD: The role of pannexin 1 hemichannels in ATP release and cell-cell communication in mouse taste buds Proc Natl Acad Sci USA 104: 6436-41, 2007.